PHOTOCROSSLINKED POLY(ANHYDRIDES) FOR SPINAL FUSION: CHARACTERIZATION AND CONTROLLED RELEASE STUDIES

By

Ashley Aston Weiner

Dissertation

Submitted to the Faculty of the

Graduate School of Vanderbilt University

in partial fulfillment of the requirements

for the degree of

DOCTOR OF PHILOSOPHY

in

Biomedical Engineering

May, 2007

Nashville, Tennessee

Approved:

V. Prasad Shastri

Todd D. Giorgio

Scott A. Guelcher

Frederick R. Haselton

Ginger E. Holt

ACKNOWLEDGEMENTS

Many people have contributed over the course of my graduate school career. First I would like to thank my advisor, Prasad Shastri, for giving me guidance throughout the course of my dissertation research. Additionally, I would like to thank the members of my doctoral dissertation committee – Todd Giorgio, Scott Guelcher, Rick Haselton, and Ginger Holt – for their suggestions and mentoring as I worked toward my degree.

I would also like to thank the members of the Shastri, Giorgio, and Haselton labs during my graduate career - Ian Dallmeyer, Ash Jayagopal, Kyle Kellinghaus, Amy Klemm, Sam Kuhn, Chrissy Marasco, Henrique Oliveira, Chris Pino, Sanjeet Rangarajan, Tricia Russ, Adam Smith, Chinmay Soman, Greg Stone, Elizabeth Vargis, and Shelby Wyatt. During my years at Vanderbilt, they have constantly motivated and encouraged me both scientifically and socially.

Undergraduate students Eileen Bock, Jordan Bush, Margaret Gipson, Marc Moore, Dani Shuck, and Amanda Walker have put many hours into the projects described in this dissertation. I appreciate their diligence and commitment to research.

A number of other faculty members have also assisted with this work. Don Stec graciously assisted with NMR analysis of the monomers. Adam List provided access to FT-IR equipment for analysis of networks. Ginger Holt has provided surgical expertise to shape preparations for the future applications of these studies. Ed Donnelly and Todd Peterson have provided guidance for usage of imaging modalities in the future surgical applications.

This work would not have been possible without our sources of funding. I would like to thank the Graduate School of Vanderbilt University for assistance with my stipend through the IBM and University Graduate Fellowship Programs and for assistance with travel funds. I would also like to acknowledge the National Science Foundation for supporting me through the NSF Graduate Research Fellowship Program. Additionally this work was funded by Vanderbilt Institute of Integrative Biology Research and Education (VIIBRE) funds and by a Vanderbilt Discovery Grant to Prasad Shastri.

Finally, I would like to thank my family – especially my parents and my husband – for their unwavering love and support during my graduate studies.

TABLE OF CONTENTS

Page

LIST OF FIGURES

Figure Page

CHAPTER II

CHAPTER IV

LIST OF TABLES

APPENDIX A

CHAPTER I

INTRODUCTION

Specific Aims

The primary goal of the National Bone and Joint decade is to foster the discovery and development of novel therapeutics and treatments for skeletal disorders. Spine-related applications would benefit greatly from the development of injectable and *in situ* curable biomaterials. Spinal fusion is a procedure that eliminates or minimizes motion at a site of degeneration in the spinal column. When fusion procedures yield new bone that welds the transverse processes or the vertebral bodies, the stability of the spinal column is enhanced without dramatically altering spine motion as a whole. The osteoinductive material of choice for grafting is autograft harvested from the iliac crest. The use of autograft is dictated by limited availability at the donor site (1) and post-operative morbidity due to long-term discomfort at the donor site (2). Furthermore, in cases of revision procedures and/or when previous iliac crest harvest has been made, the autograft option is an untenable one. These limitations form the basis and serve as the motivating elements in the development of synthetic alternatives. An ideal polymeric biomaterial for these applications provides immediate mechanical stability, degrades over time in order to promote new bone growth, and promotes no adverse immune response. To fulfill these three criteria, the following characteristics are desired for bone regenerative biomaterials: capability of *in situ* formation, conformability to the implantation site, controlled degradation and retention of mechanical characteristics.

Additionally, the material should be readily modifiable to include osteogenic factors or components which minimize local pH alterations, as local acidity can induce inflammation and impair bone healing (3). This combination of features is ideal for complex fractures, bony defects, or spinal augmentations which require immediate mechanical support yet would benefit from material degradation and eventual replacement by bone.

The focus of this work therefore, was to develop an injectable, *in situ* curable, biodegradable biomaterial for spinal fusion. In this study, photocurable methacrylated-anhydride monomers were formulated into injectable pastes. Reactive diluents (polyethylene glycol diacrylate (PEGDA) and nonreactive fillers (calcium carbonate (CaCO3)) will be incorporated. The choice of the anhydride system was based on its similarity to PMMA with respect to crosslinking chemistry, while simultaneously affording degradability to biomaterial. In this dissertation, a thorough evaluation of the *in vitro* degradation and biocompatibility of the photocrosslinked poly(anhydride) networks is provided. In addition, the capabilities of the materials to deliver bioactive molecules are assessed in *in vitro* studies. The following specific aims were pursued.

Aim 1 – Characterize in vitro degradation parameters for bone graft substitutes composed of surface-eroding poly-anhydrides

In this aim, we have evaluated the *in vitro* degradation characteristics of photocrosslinked networks composed of sebacic acid dimethacrylate (MSA), 1,6-bis-carboxyphenoxyhexane dimethacrylate (MCPH), and PEGDA in varying proportions, with or without the presence of additives such as calcium carbonate. We have evaluated the swelling, mass loss, and mechanical properties at varying time points. In

addition, the effect of degradation on local pH was evaluated as a function of time. This aim resulted in optimization of network formulation for further use in Aims 2 and 3.

Aim 2 – Evaluate in vitro release of proteins from surface eroding polyanhydrides

In this aim, we have evaluated the *in vitro* release of model proteins from three-dimensional photocrosslinked networks composed of MSA, MCPH and PEGDA. Formulations demonstrating favorable degradation parameters (including pH profile, mass loss, swelling, and mechanical strength as well as reproducibility in fabrication and ease of handling) in Aim 1 were assessed for their capabilities of sustained release of proteins. For incorporation into the photocrosslinked poly(anhydride) networks, proteins were titurated with a hydroxypropyl-β-cyclodextrin excipient to minimize the potential for free radical or photothermal damage, to stabilize the protein, and to enable accurate measurement of low levels of proteins. We employed a gelatin-based wet granulation technique on the protein:excipient mixture to further protect proteins from free radical or photothermal damage that may occur during crosslinking. By using an excess of excipient (1:100 protein:excipient) and gelatin granulation, a barrier was formed that minimizes the probability of damage occurring to the protein. Release profiles of active enzymes were assessed using horseradish peroxidase, bovine serum albumin conjugated with fluoroscein isothiocyanate, and insulin as model proteins. Metrics included establishing protein integrity after crosslinking and achieving release for a minimum of 4 weeks *in vitro*.

Aim 3 – Modulate in vitro release of proteins from surface eroding polyanhydrides via incorporation of additives

In Aim 2, the release of several model proteins has been achieved from photocrosslinked polyanhydride networks. However, in initial polymer formulations, the rate of protein release is slower than desired. In Aim 3, the methodology developed in Aim 2 was used and expanded upon to modulate rates of protein release. A particulate leaching strategy was employed to induce network microporosity and facilitate protein release. Sodium chloride crystals and gelatin microparticles were explored for their capabilities of modulating protein release. Additionally, protein-loaded gelatin microparticles were incorporated into photocrosslinked matrices as a composite vehicle for sustained release.

Overview and Rationale

The decade spanning 2002 – 2011 has been designated the National Bone and Joint decade, in part to highlight the negative impact of skeletal degenerative diseases on productivity and quality of life and in addition to foster discovery and development of new treatment options. Among disorders and diseases associated with the musculoskeletal system, low back pain has assumed epidemic proportions, accounts for more physician visits than any diagnosis other than the common cold and is estimated to affect over 90% of Americans, with a financial impact in the billions of dollars due to lost man-hours and related medical costs (4). In an ageing population, the primary cause of lower back pain is degenerative changes that arise due to overgrown joints in the lumbar region of the spine subsequent to arthritis. These degenerative changes over time can cause a progressive narrowing of the spinal canal resulting in compression of the spinal nerve roots resulting in pain, local inflammation and onset of vertebral body segments instability (4). This condition is called Lumbar Spine Stenosis (LSS), which disproportionately affects the middle-aged and elderly population, has been implicated as the primary cause of lower back pain (4). Further progressive degeneration can result in slippage of the vertebral processes, leading to a condition called *degenerative spondylolisthesis*. Currently, non-surgical options include controlling inflammation and pain through systemic and localized administration of medications and physical therapy. Surgery involves relieving the spinal nerve root compression via decompressive laminectomy along with spinal fusion. Spinal fusion is procedure used to treat conditions that result in weakening of the spinal column due to localized trauma and disorders ranging from (1) injuries to spinal vertebrae, (2)

degeneration of disk (herniated or slipped disk) leading to *degenerative spondylolisthesis* (3) abnormal curvatures (scoliosis and kyphosis) and (4) weak or unstable spine caused by infections or tumors (AAOS). The primary goal of spinal fusion, therefore, is to eliminate motion at the site of degeneration of the spinal column thereby improving overall spinal column stability. This is accomplished by "welding" the vertebral processes in question using a grafting material that is replaced by a solid volume of bone over time. This stabilization includes posterolateral intertransverse fusion to restore alignment and stability to the spine and/or interbody fusion. Since the fusion procedures typically involve no more 2-3 sequential spinal segments, overall motion to the spine is not compromised. A spinal fusion procedure is typically accompanied by augmentation of the spinal column with internal devices such as metal rods. Annually, over 400,000 spinal fusion procedures are performed in the United States, with over 50% of those involving the lower spine, namely lumbar fusion. Alarmingly, the rate of lumbar fusion surgery for the treatment of LSS saw a relative increase of 220% from 1990 to 2001 to over 122,000 lumbar fusion procedures in 2001 alone (5).

Current hurdles that clinicians face in restoring spine stability include achieving predictable bone fusion particularly in cases of revision spine surgery, elderly patients and smokers. The grafting material of choice, i.e., the 'gold standard' is autogenous bone from the iliac crest. In a human, typically no more than 15 cc of bone can be harvested from the iliac crest (1). This additional procedure results in significant pain and morbidity and furthermore, is non-tenable option in patients who have already undergone harvest for other surgical procedures (2). This has prompted the exploration

of other alternatives and they include pre-fabricated grafts, injectable tri-calcium phosphate pastes and collagen-BMP systems. Pre-fabricated grafts neither provide stability nor promote new-bone formation easily. Tri-calcium phosphate (TCP) pastes are utilized as non-weight bearing bone void fillers, and require supplementation with hydroxyapatite (HA) or growth factors such as rhBMP-2 or TGF-β to facilitate new bone growth (6). Collagen-BMP systems while capable of inducing new-bone formation do not provide immediate stabilization to the spinal column at the site of application. Therefore, the current need in spinal fusion surgery is a material that (a) provides immediate structural stability for spinal stabilization, (b) allows for easy conformability to defect site but degrades over time producing a fusion rate comparable to or better than autografts and current materials and (c) is replaced by bone. The focus of this proposal therefore, is to develop an *in situ* curable biomaterial for spinal procedures. In the proposed study, photo-curable methacrylated-anhydride monomers will be formulated into injectable pastes and augmented with osteogenic factors. The choice of the anhydride system is based on its similarity to polymethyl(methacrylate) (PMMA) with respect to crosslinking chemistry, while affording degradability to biomaterial. While, degradable alternatives to autograft have been explored, these efforts have primarily focused on the development of calcium phosphate bone cements (7-10) with the exception of poly(propylene-co-fumarate) (PPF) which is discussed later in this section. The focus of this proposal therefore, is to develop an injectable, *in situ* curable biomaterial for minimally invasive spinal procedures. The choice of the anhydride system is based on its similarity to PMMA with respect to chemistry, while affording degradability to biomaterial. In this study, photo-curable methacrylated-anhydride

monomers were formulated into injectable pastes. The paste was photocrosslinked and its *in vitro* degradation properties were evaluated. In addition, its capabilities for release of active biomolecules were assessed.

Degradable biomaterials in orthopedics

The poly(α-hydroxy acids) (PHAs) such as poly(lactic acid), poly(glycolic acid) and their copolymers have garnered the most attention amongst biocompatible, degradable polymers. Although the PHAs have had long standing success as surgical sutures, their use in bone replacement or augmentation has been limited. A primary source of this limitation is the lack or reactive moieties that prevent the PHAs from being injected and crosslinked *in situ*.

It is fairly well established that PHAs primarily undergo degradation via bulk erosion (11). A shortcoming of this degradation pattern is the accumulation of acidic degradation products due to end-stage hydrolysis (12). When the mass of the degrading polymer matrix is significantly large, the local concentration of soluble degradation products (monomers and oligomers) can reach levels adequate to lower the local pH (13). It is believed that local acidity can induce inflammation and thus impair bone healing (3). In addition, pockets of accumulated degradation products can occur, resulting in a net porosity increase throughout the degradative lifetime of the polymer. This is particularly detrimental in bone replacement situations, as the net increase in porosity causes a net decrease in mechanical strength. Thus the effective lifetime of the device could be much less than the theoretical lifetime based on mass calculations. In contrast to the PHAs, poly(anhydrides) (14, 15) (PA) undergo degradation

predominantly via surface erosion (16). The advantages of the surface eroding system in bone augmentation applications are twofold. Surface erosion is dictated by the presence of highly insoluble degradation products. Although the degradation products of the PAs are also acids, the monomers are intentionally designed to have low solubility and hence the degradation products are less likely to contribute to local acidity under physiological conditions. As a result, devices fabricated from these polymers are less likely to alter the local pH during their degradative lifetime. A second advantage conferred by the surface eroding characteristics of the PA system is the maintenance of mechanical strength during the course of degradation. Tensile modulus changes of less than 20% have been seen at up to 50% mass loss in photocrosslinked polyanhydride systems (17, 18).

Another consideration in the development of materials for use in spinal applications is control over degradation behavior. The ability to vary degradation behavior in a predictable manner is of extreme significance in ensuring new bone formation. It is desirable that the degradation/erosion rates match new bone ingrowth. In the PA system the degradative lifetime of the polymer can be varied from a few days to few years by changing the relative hydrophobicity of the monomers and the co-monomer composition in the polymer (19). Such flexibility in degradation properties is however absent in the PHAs without significant chemical modification.

Although, poly(esters) derived from propylene glycol and fumaric acid (unsaturated diacid) are being evaluated for bone cement applications with moderate success (20-22), they lack the versatility in chemical structure to allow for tailoring of erosion behavior and curing kinetics. In fact the poly(propylene-co-fumaric acid) system

(PPF), by virtue of it being an alternating polymer, has a fixed concentration of unsaturated linkages per polymer chain. This typically results in a very high cross-link density yielding brittle structures, a problem which is only offset by adding excipients and filler agents to decrease the cross linking. Furthermore, aliphatic vinyl groups have very poor reactivity, requiring the use of highly reactive and toxic reactive diluents such as vinyl pyrrolidone to improve the kinetics of cross-linking. Finally, aliphatic unsaturation in absence of an adjacent activating group is not amenable to cross-linking via light radiation.

We believe that biodegradable polymers if designed and formulated properly can yield a viable osteoconductive conduit for bone repair and replacement in spinal procedures. We have developed an anhydride based polymer system bearing reactive methacrylate functionalities that cure rapidly upon exposure to UV or visible radiation to produce high strength degradable networks that have degradative lifetimes ranging from a few days to months (17). This novel system addresses many of the limitations of the PPF system and can be developed into an injectable, photo-curable system for bone regeneration.

Polyanhydrides as drug delivery vehicles

Polyanhydrides have been studied for a variety of sustained release applications, primarily as a direct result of their surface erosion properties. The predictable degradation profile results in a similarly predictable release profile for drugs, proteins, or other molecules. Polyanhydrides are currently approved by the FDA as an implantable device for the delivery of BCNU in the treatment of glioblastoma multiforme – a fatal

form of brain cancer (23, 24). Polyanhydride microspheres have been evaluated for the release of a variety of molecules, including rhodamine B (25, 26), FITC-BSA (27), plasmid DNA (25), p-nitroaniline (26, 28), piroxicam (26), and BSA (28). In addition, photocrosslinked polyanhydride networks have demonstrated a modest capability to deliver plasmid DNA (29).

Sustained release of osteogenic cytokines and growth factors from polymer scaffolds for imparting osteoinductivity has been the focus of much research (30-36). Utilization of a potent osteoinductive molecule, such as BMP-2, in a photocrosslinked polyanhydride matrix will add an additional benefit to the system for applications in spinal repair.

Role of BMPs in bone remodeling

Bone is a very dynamic and metabolically active tissue that remodels throughout ones lifetime. This process is governed by a complex interplay between molecular cues in the form of soluble growth factors (GFs) such as bone morphogenetic proteins (BMPs), and mechanical cues. The bone healing process is a complex multi-faceted pathway which can be expedited by a bone graft. The stages of bone healing are inflammation, vascularization, osteoinduction, osteoconduction and remodeling (37). Inflammation, the first stage, lasts approximately 14 days. During the vascularization stage, capillaries begin extension throughout the graft. From days 14-21, the osteoinduction stage occurs concurrently with the vascularization stage, and results in osteoblast differentiation. The fourth stage, osteointegration, occurs as bone grows into

the graft over the course of several months. Finally, remodeling occurs over a period of months to years.

BMPs are cytokines which are members of the TGF-β superfamily of proteins. BMPs are involved in cell proliferation, differentiation, apoptosis and morphogenesis (37). The hallmark of BMPs is the ability to enhance osteoinduction in a multi-faceted approach. BMPs can contribute to osteoinduction via Smad-mediated gene expression after interaction with membrane bound BMP receptors. BMPs act as a chemotactic agent by facilitating progenitor cell migration to the graft interface. BMPs act as growth factors by stimulating stem cell proliferation and angiogenesis. BMPs act in differentiation by inducing stem cell maturation into chondrocytes, osteocytes and osteoblasts. BMP-2, on which we are focusing Aim 2, is involved in bone and cartilage formation during embryogenesis, morphogenesis, and induction of osteogenesis (lineage specific differentiation in mesenchymal progenitor cells and osteoblasts) (37).

In vivo bone formation has been demonstrated in several spinal fusion models using BMP-2. In a rat model, rhBMP-2 has demonstrated up to a tenfold increase in ectopic bone formation over bone extract (38-40). In a canine intertransverse fusion model, successful bone fusion at 3 months was evident in rhBMP-2 specimen, while no fusion was observed with autograft (41, 42). Dose dependency of BMP-2 for spinal fusion has been observed; increased dosages yield more rapid and more significant degrees of fusion (42, 43).

Current clinically used materials in spinal fusion

In response to the inadequacy of autograft for spinal fusion in patient populations, several alternative fusion materials have been studied. Healos (DuPuy Spine, Inc) is a Type I collagen/hydroxyapatite matrix provided in sheets. Healos provides no immediate structural support as a fusion mass and is only an osteoconductive conduit. It must be soaked in bone marrow aspirate to achieve osteoinductive capabilities. Healos has been found to achieve clinical outcomes similar to autograft; however, Healos yields a fusion mass that is radiologically inferior to autograft (44).

Calcium sulfate pellets (OSTEOSET, Wright Medical Technologies) are another material that has been studied as an autograft replacement for spinal fusion. This is a resorbable, osteoconductive material. In a study in which one side of the spine was augmented with iliac crest autograft and the other side was augmented with OSTEOSET, there was no significant difference in fusion between sides (45).

Coralline hydroxyapatite has also been assessed clinically for spinal fusion procedures. Although this material was found to promote bone growth, in an posterolateral intertransverse fusion study it was found that there is not enough local bone available in this procedure to produce fusion comparable to autograft (46).

rhBMP-2 has been tested in several completed, prospective, randomized clinical trials which have resulted in FDA approval for use in anterior interbody spinal fusion (47, 48). Carriers for BMP-2 used in clinical trials and/or animal studies include Gelfoam, biphasic ceramic phosphates (hydroxyapatite + tricalcium phosphate) (49), hydroxyapatite granules (50), an artificial hydroxyapatite True Bone Ceramic (9, 51), or

β-tricalcium phosphate mixed with a polymer matrix (52). While many studies utilize levels of BMP-2 loading in the 0.1 to 5 mg range, some studies, such as those by Namikawa have demonstrated success in spinal fusion with loading of less than 100 μg of BMP-2 per 3 cc of material (52).

OP-1 (rhBMP-7) is a growth factor that has been approved for clinical use in spinal fusion for symptomatic degenerative spondylolisthesis and spinal stenosis. OP-1 is applied as putty with carboxymethylcellulose and bovine collagen. In a clinical study using OP-1 for fusion in patients with lumbar degenerative spondylolisthesis, the OP-1 putty yielded fusion in 70% of patients (53, 54). However this was not statistically different from autograft controls. In another study involving the use of OP-1 for posterolateral intertransverse fusion in patients with degenerative spondylolisthesis with spinal stenosis, but fusion was only seen in 4 or 7 patients (in comparison to 7 or 9 patients who received the control, autograft, hydroxyapatite,TCP) (55).

Significance of the study

The photocurable polyanhydride system has numerous advantages for applications in spinal repair. First, the photocurable nature of the system, by virtue of methacrylate groups, allows formation of the network *in situ*, such that the polymer fits perfectly into the desired region. Second, upon crosslinking, the network forms with a mechanical strength sufficient to withstand the compressive forces of the spinal column. Since the material's modulus is comparable to that of cortico-cancellous bone, it is less likely to shield the bone from normal stresses. Next, the system versatility is clearly unique. The ratios of monomers can be altered to fit nearly any degradation rate.

Additionally, up to 30 wt% of the formulation can consist of reactive and nonreactive additives (inorganic fillers or porogens, growth factors, or viscosity modifiers) without altering crosslinking kinetics. Photocuring allows a more extensive handling time prior to crosslinking than is typically possible with chemical crosslinking (as in PMMA). Finally, system biodegradability eliminates the need for secondary surgeries to remove the device.

Development of this photo-curable poly(anhydride) system into an osteoconductive, osteoinductive biomaterial for use in spinal applications will be a paradigm shift from the current material of choice, autograft harvested from iliac crest. In summary, the research detailed in this dissertation provides a major advance in osteoconductive, osteoinductive biomaterials for use in spine applications. These studies will also generate data supporting the capability of this material for sustained release of proteins. The results from this study will lead to the development of an osteoinductive (through sustained release of BMPs), degradable, *in situ* curable material in spinal fusion applications.

References

1. Silber, J. S., Anderson, D. G., Daffner, S. D., Brislin, B. T., Leland, J. M., Hilibrand, A. S., Vaccaro, A. R., and Albert, T. J. (2003) Donor site morbidity after anterior iliac crest bone harvest for single-level anterior cervical discectomy and fusion. *Spine* 28, 134-139.

2. Sasso, R. C., LeHuec, J. C., and Shaffrey, C. (2005) Iliac crest bone graft donor site pain after anterior lumbar interbody fusion: a prospective patient satisfaction outcome assessment. *J Spinal Disord Tech* 18 Suppl, S77-81.

3. Bergsma, E. J., Rozema, F. R., Bos, R. R., and de Bruijn, W. C. (1993) Foreign body reactions to resorbable poly(L-lactide) bone plates and screws used for the fixation of unstable zygomatic fractures. *J Oral Maxillofac Surg* 51, 666-670.

4. Alvarez, J. A., and Hardy, R. H., Jr. (1998) Lumbar spine stenosis. *Am Fam Physician* 57, 1825-1834, 1839-1840.

5. Deyo, R. A., Gray, D. T., Kreuter, W., Mirza, S., and Martin, B. I. (2005) United States trends in lumbar fusion surgery for degenerative conditions. *Spine* 30, 1441-1445; discussion 1446-1447.

6. Epstein, N. E. (2006) A preliminary study of the efficacy of Beta Tricalcium Phosphate as a bone expander for instrumented posterolateral lumbar fusions. *J Spinal Disord Tech* 19, 424-429.

7. Baroud, G., Bohner, M., Heini, P., and Steffen, T. (2004) Injection biomechanics of bone cements used in vertebroplasty. *Biomed Mater Eng* 14, 487-504.

8. Boden, S. D., Martin, G. J., Jr., Morone, M. A., Ugbo, J. L., and Moskovitz, P. A. (1999) Posterolateral lumbar intertransverse process spine arthrodesis with recombinant human bone morphogenetic protein 2/hydroxyapatite-tricalcium phosphate after laminectomy in the nonhuman primate. *Spine* 24, 1179-1185.

9. Minamide, A., Kawakami, M., Hashizume, H., Sakata, R., Yoshida, M., and Tamaki, T. (2004) Experimental study of carriers of bone morphogenetic protein used for spinal fusion. *J Orthop Sci* 9, 142-151.

10. Khan, S. N., Fraser, J. F., Sandhu, H. S., Cammisa, F. P., Jr., Girardi, F. P., and Lane, J. M. (2005) Use of osteopromotive growth factors, demineralized bone matrix, and ceramics to enhance spinal fusion. *J Am Acad Orthop Surg* 13, 129-137.

11. Leenslag, J. W., Pennings, A. J., Bos, R. R., Rozema, F. R., and Boering, G. (1987) Resorbable materials of poly(L-lactide). VII. In vivo and in vitro degradation. *Biomaterials* 8, 311-314.

12. Pistner, H., Stallforth, H., Gutwald, R., Muhling, J., Reuther, J., and Michel, C. (1994) Poly(L-lactide): a long-term degradation study in vivo. Part II: Physico-mechanical behaviour of implants. *Biomaterials* 15, 439-450.

13. Martin, C., Winet, H., and Bao, J. Y. (1996) Acidity near eroding polylactide-polyglycolide in vitro and in vivo in rabbit tibial bone chambers. *Biomaterials* 17, 2373-2380.

14. Rosen, H. B., Chang, J., Wnek, G. E., Linhardt, R. J., and Langer, R. (1983) Bioerodible polyanhydrides for controlled drug delivery. *Biomaterials* 4, 131-133.

15. Domb, A. J., and Langer, R. (1987) Polyanhydrides .1. Preparation of High-Molecular-Weight Polyanhydrides. *Journal of Polymer Science Part a-Polymer Chemistry* 25, 3373-3386.

16. Tamada, J. A., and Langer, R. (1993) Erosion kinetics of hydrolytically degradable polymers. *Proc Natl Acad Sci U S A* 90, 552-556.

17. Anseth, K. S., Shastri, V. R., and Langer, R. (1999) Photopolymerizable degradable polyanhydrides with osteocompatibility. *Nat Biotechnol* 17, 156-159.

18. Muggli, D. S., Burkoth, A. K., and Anseth, K. S. (1999) Crosslinked polyanhydrides for use in orthopedic applications: degradation behavior and mechanics. *J Biomed Mater Res* 46, 271-278.

19. Domb, A., Shastri, V. & Langer, R. (1997) Polyanhydrides. In *Handbook of Biodegradable Polymers* (Domb, A., Kost, J. & Wiseman, D., ed) pp. 135-159, Harwood Academic Publishers.

20. Peter, S. J., Kim, P., Yasko, A. W., Yaszemski, M. J., and Mikos, A. G. (1999) Crosslinking characteristics of an injectable poly(propylene fumarate)/beta-tricalcium phosphate paste and mechanical properties of the crosslinked composite for use as a biodegradable bone cement. *J Biomed Mater Res* 44, 314-321.

21. Peter, S. J., Lu, L., Kim, D. J., and Mikos, A. G. (2000) Marrow stromal osteoblast function on a poly(propylene fumarate)/beta-tricalcium phosphate biodegradable orthopaedic composite. *Biomaterials* 21, 1207-1213.

22. Lewandrowski, K. U., Gresser, J. D., Wise, D. L., White, R. L., and Trantolo, D. J. (2000) Osteoconductivity of an injectable and bioresorbable poly(propylene glycol-co-fumaric acid) bone cement. *Biomaterials* 21, 293-298.

23. Brem, H., Kader, A., Epstein, J. I., Tamargo, R. J., Domb, A., Langer, R., and Leong, K. W. (1989) Biocompatibility of a biodegradable, controlled-release polymer in the rabbit brain. *Sel Cancer Ther* 5, 55-65.

24. Brem, H., Piantadosi, S., Burger, P. C., Walker, M., Selker, R., Vick, N. A., Black, K., Sisti, M., Brem, S., Mohr, G., and et al. (1995) Placebo-controlled trial of safety and efficacy of intraoperative controlled delivery by biodegradable polymers of chemotherapy for recurrent gliomas. The Polymer-brain Tumor Treatment Group. *Lancet* 345, 1008-1012.

25. Fu, J., Fiegel, J., and Hanes, J. (2004) Synthesis and characterization of PEG-based ether-anhydride terpolymers: Novel polymers for controlled drug delivery. *Macromolecules* 37, 7174-7180.

26. Berkland, C., Kipper, M. J., Narasimhan, B., Kim, K. K., and Pack, D. W. (2004) Microsphere size, precipitation kinetics and drug distribution control drug release from biodegradable polyanhydride microspheres. *J Control Release* 94, 129-141.

27. Determan, A. S., Trewyn, B. G., Lin, V. S., Nilsen-Hamilton, M., and Narasimhan, B. (2004) Encapsulation, stabilization, and release of BSA-FITC from polyanhydride microspheres. *J Control Release* 100, 97-109.

28. Hanes, J., Chiba, M., and Langer, R. (1998) Degradation of porous poly(anhydride-co-imide) microspheres and implications for controlled macromolecule delivery. *Biomaterials* 19, 163-172.

29. Quick, D. J., Macdonald, K. K., and Anseth, K. S. (2004) Delivering DNA from photocrosslinked, surface eroding polyanhydrides. *J Control Release* 97, 333-343.

30. Hedberg, E. L., Tang, A., Crowther, R. S., Carney, D. H., and Mikos, A. G. (2002) Controlled release of an osteogenic peptide from injectable biodegradable polymeric composites. *J Control Release* 84, 137-150.

31. Hedberg, E. L., Shih, C. K., Solchaga, L. A., Caplan, A. I., and Mikos, A. G. (2004) Controlled release of hyaluronan oligomers from biodegradable polymeric microparticle carriers. *J Control Release* 100, 257-266.

32. Hedberg, E. L., Kroese-Deutman, H. C., Shih, C. K., Crowther, R. S., Carney, D. H., Mikos, A. G., and Jansen, J. A. (2005) Effect of varied release kinetics of the osteogenic thrombin peptide TP508 from biodegradable, polymeric scaffolds on bone formation in vivo. *J Biomed Mater Res A* 72A, 343-353.

33. Jansen, J. A., Vehof, J. W., Ruhe, P. Q., Kroeze-Deutman, H., Kuboki, Y., Takita, H., Hedberg, E. L., and Mikos, A. G. (2005) Growth factor-loaded scaffolds for bone engineering. *J Control Release* 101, 127-136.

34. Simmons, C. A., Alsberg, E., Hsiong, S., Kim, W. J., and Mooney, D. J. (2004) Dual growth factor delivery and controlled scaffold degradation enhance in vivo bone formation by transplanted bone marrow stromal cells. *Bone* 35, 562-569.

35. Kaito, T., Myoui, A., Takaoka, K., Saito, N., Nishikawa, M., Tamai, N., Ohgushi, H., and Yoshikawa, H. (2005) Potentiation of the activity of bone morphogenetic protein-2 in bone regeneration by a PLA-PEG/hydroxyapatite composite. *Biomaterials* 26, 73-79.

36. Kamakura, S., Nakajo, S., Suzuki, O., and Sasano, Y. (2004) New scaffold for recombinant human bone morphogenetic protein-2. *J Biomed Mater Res A* 71, 299-307.

37. Samartzis, D., Khanna, N., Shen, F. H., and An, H. S. (2005) Update on bone morphogenetic proteins and their application in spine surgery. *J Am Coll Surg* 200, 236-248.

38. Boden, S. D., Schimandle, J. H., and Hutton, W. C. (1995) 1995 Volvo Award in basic sciences. The use of an osteoinductive growth factor for lumbar spinal fusion. Part II: Study of dose, carrier, and species. *Spine* 20, 2633-2644.

39. Boden, S. D., Schimandle, J. H., Hutton, W. C., and Chen, M. I. (1995) 1995 Volvo Award in basic sciences. The use of an osteoinductive growth factor for lumbar spinal fusion. Part I: Biology of spinal fusion. *Spine* 20, 2626-2632.

40. Martin, G. J., Jr., Boden, S. D., Marone, M. A., and Moskovitz, P. A. (1999) Posterolateral intertransverse process spinal arthrodesis with rhBMP-2 in a nonhuman primate: important lessons learned regarding dose, carrier, and safety. *J Spinal Disord* 12, 179-186.

41. Sandhu, H. S., Kanim, L. E., Kabo, J. M., Toth, J. M., Zeegan, E. N., Liu, D., Seeger, L. L., and Dawson, E. G. (1995) Evaluation of rhBMP-2 with an OPLA carrier in a canine posterolateral (transverse process) spinal fusion model. *Spine* 20, 2669-2682.

42. Sandhu, H. S., Kanim, L. E., Kabo, J. M., Toth, J. M., Zeegen, E. N., Liu, D., Delamarter, R. B., and Dawson, E. G. (1996) Effective doses of recombinant human bone morphogenetic protein-2 in experimental spinal fusion. *Spine* 21, 2115-2122.

43. Boden, S. D., Martin, G. J., Jr., Horton, W. C., Truss, T. L., and Sandhu, H. S. (1998) Laparoscopic anterior spinal arthrodesis with rhBMP-2 in a titanium interbody threaded cage. *J Spinal Disord* 11, 95-101.

44. Neen, D., Noyes, D., Shaw, M., Gwilym, S., Fairlie, N., and Birch, N. (2006) Healos and bone marrow aspirate used for lumbar spine fusion: a case controlled study comparing healos with autograft. *Spine* 31, E636-640.

45. Chen, W. J., Tsai, T. T., Chen, L. H., Niu, C. C., Lai, P. L., Fu, T. S., and McCarthy, K. (2005) The fusion rate of calcium sulfate with local autograft bone compared with autologous iliac bone graft for instrumented short-segment spinal fusion. *Spine* 30, 2293-2297.

46. Korovessis, P., Koureas, G., Zacharatos, S., Papazisis, Z., and Lambiris, E. (2005) Correlative radiological, self-assessment and clinical analysis of evolution in instrumented dorsal and lateral fusion for degenerative lumbar spine disease. Autograft versus coralline hydroxyapatite. *Eur Spine J* 14, 630-638.

47. Boden, S. D., Zdeblick, T. A., Sandhu, H. S., and Heim, S. E. (2000) The use of rhBMP-2 in interbody fusion cages. Definitive evidence of osteoinduction in humans: a preliminary report. *Spine* 25, 376-381.

48. Carlisle, E., and Fischgrund, J. S. (2005) Bone morphogenetic proteins for spinal fusion. *Spine J* 5, 240S-249S.

49. Akamaru, T., Suh, D., Boden, S. D., Kim, H. S., Minamide, A., and Louis-Ugbo, J. (2003) Simple carrier matrix modifications can enhance delivery of recombinant human bone morphogenetic protein-2 for posterolateral spine fusion. *Spine* 28, 429-434.

50. Konishi, S., Nakamura, H., Seki, M., Nagayama, R., and Yamano, Y. (2002) Hydroxyapatite granule graft combined with recombinant human bone morphogenic protein-2 for solid lumbar fusion. *J Spinal Disord Tech* 15, 237-244.

51. Minamide, A., Kawakami, M., Hashizume, H., Sakata, R., and Tamaki, T. (2001) Evaluation of carriers of bone morphogenetic protein for spinal fusion. *Spine* 26, 933-939.

52. Namikawa, T., Terai, H., Suzuki, E., Hoshino, M., Toyoda, H., Nakamura, H., Miyamoto, S., Takahashi, N., Ninomiya, T., and Takaoka, K. (2005) Experimental spinal fusion with recombinant human bone morphogenetic protein-2 delivered by a synthetic polymer and beta-tricalcium phosphate in a rabbit model. *Spine* 30, 1717-1722.

53. Vaccaro, A. R., Patel, T., Fischgrund, J., Anderson, D. G., Truumees, E., Herkowitz, H., Phillips, F., Hilibrand, A., and Albert, T. J. (2005) A 2-year follow-up pilot study evaluating the safety and efficacy of op-1 putty (rhbmp-7) as an adjunct to iliac crest autograft in posterolateral lumbar fusions. *Eur Spine J* 14, 623-629.

54. Vaccaro, A. R., Anderson, D. G., Patel, T., Fischgrund, J., Truumees, E., Herkowitz, H. N., Phillips, F., Hilibrand, A., Albert, T. J., Wetzel, T., and McCulloch, J. A. (2005) Comparison of OP-1 Putty (rhBMP-7) to iliac crest autograft for posterolateral lumbar arthrodesis: a minimum 2-year follow-up pilot study. *Spine* 30, 2709-2716.

55. Kanayama, M., Hashimoto, T., Shigenobu, K., Yamane, S., Bauer, T. W., and Togawa, D. (2006) A prospective randomized study of posterolateral lumbar fusion using osteogenic protein-1 (OP-1) versus local autograft with ceramic bone substitute: emphasis of surgical exploration and histologic assessment. *Spine* 31, 1067-1074.

CHAPTER II

OPTIMIZATION OF PHOTOCROSSLINKED ANHYDRIDE SYSTEMS FOR BONE AUGMENTATION APPLICATIONS: CHARACTERIZATION OF IN VITRO DEGRADATION

Ashley A. Weiner
Danielle M. Shuck
Jordan R. Bush
V. Prasad Shastri

Department of Biomedical Engineering and Biomaterials, Drug Delivery & Tissue Engineering Laboratory (BDTL)
Vanderbilt University
Nashville, TN

Abstract

In the past decade, injectable biomaterials that are capable of *in situ* formation have garnered increased interest for use in restorative orthopedic procedures. In this study, the *in vitro* degradation of photocrosslinked polyanhydride matrices, derived from methacrylic anhydrides of 1,6-bis(*p*-carboxyphenoxy)hexane (MCPH) and sebacic acid (MSA) were evaluated over a six-week period under physiological conditions. These matrices were augmented with two additives – the reactive diluent polyethylene glycol diacrylate (PEGDA) and the buffering agent calcium carbonate ($CaCO_3$). Disc shaped specimens were produced by crosslinking the components using both chemical and photoinitiators and exposure to visible light. The experimental variables studied included: MCPH:MSA ratio, PEGDA molecular weight and weight fraction, and incorporation of $CaCO_3$. The effects of these variables on local pH, water uptake, mass loss, and mechanical properties were explored. Increasing the MCPH:MSA ratio decreased the mass loss and water uptake at predetermined endpoints, and decreased buffer acidity during degradation. Both PEGDA and $CaCO_3$ were found to decrease acidity and to reduce water uptake during degradation. Incorporation of $CaCO_3$ enabled maintenance of compressive modulus during degradation. These results demonstrate that incorporation of reactive diluents and nonreactive additives into networks of photocrosslinked anhydrides can improve system properties as a material for bone replacement.

Introduction

Polymers have been explored for augmentation and/or regeneration of osseous tissue – including pins and plates in fracture fixation, fillers for long bone defects, and spinal augmentation. An ideal polymeric biomaterial for these applications provides immediate mechanical stability, degrades over time in order to promote new bone growth, and promotes no adverse immune response. To fulfill these three criteria, the following characteristics are desired for bone regenerative biomaterials: capability of *in situ* formation, conformability to the implantation site, controlled degradation and retention of mechanical characteristics. Additionally, the material should be readily modifiable to include osteogenic factors or components which minimize local pH alterations, as local acidity can induce inflammation and impair bone healing (1). This combination of features is ideal for complex fractures, bony defects, or spinal augmentations which require immediate mechanical support yet would benefit from material degradation and eventual replacement by bone.

The well-characterized homo and co-polymers of α-hydroxy acids (PHAs) such as poly(lactic acid) and poly(glycolic acid), which have great utility as surgical sutures, have garnered the most attention amongst biocompatible, degradable polymers. In fracture fixation and bone augmentation applications, solid rods, plates and membranes formed from the PHAs have been used in conjunction with bioactive glass for evaluation of osteoconductivity (2). While the PHAs do initially possess sufficient mechanical strength for load-bearing applications, their bulk degradation mechanism results in a rapid loss of strength without accompanying loss of mass. Additionally resultant from the degradation mechanism, the accumulation of hydrophilic degradation products can

cause local acidity and inflammation. Another limitation of the PHA-based systems is the inability to be processed and formed *in situ*, primarily due to an absence of reactive moieties or photocurable groups. PHAs bearing acrylate end groups have been synthesized and explored for drug delivery and tissue sealant applications (3); however, these polymers lack versatility with respect to degradation behavior.

Spine-related applications would benefit greatly from the development of injectable and *in situ* curable biomaterials. Spinal fusion is a procedure that eliminates or minimizes motion at a site of degeneration in the spinal column. When fusion procedures yield new bone that welds the transverse processes or the vertebral bodies, the stability of the spinal column is enhanced without dramatically altering spine motion as a whole. The osteoinductive material of choice for grafting is autograft harvested from the iliac crest. The use of autograft is dictated by limited availability at the donor site (4) and post-operative morbidity due to long-term discomfort at the donor site (5). Furthermore, in cases of revision procedures and/or when previous iliac crest harvest has been made, the autograft option is an untenable one. These limitations form the basis and serve as the motivating elements in the development of synthetic alternatives. Many materials are currently being studied for use in spinal fusion including calcium sulfate pellets (6), collagen/hydroxyapatite (HA) matrices (7), carriers for BMP-2 (calcium phosphates (8), HA (9-11), and combinations of calcium phosphate and HA (12)), and BMP-7 (OP-1) (13-15). Autograft and the majority of currently studied synthetic alternatives do not provide immediate load-bearing capability to the spine. Mechanical stability does not occur until a bony fusion mass is formed. Based on the surgical consideration and desired clinical outcomes, the ideal material for spinal fusion

applications is a degradable, *in situ* curable biomaterial that provided mechanical support until sufficient new bone growth occurs.

An anhydride based polymer system has been developed which bears reactive methacrylate functionalities that cure rapidly upon exposure to UV or visible radiation to produce high strength networks with variable degradative lifetimes (16). This system meets the criteria for use in bone regeneration applications and provides an alternative synthetic system to overcome the limitations of PHAs, autograft or other materials used in spinal fusion. For example, the system components can be mixed as a paste, which can be conformed to the desired region and crosslinked *in situ* by virtue of methacrylate groups. Furthermore the chemistry of the monomers (differing lipophilicities) offer a means of varying the degradation of the system from a few days to around a year without compromising the photocuring characteristics by simply changing the co-monomer composition in the polymer (16, 17). Another perceived advantage of polyanhydrides (PAs) is a degradation mechanism predominantly via surface erosion (18), a result of the hydrophobicity of the matrix and degradation products. For example, Muggli et al have shown complete degradation of discs of crosslinked MSA (an aliphatic anhydride monomer) in 50 hours, while crosslinked discs of MCPH (an aromatic, hydrophobic anhydride monomer) reached only 30% mass loss after 90 days of degradation (19). Surface-eroding materials also favor the retention of mechanical strength during the course of degradation. The dense network enables achievement of a high strength material immediately following crosslinking. Tensile modulus changes of less than 20% have been seen at up to 50% mass loss in photocrosslinked PA systems (16, 19). The surface erosion mechanism also minimizes acidity around the

degrading biomaterial, which should favor new bone deposition. Finally, in *in* vivo applications, photocrosslinked PAs have shown evidence of soft tissue biocompatibility (20, 21) as well as a dynamic interface (22) for bone growth and remodeling.

An additional benefit of the photocrosslinked PA system is the relative ease with which physical characteristics of the system can be modulated (via incorporation of additives) without chemical alterations to the monomers. Studies to date have primarily focused on the curing and degradation behavior of PA semi-interpenetrating networks (semi-IPN's). In one study, Muggli *et al* evaluated the degradation behavior of semi-IPNs composed of linear anhydride polymers within a crosslinked network of dimethacrylated anhydride monomers (19). This study demonstrated that addition of a linear polymer into the crosslinked network resulted in increased network hydrophobicity and a reduction of shrinkage and heat evolution during polymerization. Burkoth *et al* explored incorporation of lipophilic moieties bearing photoreactive groups such as monomethacrylated cholesterol and stearic acid into networks (23). In this system, both photografting and covalent incorporation of the additives decreased the degradation rate in comparison to unmodified networks.

In this study, we evaluated the *in vitro* degradation behavior of varying formulations of MCPH and MSA in the presence or absence of reactive and nonreactive additive agents, with specific emphasis on maintenance of network integrity, retention of mechanical properties and local pH control. The reactive diluent poly(ethylene glycol) diacrylate (PEGDA) was selected to modulate network crosslinking by virtue of its dual reactive acrylate groups. Fig. 1 shows a photocrosslinking schematic for the anhydride monomers and PEGDA. The inorganic buffering phase calcium carbonate ($CaCO_3$)

was selected as a pH buffer to minimize acidity during degradation. These two constituents were easily incorporated into the system prior to crosslinking. Since one-dimensional degradation best enables characterization of surface erosion, most studies of photopolymerizable anhydrides evaluate crosslinked discs which are typically 12-16 mm in diameter and <2 mm in height. Since this does not approximate the three-dimensional nature of most *in vivo* situations, in this study, samples of dimensions 8 mm diameter, 4 mm height were studied. The overall effect of each additive (PEGDA or $CaCO_3$) was based on criteria for usage of the material in spinal augmentation applications - curing efficiency, degradation rate, water uptake, pH during degradation, and mechanical properties. The objectives of this study therefore was to deduce the effects of these additives on 1) network water uptake and mass loss, 2) acidity during degradation, and 3) maintenance of mechanical strength and integrity during degradation to enable the identification of an optimal system for spinal fusion applications.

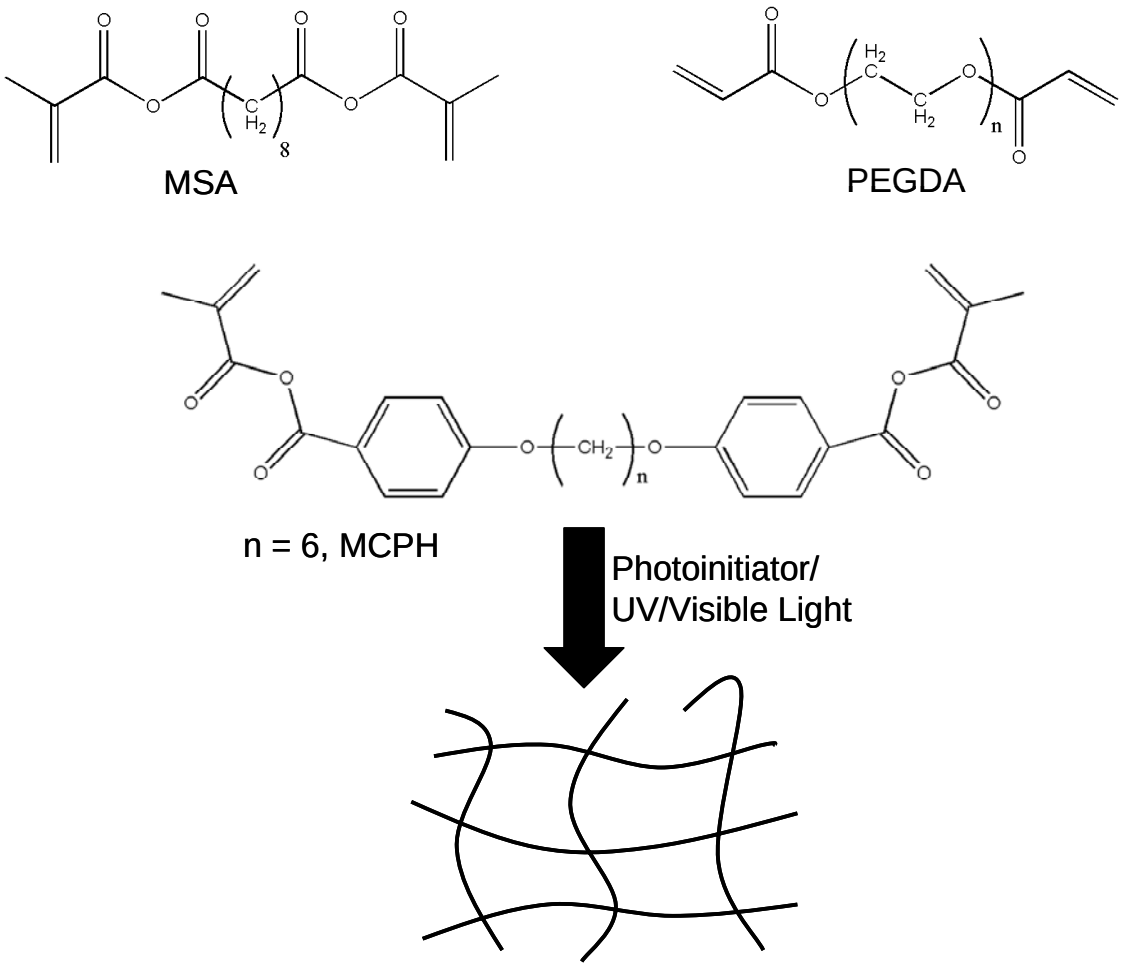

Fig. 1: Photopolymerization scheme for dimethacrylated and diacrylated monomers. MSA - sebacic acid dimethacrylate, MCPH - 1,6-bis(p-carboxyphenoxy)hexane dimethacrylate, PEGDA – poly(ethylene glycol) diacrylate.

Experimental

Materials

Methacrylic acid, sebacoyl chloride, triethylamine, methylene chloride, sodium bicarbonate, sodium sulfate, 4-hydroxybenzoic acid, 1,6-dibromohexane, methacryloyl chloride, poly(ethylene gycol) diacrylate, camphorquinone, ethyl 4-

(dimethylamino)benzoate, benzoyl peroxide, dimethyl toluidine, n-methyl pyrrolidone, sodium chloride, potassium chloride, Tris, sodium phosphate monobasic, magnesium chloride, calcium chloride, calcium carbonate, and hydrochloric acid were obtained from Sigma-Aldrich. Sulfuric acid and acetone were obtained from Fisher Scientific. All chemicals were used as received.

Experimental design

Effect of incorporation of PEGDA

In order to assess the effects of the reactive additive PEGDA in photocurable PAs, 15 sample formulations were evaluated. Two variables were considered: 1) mass fraction of PEGDA in the formulation and 2) ratio of MCPH to MSA. High, intermediate and low levels for each variable were selected, and used in a full factorial experimental design. Three mass fractions of PEGDA were evaluated – 0%, 5%, 10%, 20% and 40 w/w %. Three MCPH:MSA ratios were evaluated – 30:70, 50:50, and 70:30. The values for all parameters and all combinations can be seen in Table 1 (a) and (b).

Table 1: PEGDA MW 700, MSA, and MCPH experimental design

a. Levels of parameters tested in the experimental design

wt % PEGDA		MCPH:MSA ratio	
Low level (0)	0%	Low level (0)	30:70
Low intermediate level (1)	5%	Intermediate level (1)	50:50
Intermediate level (2)	10%	High level (2)	70:30
High intermediate level (3)	20%		
High level (4)	40%		

b. Combinations of the experimental levels and parameters in the full factorial design

Formulation	wt% PEGDA	MCPH:MSA ratio
F00	0%	30:70
F01	0%	50:50
F02	0%	70:30
F10	5%	30:70
F11	5%	50:50
F12	5%	70:30
F20	10%	30:70
F21	10%	50:50
F22	10%	70:30
F30	20%	30:70
F31	20%	50:50
F32	20%	70:30
F40	40%	30:70
F41	40%	50:50
F42	40%	70:30

An additional variable, PEGDA molecular weight, was also assessed. Two PEGDA molecular weights were evaluated - MW 575 and MW 700. The values for all parameters and all combinations for the MW 700 experiments can be seen in Table 1 (a) and (b). The values for all parameters and all combinations for the MW 575 experiments can be seen in Table 2 (a) and (b).

Effect of incorporation of $CaCO_3$

In order to assess the effects of the nonreactive additive $CaCO_3$ in photocurable PAs, four sample formulations were evaluated. Three variables were considered: 1) presence or absence of $CaCO_3$, 2) ratio of MCPH to MSA, and 3) presence or absence of PEGDA. High and low levels were selected for each parameter, and used in a full factorial experimental design. The values for all parameters and all combinations for the $CaCO_3$ experiments can be seen in Table 3 (a) and (b).

Monomer synthesis

Sebacic acid dimethacrylate

Sebacic acid dimethacrylate (MSA) was synthesized from methacrylic acid and sebacoyl chloride as described by Tarcha (24). Methacrylic acid (9 g) and triethylamine (Et_3N) (11.63 g) were dissolved in methylene chloride (150 ml), and the mixture was stirred at 0°C for 30 min. Sebacoyl chloride (12.5 g) was added dropwise to the solution. Stirring was continued for 1 h at a reduced temperature, followed by vacuum filtration for removal of the precipitated triethyl ammonium chloride. The filtrate was diluted with an additional 100 mL of methylene chloride and cooled to 0°C. The solution was washed sequentially with saturated $NaHCO_3$

Table 2: PEGDA MW 575, MSA and MCPH experimental design

a. Levels of parameters tested in the experimental design			
wt% PEGDA		MCPH:MSA ratio	
Low level (0)	0%	Low level (0)	30:70
Intermediate level (1)	20%	Intermediate level (1)	50:50
High level (2)	40%	High level (2)	70:30

b. Combinations of the experimental levels and parameters in the full factorial design		
Formulation	wt% PEGDA	MCPH:MSA ratio
P00	0%	30:70
P01	0%	50:50
P02	0%	70:30
P10	20%	30:70
P11	20%	50:50
P12	20%	70:30
P20	40%	30:70
P21	40%	50:50
P22	40%	70:30

Table 3: $CaCO_3$, MSA, MCPH, and PEGDA experimental design

a. Low, intermediate, and high levels tested in the factorial design			
	wt% $CaCO_3$	MCPH:MSA ratio	wt% PEGDA
Low level	0%	30:70	0%
High level	20%	50:50	20%

b. Combinations of the experimental values in the full factorial design			
Formulation	wt% $CaCO_3$	MCPH:MSA ratio	wt% PEGDA
F00	0%	30:70	0%
F03	0%	30:70	20%
F13	0%	50:50	20%
F10	0%	50:50	0%
C00	20%	30:70	0%
C01	20%	50:50	0%
C30	20%	30:70	20%
C31	20%	50:50	20%

(250mL × 2) and distilled H_2O (250mL × 2) and dried over Na_2SO_4. Methylene chloride was then removed in vacuo at 0°C.

1,6-bis(p-carboxyphenoxy)hexane

1,6-bis(p-carboxyphenoxy)hexane (CPH) was synthesized from 4-hydroxybenzoic acid and 1,6-dibromohexane based on the synthesis of 1,3-bis-(p-carboxyphenoxy)propane described by Conix (25). NaOH (20 g) was dissolved in distilled water (100 ml) in a 500 ml round-bottom flask equipped with a reflux condenser, an addition funnel and a stirbar. To this solution, 4-hydroxybenzoic acid (29 g) was added, and the system was heated until reflux. 1,6-dibromohexane (24.6 g) was added dropwise over 2 hours. The reaction was stirred for several hours under reflux. The product (disodium salt of CPH) was dried by vacuum filtration and washed twice with methanol. The product was dissolved in distilled water, warmed to 60°C and acidified to pH 2 with H_2SO_4. This resulted in the free acid of CPP or CPH as a white frothy precipitate. The product was then isolated by vacuum filtration and washed with distilled H_2O (200 ml × 2) and acetone (200 ml × 2) to remove any trace organics, water, and unreacted 4-hydroxybenzoic acid. The final product was then dried overnight in a 60°C oven.

1,6-bis(p-carboxyphenoxy)hexane dimethacrylate

1,6-bis(p-carboxyphenoxy)hexane dimethacrylate (MCPH) was synthesized from CPH and methacryloyl chloride as described by Tarcha (24). 1,6-bis(p-carboxyphenoxy)hexane (11.3 g) and Et_3N (8.08 g) were dissolved in methylene chloride (120 mL) and stirred at 0 °C for 45 min. Methacryloyl chloride (7.1g) was added dropwise to this solution. Stirring was continued at a reduced temperature for 3.5 h,

followed by vacuum filtration for removal of precipitated triethyl ammonium chloride. The filtrate was washed sequentially with saturated $NaHCO_3$ (200 mL × 2) and distilled H_2O (200 mL × 2). The solution was dried over anhydrous Na_2SO_4, and CH_2Cl_2 was removed in vacuo; a slurry was thereby produced. Then, anhydrous ethyl ether was added and removed in vacuo to facilitate the removal of any remaining methylene chloride.

Sample preparation and photopolymerization

Photopolymerizations were initiated with a dual initiator strategy, composed of camphorquinone (CQ)/ ethyl 4-(dimethylamino)benzoate (4-EDMAB) for light-initiated crosslinking, and benzoyl peroxide (BPO)/dimethyl toluidine (DMT) for chemically-initiated crosslinking. Sample formulations were prepared by thoroughly mixing the monomers in appropriate amounts, followed by adding an appropriate quantity of a BPO/CQ in N-methyl pyrrolidone (NMP) followed by 4-EDMAB/DMT in NMP to yield a final quantity of up to 0.1 wt% for each of CQ, BPO, 4-EDMAB, and DMT in the formulation. Uniform discs (4 mm in height and 8 mm in diameter) were prepared in Teflon molds Samples were polymerized with a blue dental lamp (3M CuringLight XL1500).

Simulated body fluid preparation

Simulated body fluid (SBF), first described by Kokubo (26), was prepared by ion concentrations nearly equivalent to the inorganic components of human plasma – 142 mM Na^+, 5 mM K^+, 1.5 mM Mg^{2+}, 2.5 mM Ca^{2+}, 148.8 mM Cl^-, 4.2 mM HCO_2^-, and 1

mM SO_4^{2-}, buffered with 50 mM Tris. Bayraktar's modifications to Kokubo's SBF were used in this study (27).

In vitro degradation studies

In vitro degradation parameters were assessed in simulated body fluid (SBF), pH 7.4 at 37°C to most thoroughly mimic physiological conditions. Samples were maintained at 60 rpm on an orbital shaker throughout degradation studies. The discs were degraded in seven ml of SBF. Buffer was replaced daily for the first two weeks, every other day for the next two weeks, and once every three days for the last two weeks of the study to maintain sink conditions. Buffer pH was measured and recorded at each timepoint prior to buffer exchanges. At pre-selected time points (2 and 6 weeks), four samples of each formulation were removed for assessment.

Gravimetric analysis

The dry mass of the samples (m_0) was measured prior to commencement of degradation studies in SBF. At pre-determined time points, samples were removed, rinsed with PBS and the excess liquid dabbed using a Kimwipe® before recording their wet mass (m_w). Samples were then flash frozen in liquid nitrogen and freeze-dried overnight. Next, they were vacuum-dried for an additional 48 hours and weighed to obtain the dry mass after degradation (m_d). The mass loss (ML, Eq. 1) and water uptake (WU, Eq. 2) of the samples were then determined by the following equations:

$$ML = \frac{m_0 - m_d}{m_0} \quad (1)$$

$$WU = \frac{m_w - m_d}{m_d} \quad (2)$$

Minimums of four (n =4) samples were measured for each composition and time point.

Mechanical testing

Compressive mechanical testing was conducted using an AGS-J mechanical tester (Shimadzu, Kyoto, Japan) with a 1 kN load cell on dried samples (n = 4). The cylinders were compressed between two plates moving at a crosshead speed of 1 mm/min until failure, while load and displacement was recorded throughout. Based on sample geometry, the stress versus strain behavior was obtained and plotted. The compressive modulus was determined from the stress-strain curve using Trapezium software (Shimadzu) and Microsoft Excel.

Scanning electron microscopy

Dried PA samples before and after degradation were cryo-fractured by cooling in liquid nitrogen and the cross-section was analyzed using scanning electron microscopy (SEM). The pellets were sputter-coated with gold-palladium to minimize charging and then mounted onto aluminum stubs using conductive tape for imaging. SEM images were obtained using a Hitachi S-4200 SEM at an acceleration voltage of 5 keV.

Statistical analysis

Results are reported as mean ± standard deviation. Data analysis was performed using SigmaStat version 3.1 and SigmaPlot version 9.0 (Systat Software, Inc. Point Richmond, CA, USA). To determine differences between time points for each

formulation, a one-way analysis of variance (ANOVA) or a non-parametric ANOVA (Kruskal-Wallis Test) was first performed to determine statistical significance ($p < 0.05$) within each data set. When the analysis of variance detected significance, a Tukey Multiple Comparison Test (one-way ANOVA) or a Dunn's Multiple Comparison Test (Kruskal-Wallis Test) was run with a confidence level of 95%. To determine differences between different formulations at the two timepoints, a t-test or a Mann-Whitney Rank Sum Test was performed to determine statistical significance ($p<0.05$). In addition to statistical analysis by ANOVA, the main effects of experimental parameters (MCPH:MSA ratio, PEGDA amount, $CaCO_3$ amount) on mass loss and water uptake were calculated at each timepoint as enabled by the factorial experimental design (28).

Results

Nomenclature

Polymer formulations are described in the following manner. For the samples containing PEGDA MW700, the formulations are defined as F(*x*)(*y*) where *x* refers to the wt% of PEGDA with 0=0%, 1=5%, 2=10%, 3=20%, and 4=40% and *y* refers to the MCPH:MSA ratio where 0=30:70, 2=50:50, and 3=70:30. For the samples containing PEGDA MW575, the formulations are defined as P(*x*)(*y*) where *x* refers to the wt% of PEGDA with 0=0%, 1=20%, and 2=40%, and *y* refers to the MCPH:MSA ratio where 0=30:70, 2=50:50, and 3=70:30. Finally, samples containing $CaCO_3$ were described by the notation C(*x*)(*y*) where the C denotes the presence of $CaCO_3$ at 20 wt%, *x* represents the wt% of PEGDA, with 0=0% and 3=20% (to correspond with the

respective F formulations) and *y* represents the MCPH:MSA ratio with 0=30:70 and 1=50:50.

General observations

In order to maximize the impact of the experimental variables, a more efficient dual initiator curing system was explored. Instead of only a conventional photoinitiator/accelerator system commonly used in photocrosslinking applications, this system was augmented with a chemical curing agent and accelerator (benzoyl peroxide/dimethyl toluidine). By combining these two systems, the initiator concentration required for induction of polymerization was 10-fold lower. The low initiator concentrations allowed longer working times of the paste than were previously enabled. However, more importantly, the addition of chemical curing resulted in rapid photocrosslinking (~ 60-90 seconds) with excellent depth of cure (up to 10 mm).

Some formulations did not maintain network integrity during the course of the *in vitro* degradation. These formulations included the 40% PEGDA MW 700 formulations (F40, F41, F42), the 40% PEGDA MW 575 formulations (P20, P21, P22), and most of the 20% PEGDA MW 575 formulations (P10, P11). These results suggest an upper limit for PEGDA wt% within the matrices.

pH profiles

To evaluate the acidity as a result of the polymer degradation products, pH of the degradation buffer was measured prior to each buffer exchange. The degradation buffer was exchanged daily for the first week of degradation, every other day for the

next two weeks, and every third day for the final two weeks. The pH profiles for each formulation showed the same general shape. During days one and two there was a dramatic drop in degradation buffer pH. From days three to 14, the pH level slowly increased to a level near 7.4 (the initial degradation buffer pH). At day 14, when degradation buffer exchanges were changed from daily to every other day, there is an initial drop in pH. This drop gradually recovered over the next few days. By day 40, the pH for all samples was approaching 7.4.

Selected pH profiles are shown in Fig. 2 to demonstrate trends based on formulation. As expected based on degradation rates reported in other studies (16), an increase in MCPH:MSA ratio resulted in decreased acidity during the course of degradation. This trend was seen in both unmodified formulations (without PEGDA), shown in Fig. 1A, and in formulations containing PEGDA. Additionally, as shown in Fig. 2B, the inclusion of PEGDA in the crosslinked network resulted in a net decrease in acidity in a dose dependant manner. While the intermediate levels of PEGDA (5 and 10 wt%), were not dramatically different in pH response, the high level of PEGDA (20%) caused less buffer acidity during degradation and the formulations without PEGDA resulted in increased buffer acidity during degradation. During the first 30 days of degradation, the degradation buffer of formulations containing PEDGA MW 575 was less acidic than formulations containing PEGDA MW 700. However, after 30 days there was negligible difference in the pH response of the formulations. Both formulations were less acidic than unmodified formulations. The pH profiles for these formulations are shown in Fig. 2C.

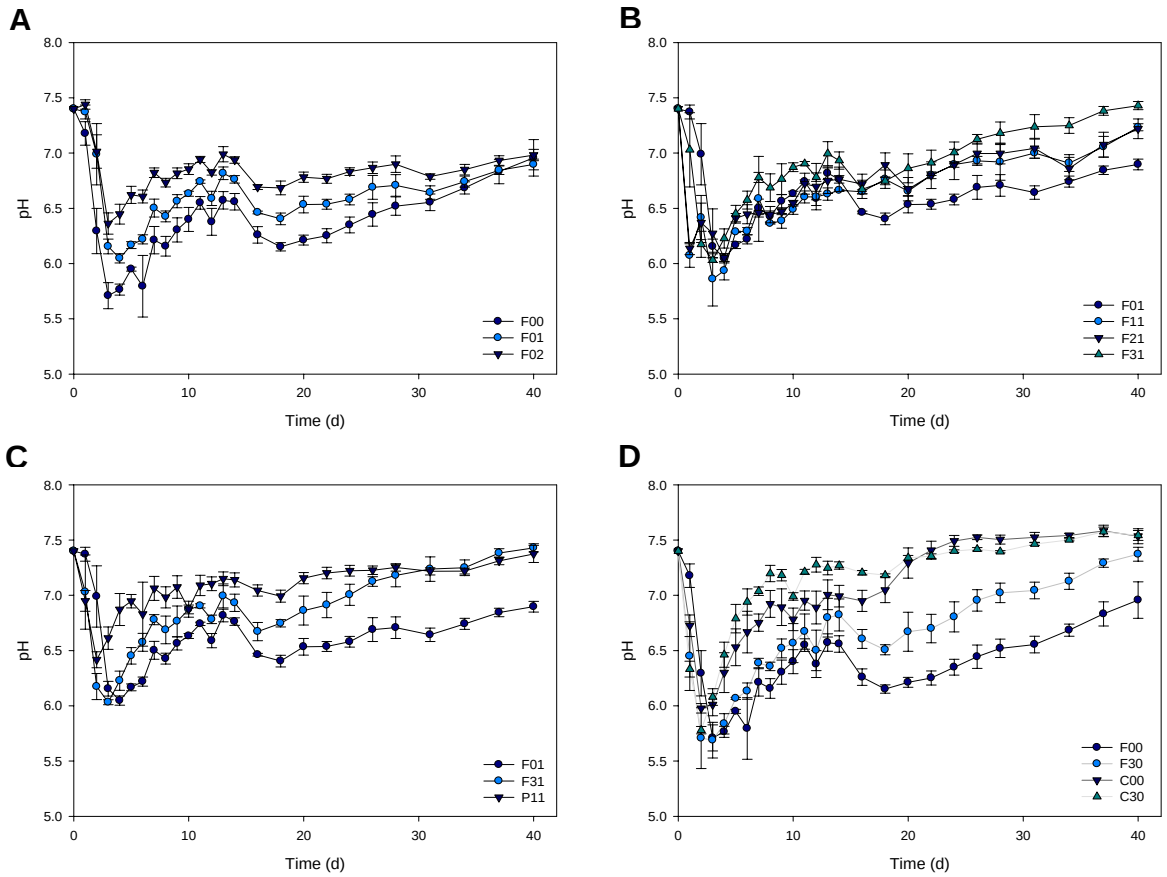

Fig. 2: pH profiles of selected formulations. A. Samples with higher MCPH:MSA ratios (ie F02) undergo less acidity during degradation than samples with intermediate MCPH:MSA ratios (F01) or low MCPH:MSA ratios (F00). This trend is evident in unmodified network and in networks containing PEGDA). B. By increasing the percentage of PEDGA in a formulation, acidity is decreased. C. Regardless of PEDGA MW, PEGDA incorporation decreases acidity during degradation in comparison to formulations that do not contain PEGDA (F01). Until day 30, formulations containing PEGDA MW 700 (F31) have less acidity than formulations containing PEGDA MW 575 (P11). However after day 30, the acidity levels are comparable. D. Samples containing CaCO3 (C00) or CaCO3 + PEGDA MW 700 (C30) demonstrate the least acidity during degradation, in comparison with formulations with PEGDA MW 700 (F30) or formulations containing anhydride monomers alone (F00). Data is represented as means ± standard deviations for n = 3-4.

The addition of $CaCO_3$ to sample formulations provided the most dramatic decrease in degradation buffer acidity during sample degradation, shown in Fig. 2D. Formulations with $CaCO_3$ or $CaCO_3$ + PEGDA exhibited the least acidity of any formulation; however, these formulations were not different from each other. In comparison, the unmodified samples exhibited the most acidic degradation buffer, while the samples containing PEGDA alone had intermediate buffer pH levels.

Gravimetric analysis

Mass loss

Percent mass loss was determined after two and six weeks of *in vitro* degradation to assess the extent of erosion that occurred in photocrosslinked PA networks (Fig. 3). In general, a statistically significant difference in mass loss between weeks two and six was seen only in the samples containing 0% PEGDA (F00, F01, F02) and two samples containing 5% PEGDA (F11 and F12). Likewise, samples containing 10% or 20% PEGDA did not exhibit statistically significant changes in mass loss between two and six weeks. In general, samples containing PEGDA underwent less change in mass than samples without PEGDA. In addition, samples with a higher MCPH:MSA ratio exhibited less mass loss than samples with a lower MCPH:MSA ratio. The main effects of each parameter ($CaCO_3$, MCPH:MSA ratio, PEGDA) on mass loss are summarized in Fig. 4. When $CaCO_3$ is increased from a low level (0%) to a high level (25%) mass loss was increased. This effect was more pronounced after two weeks of degradation than after six weeks. Increasing the MCPH:MSA ratio from a low

level (30:70) to a high level (50:50), resulted in a decrease in mass loss. Altering PEGDA content from a low level (0%) to a high level (20%) also decreased mass loss.

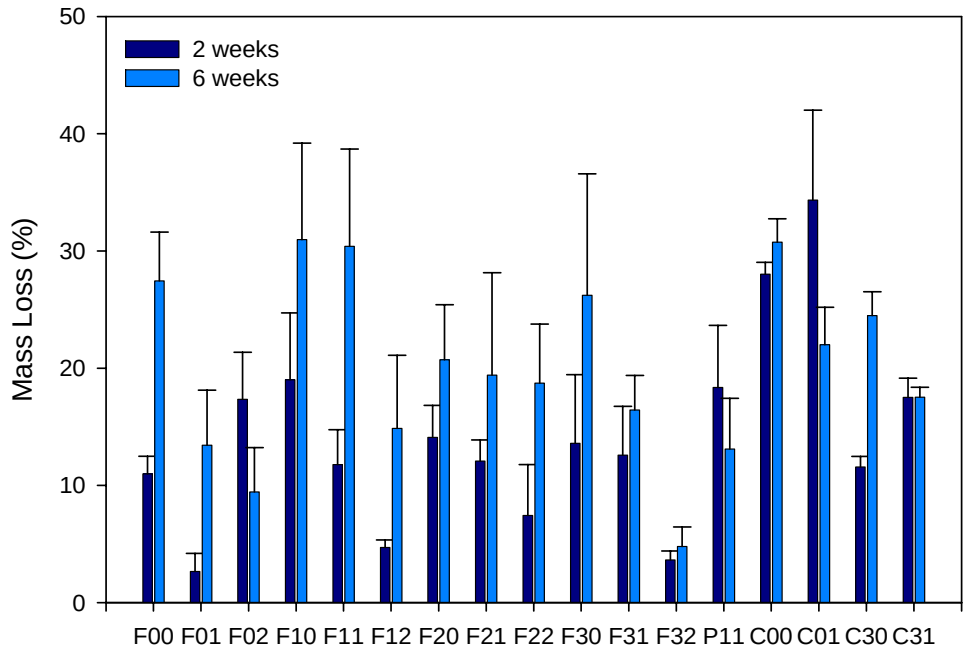

Fig. 3: Percent change in polymer mass during *in vitro* degradation for unmodified photocrosslinked anhydride networks (F00, F01, F02), photocrosslinked anhydride networks contained PEGDA MW700 (F10 – F32) or MW575 (P11), photocrosslinked anhydride networks containing $CaCO_3$ (C00, C01) or photocrosslinked anhydride networks containing $CaCO_3$ and PEGDA MW700 (C30 and C31). Results are presented as means ± standard deviation for n = 3-4.

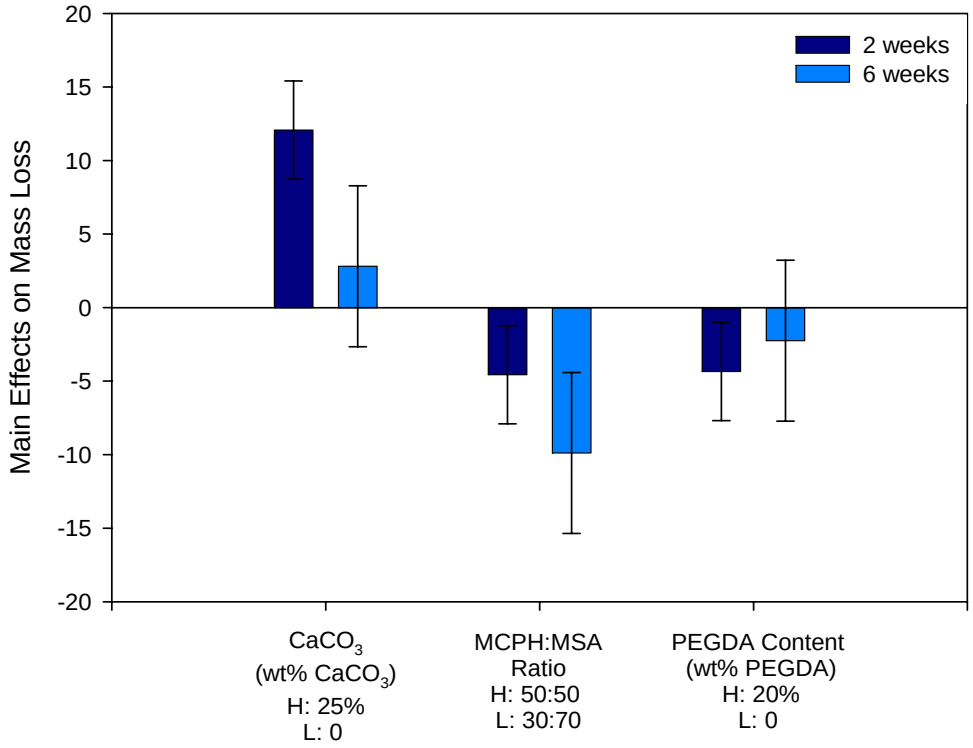

Fig. 4: Main effects of $CaCO_3$ incorporation, PEGDA incorporation, and MCPH:MSA ratio percent on mass loss of photocrosslinked anhydride networks for 2 and 6 weeks. A positive number indicates that the particular parameter had an increasing effect on the mass loss as the value was changed from a low (L) level to a high (H) level. A negative number indicates a decrease in the normalized cumulative mass loss as the parameter was changed from the low (L) level to a high (H) level. Formulations described in Table 1 were used for this analysis. Error bars represent the standard deviations of the effect.

Water uptake

Percent water uptake was determined after two and six weeks of *in vitro* degradation (Fig. 5). All samples exhibited a greater percent water uptake at 6 weeks than at 2 weeks ($p<0.02$ for all formulations). After two weeks of degradation, within a given MCPH:MSA ratio, samples containing any weight percent of PEGDA exhibited significantly less water uptake than the samples without PEGDA ($p<0.001$). After six

weeks of degradation, there was a statistically significant difference in water uptake between all formulations except between F10 and F20, and F20 and F30. Increasing the PEGDA content of the photocrosslinked networks decreased the water uptake during *in vitro* degradation. Dose-dependency of this effect was not seen after two weeks of degradation, but was evident after 6 weeks of degradation. A trend was also seen to correlate MCPH:MSA ratio with water uptake. In general, an increase in MCPH:MSA ratio (within a given PEGDA weight percent) resulted in a decrease in water uptake during degradation.

The main effects of each parameter ($CaCO_3$, MCPH:MSA ratio, PEGDA content) on water uptake are summarized in Fig. 6. Changing $CaCO_3$ content from a low level (0%) to a high level (25%) resulted in increased water uptake after two weeks of degradation. Alternatively, the same increase in $CaCO_3$ content resulted in decreased water uptake after six weeks of degradation. Increasing the MCPH:MSA ratio from a low level (30:70) to a high level (50:50), resulted in a decrease in water uptake. Altering PEGDA content from a low level (0%) to a high level (20%) also decreased water uptake.

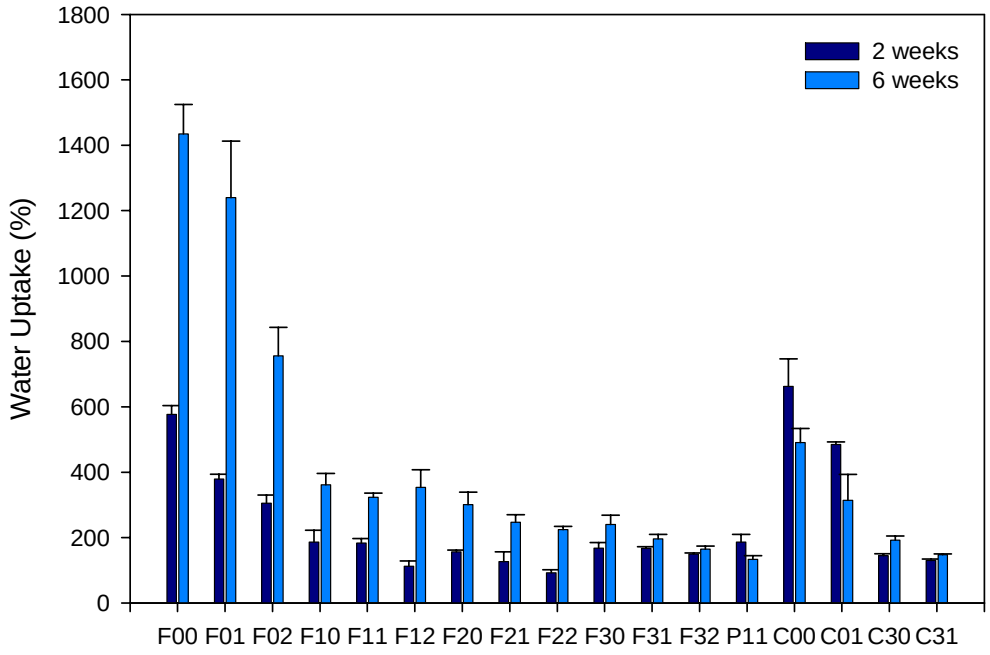

Fig. 5: Percent water uptake during *in vitro* degradation for unmodified photocrosslinked anhydride networks (F00, F01, F02), photocrosslinked anhydride networks containing PEGDA MW700 (F10 – F32) or MW575 (P11), photocrosslinked anhydride networks containing $CaCO_3$ (C00, C01) or photocrosslinked anhydride networks containing $CaCO_3$ and PEGDA MW700 (C30, C31). Results are presented as means ± standard deviation for n = 3-4.

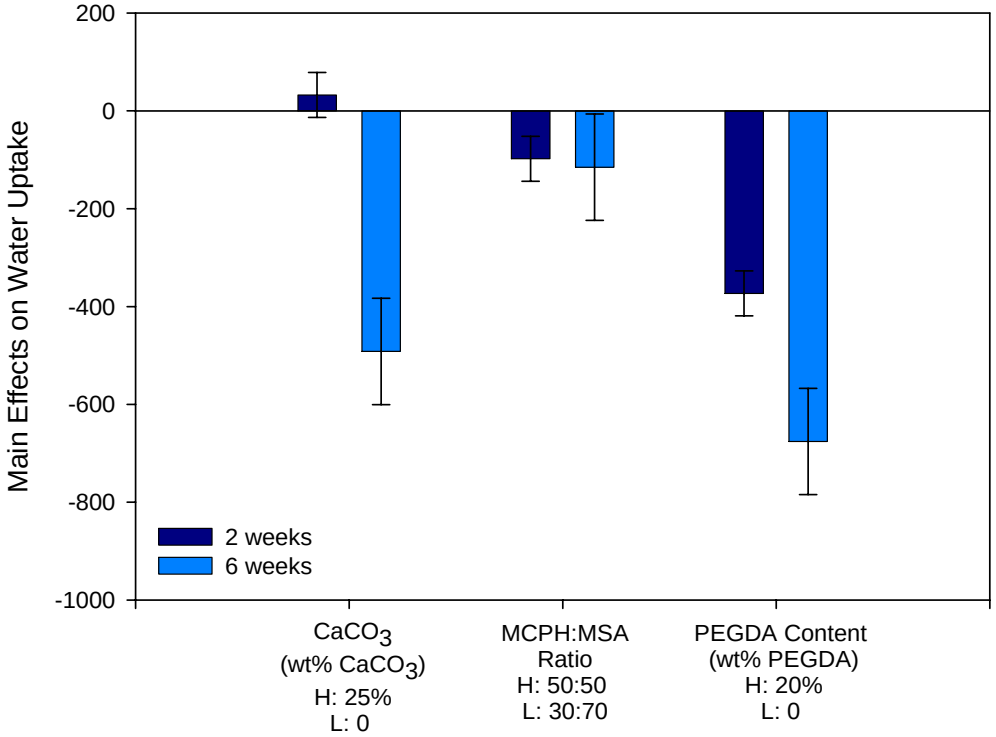

Fig. 6: Main effects of $CaCO_3$ incorporation, PEGDA incorporation, and MCPH:MSA ratio on percent water uptake of photocrosslinked anhydride networks for 2 and 6 weeks. A positive number indicates that the particular parameter had an increasing effect on the water uptake as the value was changed from a low (L) level to a high (H) level. A negative number indicates a decrease in the normalized cumulative water uptake as the parameter was changed from the low (L) level to a high (H) level. Formulations described in Table 3 were used in this analysis. Error bars represent the standard deviations of the effect.

Scanning electron microscopy

Formulations that did not contain $CaCO_3$ showed no microporosity at the degrading zone. In contrast, as seen in Fig. 7, microporosity is evident in samples containing 20 wt% $CaCO_3$ in the region of the degradation front. The degradation front for samples with $CaCO_3$ was significantly thicker than the relatively thin front of degradation for samples without $CaCO_3$ (data not shown).

Mechanical testing

Compressive mechanical testing was performed on freeze-dried samples that were not subjected to degradation and those that had been subjected to either two or six weeks of *in vitro* degradation. As seen in Fig. 8, inclusion of $CaCO_3$ enabled maintenance of compressive modulus during *in vitro* degradation in comparison to samples which did not contain $CaCO_3$. Although samples with or without $CaCO_3$ had a similar compressive modulus prior to degradation, after two weeks of degradation, samples containing $CaCO_3$ had a significantly greater compressive modulus (104±12 MPa) than samples without $CaCO_3$ (68±14 MPa) ($p=0.015$). Interestingly, after six weeks of degradation samples containing $CaCO_3$ had a compressive modulus of 127±9 MPa, which is greater than the compressive modulus prior to degradation or after only two weeks of degradation. After six weeks of degradation, samples without $CaCO_3$ underwent further loss of compressive modulus to 21±3 MPa ($p<0.01$).

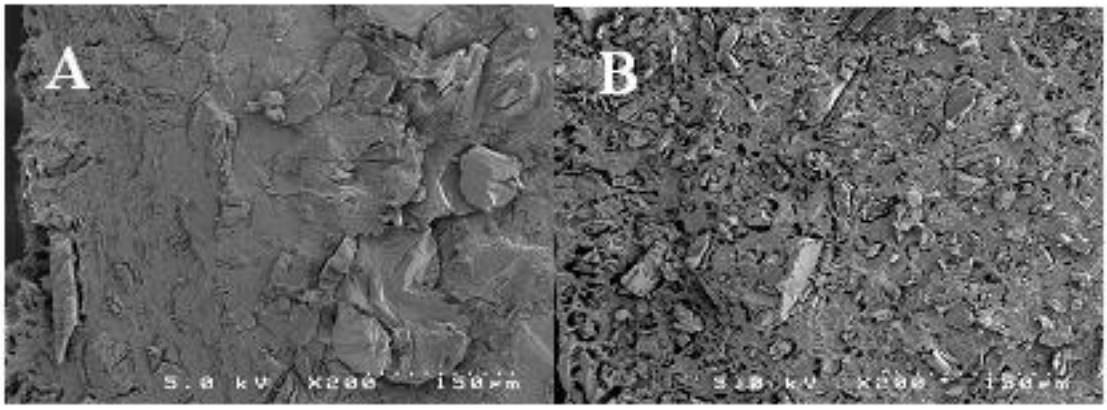

Fig. 7: SEM images of the front of degradation for a photocrosslinked polyanhydride network (A) and for a photocrosslinked poly(anhydride) network containing 20 wt% $CaCO_3$ (B).

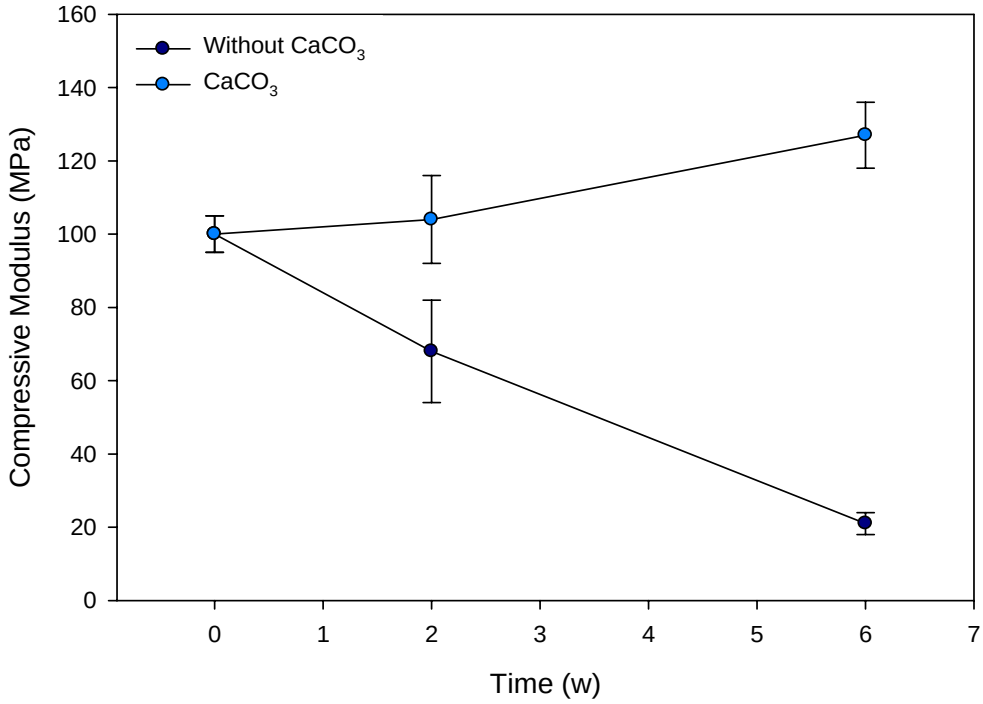

Fig. 8: $CaCO_3$ incorporation into photocrosslinked anhydride matrices – effect on compressive modulus. Results are presented as means ± standard deviation for n = 3-4.

Discussion

Many orthopedic applications can benefit from the development of a high-strength, degradable, *in situ* curable polymeric system. Criteria for success as a bone regenerative material include: capability of *in situ* formation, conformability to the implantation site, controlled degradation (water uptake and mass loss) and retention of mechanical characteristics. Additionally, the degradation of the material should minimally affect local pH. In recent years a family of photopolymerizable anhydride network systems based on difunctional methacrylated monomers derived from sebacic anhydride, 1,3-bis(*p*-carboxyphenoxy)propane, and 1,6-bis(*p*-carboxyphenoxy)hexane have been developed (16) and explored for tissue contacting and drug delivery

applications. These difunctional moieties can be crosslinked upon exposure to UV or visible light in the presence of a photoinitiator. The photocurable nature of the system fulfills two desirable characteristics for a bone regenerative material – namely *in situ* formation and conformability to an implantation site or three dimensional mold (16).

The incorporation of PEGDA was expected to promote the crosslinking efficiency of the system at the expense of increased network hydrophilicity and water uptake. Surprisingly, PEGDA incorporation into the photocrosslinked PA system resulted in a dramatic decrease in water uptake during degradation. This phenomenon occurred in a somewhat dose-dependent fashion; with even 5 wt% PEGDA incorporation resulting in a 10-fold decrease in water uptake after six weeks of degradation (see Fig. 5). Increases in PEGDA concentrations to 10 or 20 wt% further decreased water uptake at a modest level. The reduction of water uptake was seen in all formulations regardless of MCPH:MSA ratio or the inclusion of $CaCO_3$. This observation was contrary to the initial premise that inclusion of PEGDA would result in increased water uptake by nature of the molecule's hydrophilicity. Excessive system water uptake or swelling is undesirable, as it would preclude adequate filling of a void *in vivo* and would adversely affect the rate of degradation. The most likely cause of the decrease in water uptake for the PEGDA-containing formulations is the presence of a denser network with increased crosslinking that minimizes water uptake. Additionally, the introduction of PEGDA likely reduces the concentration of unreacted monomer that can lead to autocatalytic events promoted by the hydrolysis of the monomers. PEGDA may be a useful additive for modulating water uptake behavior in *in vivo* applications for photocrosslinked PA networks.

Interestingly, $CaCO_3$ inclusion also affected the water uptake behavior of degrading matrices (see Fig. 5). Samples containing both PEGDA and $CaCO_3$ displayed similar water uptake behavior as comparable formulations (same MCPH:MSA ratio) containing only PEGDA. However, in anhydride matrices augmented with only $CaCO_3$ significantly different water uptake behavior was observed. After two weeks of degradation, the presence of $CaCO_3$ resulted in slightly increased water uptake, presumably a direct result of microporosity induced by the presence of the additive. The microporosity induced in the region of the degradation front facilitated water influx. Alternatively, after six weeks of degradation, the water uptake of samples containing $CaCO_3$ was significantly decreased in comparison with corresponding formulations without $CaCO_3$. This phenomenon suggests some ionic interaction between the crosslinked network and the $CaCO_3$ that effectively tightens the network. This mechanism may be similar to the effects seen during ionotropic gelation of alginate by divalent cations (29). Crosslinking of alginate with calcium chloride serves to stiffen the polymer and to reduce solvent swelling (30); a similar effect as is seen in PA networks modulated with $CaCO_3$. Modulation of photocrosslinked PAs with $CaCO_3$ may be useful for eliminating longterm water uptake in *in vivo* applications.

One additional property of importance in the development of a material for use in spinal applications is mechanical strength. The compressive modulus was similar for all formulations prior to degradation. However, after degradation, the compressive modulus for formulations without $CaCO_3$ (regardless of PEGDA content) significantly decreased (see Fig. 8). A 25% loss of modulus was seen after two weeks of degradation, and a 60% loss of modulus was seen after six weeks of degradation. In

contrast, formulations containing $CaCO_3$ (regardless of PEGDA content) displayed maintenance of modulus throughout the six week degradation period. The mechanism for the maintenance of mechanical strength is most likely the ionotropic effect proposed as the mechanism for decreasing water uptake in the longterm. Interactions between the anhydride network and Ca^{2+} strengthen the system, which will prove critical for load bearing applications in the spine.

Another important and surprising outcome of the incorporation of PEGDA was the reduction in buffer acidity during sample degradation. During the final four weeks of degradation, PEGDA incorporation significantly reduced acidity in the sample degradation buffer, with pH differences between samples containing PEGDA and samples without PEGDA of ~0.5 pH units (see Fig. 2B). This elevation in pH was greater than would occur purely by a reduction in concentration of anhydride bonds. Additionally, PEGDA of a lower molecular weight favored less changes in pH during the first 30 days of degradation (see Fig. 2C), an observation that is consistent with a denser network (decreased elasticity). A portion of this effect is dictated by the amount of PEGDA measured as a weight percent instead of a mole percent – with this measurement, there are more molecules of PEGDA MW 575 in the system with an equal weight percent. Again, with pH differences near 0.5 pH units, it seems unlikely that the molar difference can account completely for the reduction in acidity. Although PEGDA has been incorporated into a variety of degradable polymers, similar pH effects have not been reported.

Although the incorporation of $CaCO_3$ into the PA matrices did not significantly impact the initial drop in pH observed in all samples, the pH of the degradation buffer of

samples containing $CaCO_3$ was restored to physiological pH by day 20. Such a normalization of pH was not observed in samples without $CaCO_3$. Interestingly, formulations containing both $CaCO_3$ and PEGDA had similar pH profiles to formulations containing $CaCO_3$ alone, an effect greater than that of PEGDA alone. Furthermore, while introduction of PEGDA yielded small changes in pH (reduced acidity) in comparison to samples containing $CaCO_3$, the incorporation of both yielded similar pH profiles as $CaCO_3$ alone. More importantly, the beneficial effect of $CaCO_3$ was more pronounced after two weeks. This suggests that the events that contributed to acidity in the first two weeks are not easily mitigated by simple formulation changes and are induced by initial network hydrolysis. The buffering capability of $CaCO_3$ has been studied in conjunction with degradable polymers including PLGA(50:50) (31) and poly(ortho esters) (32). Additionally, carbonated calcium phosphates as well as $CaCO_3$ are capable of buffering pH of lactic acid in the physiological range (33). Inclusion of $CaCO_3$ into photocrosslinked PA networks enabled pH buffering in the physiological range, a property of importance in bone regeneration applications.

The effect of MCPH:MSA ratio on mass loss, water uptake, and pH was consistent with results from previous studies (16, 19). In the photocrosslinked PA system, mass loss and water uptake are functions of network hydrophobicity. In general, MCPH:MSA ratio affects the system degradation in a predictable manner. Increases in MCPH:MSA ratio decrease the mass loss (see Fig. 3) and decrease system water uptake (see Fig. 5). Increasing the MCPH:MSA ratio also decreases the acidity that occurs during degradation (see Fig. 2A). This may be attributed to an overall increase in hydrophobicity of the system, which would be expected based on

chemical structure considerations of MCPH and MSA. MCPH, with its two aromatic groups and long hydrocarbon chain as a backbone, is a much more hydrophobic moiety than MSA, with only a shorter aliphatic hydrocarbon backbone. A more hydrophobic system is expected to less readily uptake water, favoring a slower degradation rate. The lower aqueous solubility of MCPH in comparison with MSA is also expected to favor reduced acidity.

The inclusion of the additives PEGDA and $CaCO_3$ also affected mass loss in the system. When PEGDA was included in the system, generally a decrease in mass loss was observed, which can be attributed to the increased crosslinking density and decreased penetration of water in the system. In addition, some loss of control of the degradation rate dictated by MCPH:MSA ratio occured. The inclusion of $CaCO_3$ in the system increased the system mass loss, a result of microporosity introduced by leaching of the additive. This effect was more pronounced after two weeks of degradation than after six weeks of degradation. We theorize that the effect on mass loss is less prominent in the long term due to the ionotropic interactions between the calcium ion and the crosslinked network.

Conclusions

In conclusion, the photocrosslinked PA system described here clearly possesses necessary characteristics for usage in bone replacement applications. These characteristics are enhanced by the inclusion of PEGDA and $CaCO_3$ as additives. The incorporation of additives does not alter the curing ability or formability of the system. Incorporation of PEGDA and $CaCO_3$ serve both to decrease water uptake and to

modulate local acidity during degradation. Surprisingly, inclusion of $CaCO_3$ enables maintenance of compressive modulus throughout the degradative lifetime of the material. In this study, we have revealed additional mechanisms for tuning material properties via incorporation of additive agents to expand the scope and functionality of the system. Finally, this study demonstrates that additives can be easily and successfully incorporated into photocrosslinked PA networks to address a variety of physical characteristics. In the future, these strategies can be applied to impart osteoinductivity to the network by incorporation of growth factors.

Selection of a polymer formulation for future work is based on several parameters determined in this study. First, we have determined that roughly 20% mass loss after six weeks of degradation is an optimal design criterion for use in drug delivery and *in vivo* bone augmentation applications. This amount of mass loss will provide mechanical stability which lasts until a bony fusion mass can be formed, while still allowing substantial release of any osteoinductive factors which will be incorporated in the matrix. The samples containing 10% PEGDA (F20, F21, F22) and the samples containing $CaCO_3$ and 20% PEGDA (C30, C31) best meet this criteria. Additionally, based on the results of this study, PEGDA and $CaCO_3$ are additives that improve the material properties. Therefore PEGDA (at 10-20 wt%) and $CaCO_3$ (at a maximum of 20 wt%) will be components of the design criteria for future work in drug delivery and bone augmentation.

Acknowledgements

The authors are grateful for financial support from the Vanderbilt Institute for Integrative Biology and Education (VIIBRE) and a Vanderbilt University Discovery Grant. They would also like to acknowledge support for AAW from the National Science Foundation Graduate Research Program.

References

1. Bergsma, E. J., Rozema, F. R., Bos, R. R., and de Bruijn, W. C. (1993) Foreign body reactions to resorbable poly(L-lactide) bone plates and screws used for the fixation of unstable zygomatic fractures. *J Oral Maxillofac Surg* 51, 666-670.

2. Kellomaki, M., Niiranen, H., Puumanen, K., Ashammakhi, N., Waris, T., and Tormala, P. (2000) Bioabsorbable scaffolds for guided bone regeneration and generation. *Biomaterials* 21, 2495-2505.

3. Sawhney, A. S., Pathak, C. P., van Rensburg, J. J., Dunn, R. C., and Hubbell, J. A. (1994) Optimization of photopolymerized bioerodible hydrogel properties for adhesion prevention. *J Biomed Mater Res* 28, 831-838.

4. Silber, J. S., Anderson, D. G., Daffner, S. D., Brislin, B. T., Leland, J. M., Hilibrand, A. S., Vaccaro, A. R., and Albert, T. J. (2003) Donor site morbidity after anterior iliac crest bone harvest for single-level anterior cervical discectomy and fusion. *Spine* 28, 134-139.

5. Sasso, R. C., LeHuec, J. C., and Shaffrey, C. (2005) Iliac crest bone graft donor site pain after anterior lumbar interbody fusion: a prospective patient satisfaction outcome assessment. *J Spinal Disord Tech* 18 Suppl, S77-81.

6. Chen, W. J., Tsai, T. T., Chen, L. H., Niu, C. C., Lai, P. L., Fu, T. S., and McCarthy, K. (2005) The fusion rate of calcium sulfate with local autograft bone compared with autologous iliac bone graft for instrumented short-segment spinal fusion. *Spine* 30, 2293-2297.

7. Neen, D., Noyes, D., Shaw, M., Gwilym, S., Fairlie, N., and Birch, N. (2006) Healos and bone marrow aspirate used for lumbar spine fusion: a case controlled study comparing healos with autograft. *Spine* 31, E636-640.

8. Namikawa, T., Terai, H., Suzuki, E., Hoshino, M., Toyoda, H., Nakamura, H., Miyamoto, S., Takahashi, N., Ninomiya, T., and Takaoka, K. (2005) Experimental spinal

fusion with recombinant human bone morphogenetic protein-2 delivered by a synthetic polymer and beta-tricalcium phosphate in a rabbit model. *Spine* 30, 1717-1722.

9. Minamide, A., Kawakami, M., Hashizume, H., Sakata, R., Yoshida, M., and Tamaki, T. (2004) Experimental study of carriers of bone morphogenetic protein used for spinal fusion. *J Orthop Sci* 9, 142-151.

10. Minamide, A., Kawakami, M., Hashizume, H., Sakata, R., and Tamaki, T. (2001) Evaluation of carriers of bone morphogenetic protein for spinal fusion. *Spine* 26, 933-939.

11. Konishi, S., Nakamura, H., Seki, M., Nagayama, R., and Yamano, Y. (2002) Hydroxyapatite granule graft combined with recombinant human bone morphogenic protein-2 for solid lumbar fusion. *J Spinal Disord Tech* 15, 237-244.

12. Akamaru, T., Suh, D., Boden, S. D., Kim, H. S., Minamide, A., and Louis-Ugbo, J. (2003) Simple carrier matrix modifications can enhance delivery of recombinant human bone morphogenetic protein-2 for posterolateral spine fusion. *Spine* 28, 429-434.

13. Kanayama, M., Hashimoto, T., Shigenobu, K., Yamane, S., Bauer, T. W., and Togawa, D. (2006) A prospective randomized study of posterolateral lumbar fusion using osteogenic protein-1 (OP-1) versus local autograft with ceramic bone substitute: emphasis of surgical exploration and histologic assessment. *Spine* 31, 1067-1074.

14. Vaccaro, A. R., Anderson, D. G., Patel, T., Fischgrund, J., Truumees, E., Herkowitz, H. N., Phillips, F., Hilibrand, A., Albert, T. J., Wetzel, T., and McCulloch, J. A. (2005) Comparison of OP-1 Putty (rhBMP-7) to iliac crest autograft for posterolateral lumbar arthrodesis: a minimum 2-year follow-up pilot study. *Spine* 30, 2709-2716.

15. Vaccaro, A. R., Patel, T., Fischgrund, J., Anderson, D. G., Truumees, E., Herkowitz, H., Phillips, F., Hilibrand, A., and Albert, T. J. (2005) A 2-year follow-up pilot study evaluating the safety and efficacy of op-1 putty (rhbmp-7) as an adjunct to iliac crest autograft in posterolateral lumbar fusions. *Eur Spine J* 14, 623-629.

16. Anseth, K. S., Shastri, V. R., and Langer, R. (1999) Photopolymerizable degradable polyanhydrides with osteocompatibility. *Nat Biotechnol* 17, 156-159.

17. Domb, A., Shastri, V. & Langer, R. (1997) Polyanhydrides. In *Handbook of Biodegradable Polymers* (Domb, A., Kost, J. & Wiseman, D., ed) pp. 135-159, Harwood Academic Publishers

18. Tamada, J. A., and Langer, R. (1993) Erosion kinetics of hydrolytically degradable polymers. *Proc Natl Acad Sci U S A* 90, 552-556.

19. Muggli, D. S., Burkoth, A. K., and Anseth, K. S. (1999) Crosslinked polyanhydrides for use in orthopedic applications: degradation behavior and mechanics. *J Biomed Mater Res* 46, 271-278.

20. Shastri, V. P., Marini, R. P., Padera, R. F., Kirchain, S., Tarcha, P., and Langer, R. (1999) Osteocompatibility of photopolymerizable anhydride networks. *Mat. Res. Soc. Symp. Proc* 530, 93-98.

21. Shastri, V. P., Padera, R. F., Tarcha, P., and Langer, R. (2004) A preliminary report on the biocompatibility of photopolymerizable semi-interpenetrating anhydride networks. *Biomaterials* 25, 715-721.

22. Ibim, S. E., Uhrich, K. E., Attawia, M., Shastri, V. R., El-Amin, S. F., Bronson, R., Langer, R., and Laurencin, C. T. (1998) Preliminary in vivo report on the osteocompatibility of poly(anhydride-co-imides) evaluated in a tibial model. *J Biomed Mater Res* 43, 374-379.

23. Burkoth, A. K., Burdick, J., and Anseth, K. S. (2000) Surface and bulk modifications to photocrosslinked polyanhydrides to control degradation behavior. *J Biomed Mater Res* 51, 352-359.

24. Tarcha, P. J., Su, L., Baker, T., Langridge, D., Shastri, V., and Langer, R. (2001) Stability of photocurable anhydrides: Methacrylic acid mixed anhydrides of nontoxic diacids. *J Polym Sci Pol Chem* 39, 4189-4195.

25. Conix, A. (1966) Poly[1,3-bis(p-carboxyphenoxy)propane anhydride]. *Macromol. Synth.* 2, 95-98.

26. Kokubo, T., Kushitani, H., Sakka, S., Kitsugi, T., and Yamamuro, T. (1990) Solutions able to reproduce in vivo surface-structure changes in bioactive glass-ceramic A-W. *J Biomed Mater Res* 24, 721-734.

27. Bayraktar, D., and Tas, A. (2000) Biomimetic Preparation of HA Powders at 37°C in Urea-and Enzyme Urease-Containing Synthetic Body Fluids. *Turk J Med Sci* 30, 235-245.

28. Montgomery, D. C. (1997) *Design and analysis of experiments*, Wiley, New York.

29. Pillay, V., Dangor, C. M., Govender, T., Moopanar, K. R., and Hurbans, N. (1998) Ionotropic gelation: encapsulation of indomethacin in calcium alginate gel discs. *J Microencapsul* 15, 215-226.

30. Al-Musa, S., Abu Fara, D., and Badwan, A. A. (1999) Evaluation of parameters involved in preparation and release of drug loaded in crosslinked matrices of alginate. *J Control Release* 57, 223-232.

31. Agrawal, C. M., and Athanasiou, K. A. (1997) Technique to control pH in vicinity of biodegrading PLA-PGA implants. *J Biomed Mater Res* 38, 105-114.

32. Zignani, M., Le Minh, T., Einmahl, S., Tabatabay, C., Heller, J., Anderson, J. M., and Gurny, R. (2000) Improved biocompatibility of a viscous bioerodible poly(ortho

ester) by controlling the environmental pH during degradation. *Biomaterials* 21, 1773-1778.

33. Schiller, C., and Epple, M. (2003) Carbonated calcium phosphates are suitable pH-stabilising fillers for biodegradable polyesters. *Biomaterials* 24, 2037-2043.

CHAPTER III

PHOTOCROSSLINKED ANHYDRIDE SYSTEMS FOR LONG-TERM PROTEIN RELEASE

Ashley A. Weiner
Margaret E. Gipson
Eileen A. Bock
V. Prasad Shastri

Department of Biomedical Engineering and Biomaterials, Drug Delivery & Tissue Engineering Laboratory (BDTL)
Vanderbilt University
Nashville, TN

Abstract

Injectable delivery systems are attractive as vehicles of localized delivery of therapeutics especially in the context of regenerative medicine. In this study, the potential of photocrosslinked polyanhydride (PA) networks as an encapsulation matrix for long-term delivery of macromolecules was studied. The *in vitro* release of three model proteins (horseradish peroxidase (HRP), bovine serum albumin labeled with fluorescein isothiocyanate (FITC-BSA), and insulin) were evaluated from cross-linked anhydride networks composed of sebacic acid dimethacrylate (MSA), 1,6-bis-carboxyphenoxyhexane dimethacrylate (MCPH), and poly(ethylene glycol) diacrylate (PEGDA), supplemented with calcium carbonate. The proteins were formulated into granules first by dilution with a cyclodextrin excipient through trituration, followed by gelatin-based wet-granulation prior to incorporation into the networks. Protein release was quantified over predetermined time periods by activity assay (HRP), fluorescence (FITC-BSA), or ELISA (insulin). All proteins were readily released from the photocrosslinked PA networks; however, each protein displayed a unique release behavior. Most importantly, release of protein with retention of activity and antigenicity was achieved for durations ranging from one week to over four months. In general, a more hydrophobic network (higher MCPH:MSA ratio) resulted in slower rates of protein release. Incorporation of PEGDA into the matrices was found to be critical for maintenance of integrity during degradation and protein release. These results suggest that a photocrosslinked PA system may useful as injectable delivery systems for long-term delivery of peptides and growth factors in tissue regeneration applications**.**

Introduction

Polymers are routinely used in the development of sustained drug delivery systems. Some of the notable examples of polymer-based sustained release systems are Lupron Depot, an implantable ethylene-co-vinyl acetate based system for the delivery of GnRH agonist, Nutropin Depot, injectable microspheres of poly(α-hydroxy acid) for the delivery of recombinant human growth hormone and the Norplant family of Silastic-based implantable devices for the delivery of female contraceptives (1, 2). One of the drawbacks of using non-degradable polymer implantable systems is the need to excise the implant at the end of use. Therefore, when long-term systemic or localized delivery is sought, implementation of systems derived from degradable polymers is desirable; a need currently met by co-polymers of lactic acid and glycolic acid (PLGA). Some of the perceived limitations of the PLGA system include reproducibility of release behavior, difficulty in readily providing zero-order release and inability to form the delivery vehicle *in situ*. This last limitation is particularly relevant for tissue regeneration applications in which placement of a delivery system within a trauma site and physical conformation of the device to the implant site are important prerequisites to promote optimal tissue healing. Linear polymers containing anhydride linkages (polyanhydrides (PA)), which are capable of undergoing surface erosion, fulfill some of these criteria by achieving predictable near-zero order release.

In the PA system, the rate of matrix degradation and drug release can be easily modulated by simple modification of polymer hydrophobicity via polymer chemistry as well as by alterations in fabrication technique, additive components, and/or geometry (3, 4). Sustained release from linear PAs has been focused on a variety of drugs including

antibiotics (5, 6), local anesthetics (7), hormones (8), heparin (9), and many types of small molecules for the treatment of cancers (5, 10-15). Gliadel®, one of the most successful commercially available polyanhydride drug delivery vehicles, delivers BCNU (carmustine) directly in the site of surgical resection for treatment of glioblastoma multiforme (16, 17).

While small molecules form the basis for a majority of new therapeutic agents, recombinant protein technologies are becoming increasingly prevalent. Unlike small molecules, proteins are complex three-dimensional molecules whose function is dependent on structure. Proteins are susceptible to chemical and physical modifications, which may adversely affect both structure and function. The environment of a protein delivery vehicle is therefore a critical parameter for successful long-term protein release. Matrices derived from linear PA have been explored for release of insulin (18), trypsin (19), bovine serum albumin (20), FITC-BSA (21), water-soluble bone proteins (22), and the neuropeptide TRH (23). The utility of PA have been further improved by recent adaptation. A polymer system based on anhydride monomers with reactive methacrylate functionalities has been developed for use in orthopedic tissue repair and regeneration (24). Upon exposure to light radiation, this system can be rapidly crosslinked *in situ* into a high strength degradable network. Such systems address one of the limitations of the PLGA system as they are amenable to minimally invasive surgical interventions. In our laboratory, we have shown that a traditional photocrosslinked PA system composed of MCPH and MSA can be easily modified with additives such as $CaCO_3$ and PEGDA to modulate degradation properties such as mass loss, water uptake, pH and mechanical strength with no adverse impact on the

crosslinking capabilities of the system (25). The versatility for additive incorporation demonstrated in this study suggests that this system can be further modified to include therapeutic macromolecules without affecting crosslinking parameters. With the incorporation and bioactive molecules, the photocrosslinked PA system can serve as an injectable delivery system for sustained release. Although previous studies of the photocrosslinked PA system have focused on orthopedic applications, a more general application would involve intra-muscular and sub-dermal injectable systems capable of long-term delivery of macromolecules.

While the hydrophobic nature and surface erosion behavior of PAs protects bio-encapsulants such as proteins from moisture-induced aggregation that can readily occur with other polymeric delivery vehicles (such as poly(D,L-lactide-co-glycolide), augmentation with secondary protection strategies is imperative to ensure peptide an protein stability in photocurable PA systems. For example, inclusion of sugar-based excipients can prevent aggregation of proteins within a polymeric delivery vehicle (26). Additionally, inclusion of basic compounds can minimize acidity during degradation of the carrier and further enhance protein stabilization (27). While several studies describe the long-term protein release of proteins and growth factors such as BSA, TGF-β1, HRP and IGF-1 from photocurable matrices derived from PEGDA exist (28-31) no such studies have been undertaken with photocurable PA, with the notable exception of plasmid DNA release (32).

For this study, three model proteins (HRP, FITC-BSA, and insulin) were selected for release from photocrosslinked PA networks. As seen in Table 1, these proteins differ in molecular weight, isoelectric point, and detection strategy. Recently, we

developed a dual-purpose photocurable PA system, with optimized degradation characteristics and mechanical properties that is suitable as both an autograft extender and delivery vehicle for spinal fusion applications (25). In this study we have implemented a protein stabilization strategy previously developed in our laboratory to protect proteins from free radicals during polymerization (33), with some minor modifications to stabilize and disperse the protein in the PA system developed for the spinal fusion application. The overall objective of this study is therefore, to demonstrate the suitability of this system (see Fig. 1) for sustained delivery of peptides and proteins. Specifically, we aim to answer the following questions: (1) To what extent can the delivery of macromolecules be controlled by the chemistry of photocrosslinked PA networks? (2) Do the released proteins maintain activity and/or antigenicity after incorporation into and release from the matrix? (3) Can active protein release be achieved over a long-term period (>three months)?, and (4) Can a variety of macromolecules with differing physical properties be released from the networks? By answering these questions, the feasibility of the photocrosslinked PA system for the long-term delivery of active macromolecules has been established.

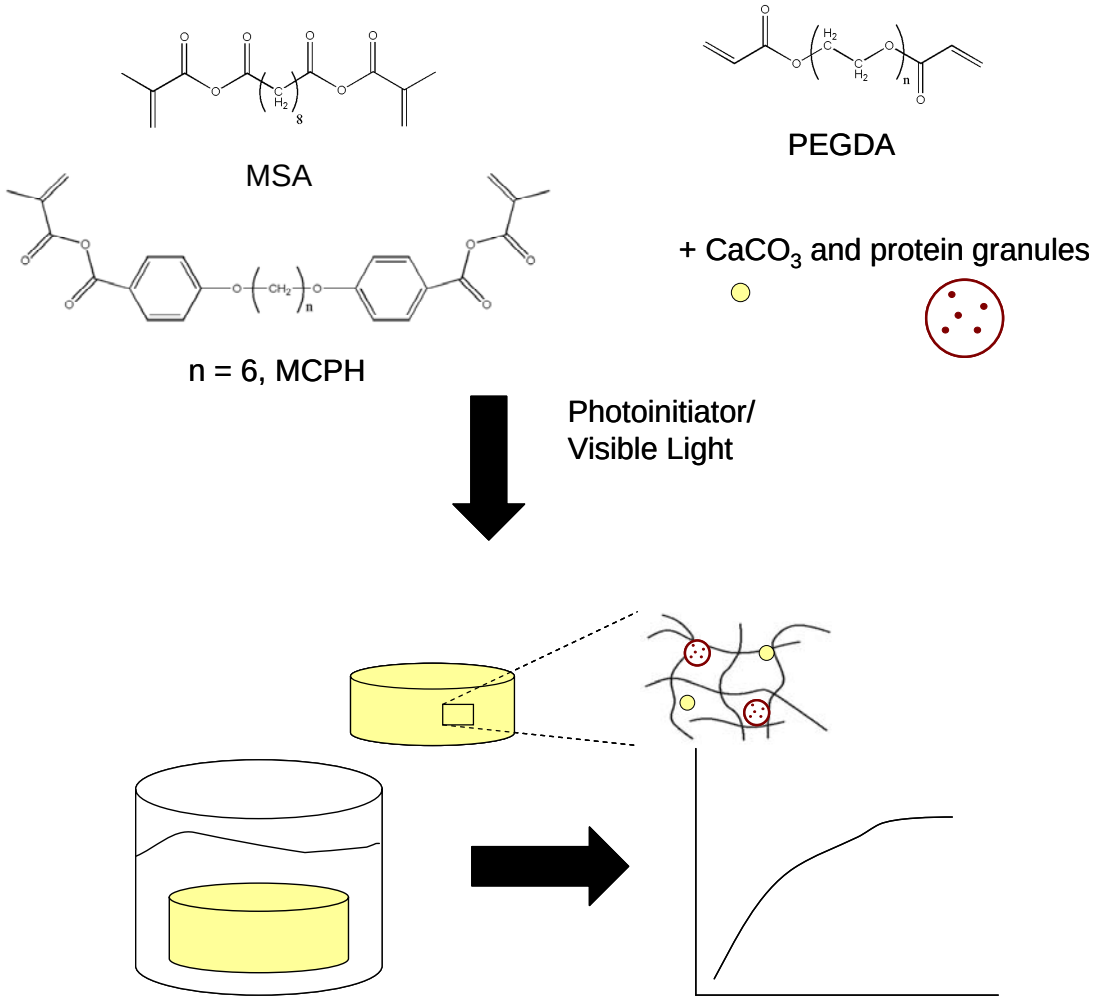

Fig. 1: A. Schematic of photocrosslinking. Anhydride monomers (MSA, MCPH), PEGDA, $CaCO_3$ and protein granules were mixed to form a paste. Mixtures were photocrosslinked after addition of photoinitiators and exposure to visible light. B. Photocrosslinked discs were subjected to in vitro degradation. At predetermined timepoints, the release buffer was removed and protein release was quantified.

Table 1: Physiochemical properties and methods of detection for model proteins.

Protein	MW	pI	Structural information	Detection method
Insulin	6.7 kDa	5.3	2 subunits, connected by disulfides	ELISA
HRP	43 kDa	9.0	Disulfides Heme group	Activity assay (oxidation of TMB)
FITC-BSA	67 kDa	4.8	Roughly 54% α-helix	Fluorescence (FITC)

Experimental

Materials

Methacrylic acid, sebacoyl chloride, triethylamine, methylene chloride, sodium bicarbonate, sodium sulfate, 4-hydroxybenzoic acid, 1,6-dibromohexane, methacryloyl chloride, poly(ethylene gycol) diacrylate (PEGDA), camphorquinone, ethyl 4-(dimethylamino)benzoate (4-EDMAB), benzoyl peroxide, dimethyl toluidine, n-methyl pyrrolidone, bovine serum albumin fluorescein isothiocyanate conjugate (FITC-BSA), bovine insulin, and calcium carbonate were obtained from Sigma-Aldrich. Horseradish peroxidase, TMB substrate kits and Coomassie-based Bradford assay kits were purchased from Pierce. Rat insulin ELISA kits were obtained from Crystal Chem.

Monomer synthesis

Sebacic acid dimethacrylate

Sebacic acid dimethacrylate (MSA) was synthesized from methacrylic acid and sebacoyl chloride as described by Tarcha (34). Methacrylic acid (9 g) and triethylamine (Et_3N) (11.63 g) were dissolved in methylene chloride (150 ml), and the mixture was stirred at 0°C for 30 min. Sebacoyl chloride (12.5 g) was added dropwise to the solution. Stirring was continued for 1 h at a reduced temperature, followed by vacuum filtration for removal of the precipitated triethyl ammonium chloride. The filtrate was diluted with an additional 100 mL of methylene chloride and cooled to 0°C. The solution was washed sequentially with saturated $NaHCO_3$ (250mL × 2) and distilled H_2O (250mL × 2) and dried over Na_2SO_4. Methylene chloride was then removed *in vacuo* at 0°C.

1,6-bis-carboxyphenoxyhexane

1,6-bis-carboxyphenoxyhexane (CPH) was synthesized from 4-hydroxybenzoic acid and 1,6-dibromohexane based on the synthesis of 1,3-bis-carboxyphenoxypropane described by Conix (35). NaOH (20 g) was dissolved in distilled water (100 ml) in a 500 ml round-bottom flask equipped with a reflux condenser, an addition funnel and a stirbar. 4-hydroxybenzoic acid (29 g) was added to this solution, and the system was heated until reflux. 1,6-dibromohexane (24.6 g) was added dropwise over 2 hours. The reaction was stirred for several hours under reflux. The product (disodium salt of CPH) was dried by vacuum filtration and washed twice with methanol. The product was dissolved in distilled water, warmed to 60°C and acidified to pH 2 with H_2SO_4. This resulted in the free acid of CPP or CPH as a white frothy precipitate. The product was then isolated by vacuum filtration and washed with distilled H_2O (200 ml × 2) and acetone (200 ml × 2) to remove any trace organics, water, and unreacted 4-hydroxybenzoic acid. The final product was then dried overnight in a 60°C oven.

1,6-bis-carboxyphenoxyhexane dimethacrylate

1,6-biscarboxyphenoxyhexane dimethacrylate (MCPH) was synthesized from CPH and methacryloyl chloride as described by Tarcha (34). 1,6-bis(p-carboxyphenoxy)hexane (11.3 g) and Et_3N (8.08 g) were dissolved in methylene chloride (120 mL) and stirred at 0 °C for 45 min. Methacryloyl chloride (7.1g) was added dropwise to this solution. Stirring was continued at a reduced temperature for 3.5 h, followed by vacuum filtration for removal of precipitated triethyl ammonium chloride. The filtrate was washed sequentially with saturated $NaHCO_3$ (200 mL × 2) and distilled H_2O (200 mL × 2). The solution was dried over anhydrous Na_2SO_4, and CH_2Cl_2 was

removed *in vacuo*; a slurry was thereby produced. Then, anhydrous ethyl ether was added and removed *in vacuo* to facilitate the removal of any remaining methylene chloride.

Protein formulation

HRP, FITC-BSA and insulin were used as model proteins. The formulation for incorporation into photocrosslinked polyanhydride matrices was based on methods described by Baroli (33). In brief, each protein (P) was first pulverized by trituration in a Teflon dish with a Teflon-coated spatula. Pulverized protein was then mixed with hydroxypropyl-β-cyclodextrin (HPβCD), in a ratio of 1:1 (insulin), 1:50 (FITC-BSA), or 1:100 (HRP) w/w (P:HPβCD), by geometric dilutions until a homogeneous powder was obtained. Subsequently, this P–HPβCD mixture was granulated with a 5% aqueous solution of gelatin B (100 mg of gelatin solution per 1 g of P–HPβCD mixture) to produce a slightly wet mass, which was then forced through a 250 μm sieve to yield granules. The granulated P–HPβCD mixture was stored at -20°C and analyzed for fluorescence (FITC-BSA), antigenicity (insulin) or enzymatic activity (HRP) prior to use.

To verify the homogeneity of the protein distribution in freshly prepared powders, a content uniformity test was used. Prior to granulation, the P–HPβCD mixtures were sampled uniformly over their entirety without mixing. Using a sample size of 10 mg (n=10 per each formulation), the mixtures were then quantified for enzyme content using a Coomassie-based Bradford Assay. For each set of 10 samples, the mean and the standard deviation was calculated. Requirements of the test were considered met if the amount of enzyme was within the limits of 85 and 115% of the expected values, and

the relative standard deviation (expressed as a percentage) was less than or equal to 6%.

Sample preparation and photopolymerization

Photopolymerizations were initiated with a dual initiator strategy, composed of camphorquinone (CQ)/4-EDMAB for light-initiated crosslinking, and benzoyl peroxide (BPO)/dimethyl toluidine (DMT) for chemically-initiated crosslinking. Sample formulations were prepared by thoroughly mixing the monomers in appropriate amounts, followed by adding an appropriate quantity of a BPO/CQ in N-methyl pyrrolidone (NMP) followed by 4-EDMAB/DMT in NMP to yield a final quantity of up to 0.1 wt% for each of CQ, BPO, 4-EDMAB, and DMT in the formulation. Uniform discs (4 mm in height and 9 mm in diameter) were prepared in Teflon molds. Samples were polymerized with a blue dental lamp (CuringLight XL1500).

In vitro release studies

In vitro protein release was assessed in phosphate buffered saline, pH 7.4 at 37°C to mimic physiological conditions. Samples were maintained at 60 rpm on an orbital shaker throughout degradation studies. The discs were degraded in 10 ml of buffer. Buffer was replaced at predetermined timepoints for entire duration of the study to minimize the effects enzyme deactivation in solution and to maintain sink conditions for degradation.

HRP activity assay

Enzymatic activity of HRP was calculated by quantification of oxidized TMB substrate in a peroxide solution using a TMB Substrate Kit. Serial dilutions of HRP release buffer were performed in PBS. 100 μl of each appropriate dilution was added to a 96 well plate. Using a multichannel pipettor, 100 μl of TMB substrate in a peroxidase buffer was added and the plate was immediately transferred to a plate reader for analysis. The concentration of the oxidized product was measured every 5 minutes for 30 minutes total at 462 nm on a BioTek II microplate reader. HRP concentrations in release buffer were compared to freshly prepared HRP standards ranging from 0.01 mU/ml to1 mU/ml. The linear range for a 30 minute incubation was between 0.01 mU/ml and 0.25 mU/ml. The detection limit was 0.01 mU/ml.

Insulin ELISA

ELISA was used to quantify insulin release and antigenicity, according to the manufacturer's instructions. In brief, samples and standards were incubated for two hours at 4°C in a 96 well plate that had been preadsorbed with anti-insulin antibody. The plate was washed five times, and was then incubated with 100 μl anti-insulin enzyme conjugate for 30 minutes at room temperature. The plate was then washed seven times and incubated with 100 μl of TMB substrate for 40 minutes at room temperature. Immediately following the TMB incubation, 100 μl of 2N sulfuric acid was added to stop the reaction. The absorbance at 450 nm was measured on a BioTek II microplate reader, with a subtraction of the absorbance at 630 nm. Insulin

concentrations were compared to freshly prepared standards ranging from 0.01 to 6.4 ng/ml. The detection limit for the assay was 0.01 ng/ml.

Quantification of FITC-BSA fluorescence

Concentration of FITC-BSA was quantified by fluorescence at 488 nm on a BioTek II microplate reader. 200 μl FITC-BSA containing release buffer was loaded in wells of a 96b well plate. FITC-BSA concentrations were compared to freshly prepared standards ranging from 0.01 to 2 μg/ml. The detection limit for the assay was 0.01 μg/ml.

Statistical analysis

Statistical analysis for comparison of burst release, cumulative release, and rates of release was performed using a Student's t-test with a minimum confidence level of 0.05 for statistical significance. All experiments were performed with n = 3-5 and are reported as mean ± standard deviation of the mean.

Results and Discussion

Experimental design

We have developed a method for protecting proteins from the detrimental effects that can occur during incorporation into a photocrosslinked system, such as free radical damage (33). In the current study, HPβCD was selected instead of lactose as the excipient, to avoid potential detrimental effects of the reducing sugar. Cyclodextrins have been shown to minimize solution-based and lyophilization-induced aggregation in

proteins, as well as to stabilize against degradation and denaturation (36). The resulting uniform powder was then subjected to wet granulation with a 5% aqueous bovine gelatin solution. This excipient and wet granulation strategy served to protect the proteins in two ways. First, the physical barrier of the gelatin granule prevented access of the free radicals to the sensitive protein molecules. Second, the excess of HPβCD molecules in comparison to protein minimized the probability of interaction between free radicals and the protein. The prepared granules were then incorporated into monomer mixtures prior to photocrosslinking.

Monomer formulations, protein:excipient ratios, and maximum experimental lengths are summarized in Table 2. Protein:excipient ratios were utilized such that the lowest level of protein loading that allowed measurable levels during the entire experimental length. This necessitated different levels of loading for the different proteins related to release rate and detection sensitivity. PEGDA incorporation into matrices enabled a reduction in water uptake, as shown in previous studies (25). Additionally, samples without PEGDA that were loaded with protein granules did not maintain structural integrity during degradation (data not shown). This finding supported previous conclusions that PEGDA serves to improve network elasticity via crosslinking. MCPH:MSA ratio was a metric for network hydrophobicity, and therefore was a dictator of degradation rate (higher ratio was a more hydrophobic network with a slower rate of degradation).

Table 2: Experimental design – Model proteins, protein:excipient ratios, tested matrix formulations, and experimental lengths.

Protein	Protein:Excipient ratio	Matrix formulations	Length of Experiment
Insulin	1:1	10% PEGDA 70:30 MCPH:MSA	7 days
		10% PEGDA 30:70 MCPH:MSA	7 days
HRP	1:100	0% PEGDA 70:30 MCPH:MSA	N/A
		0% PEGDA 30:70 MCPH:MSA	N/A
		5% PEGDA 70:30 MCPH:MSA	27 days
		5% PEGDA 30:70 MCPH:MSA	27 days
		10% PEGDA 70:30 MCPH:MSA	120 days
		10% PEGDA 50:50 MCPH:MSA	120 days
		10% PEGDA 30:70 MCPH:MSA	120 days
		20% PEGDA 70:30 MCPH:MSA	27 days
		20% PEGDA 30:70 MCPH:MSA	27 days
FITC-BSA	1:50	10% PEGDA 70:30 MCPH:MSA	27 days
		10% PEGDA 50:50 MCPH:MSA	27 days
		10% PEGDA 30:70 MCPH:MSA	27 days

Short term release of Insulin, HRP, and FITC-BSA

For evaluation of protein release from photocrosslinked PA networks, three model proteins were selected – HRP, FITC-BSA, and insulin. These proteins possess different physiochemical characteristics and can be detected and quantified in solution by different assays; these properties are summarized in Table 1. HRP is a 43 kDa protein which is positively charged at a neutral pH (pI = 9.0). Its structure is characterized by four disulfide bonds, seven N-linked carbohydrate residues, one pyrrolidone residue, and one heme group. HRP detection is achieved by enzymatic reaction, generally the oxidation of tetramethylbenzidene (TMB) substrate in a peroxide buffer. Detection by enzymatic activity requires maintenance of protein activity during and after release. FITC-BSA is a 67 kDa globular protein with a pI of roughly 4.8 and a secondary structure that is roughly 54% α-helix. Although it has no measurable biological activity, labeling of BSA with FITC enables simple, sensitive quantification of protein release. Insulin is a polypeptide of 6.7 kDa with a pI of 5.3. It is composed of

two subunits that are linked by two disulfide bonds. Detection of insulin is carried out by ELISA, which verifies maintenance of antigenicity of the epitopes recognized by the antibodies. Selection of these three model proteins with differing characteristics serves to verify the robust capabilities for protein delivery in the photocrosslinked PA system.

Initially insulin, HRP, and FITC-BSA release were quantified for 7 days (Fig. 2). PAs are commonly studied for drug delivery applications as a result of a near zero order drug release profile. In this study, the release profiles deviated from linear release profiles. During the first seven days of degradation and release, FITC-BSA release is the most nearly linear (R^2 = 0.98) of the three model proteins studied here, followed by HRP (R^2 = 0.87) and insulin (R^2 = 0.83). Traditional PA matrices used in release studies are one-dimensional wafers, which best allow linear release approximation. However, in this study, three-dimensional discs were used to more accurately mimic potential *in vivo* applications. Therefore network dimensions could be one potential cause for deviations from a zero order release curve. Additionally, the detection strategy for FITC-BSA (fluorescence) enables the quantification of total protein release. In the cases of HRP and insulin, the detection strategies of activity assay or ELISA respectively enabled only the quantitation of released protein that has maintained activity or antigenicity. The low levels of protein release in this study prevented quantification of total protein release by alternative methodology such as Bradford or BCA assay. If nonlinearities in protein activity or antigenicity occurred, these presented themselves in the release profile.

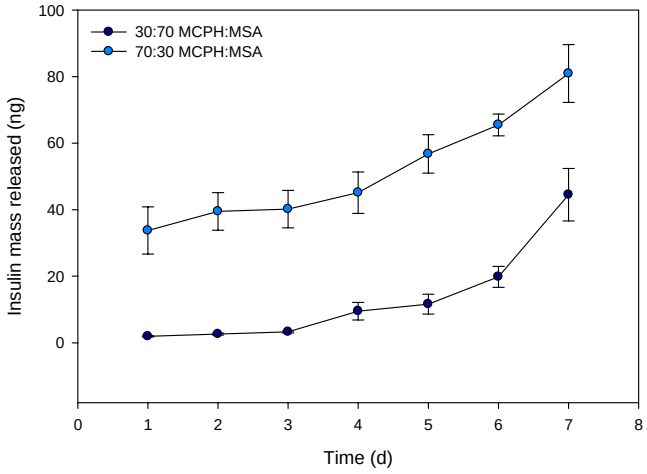

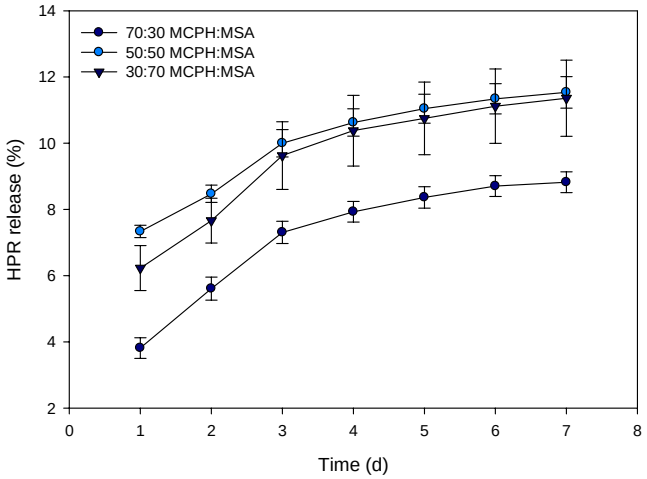

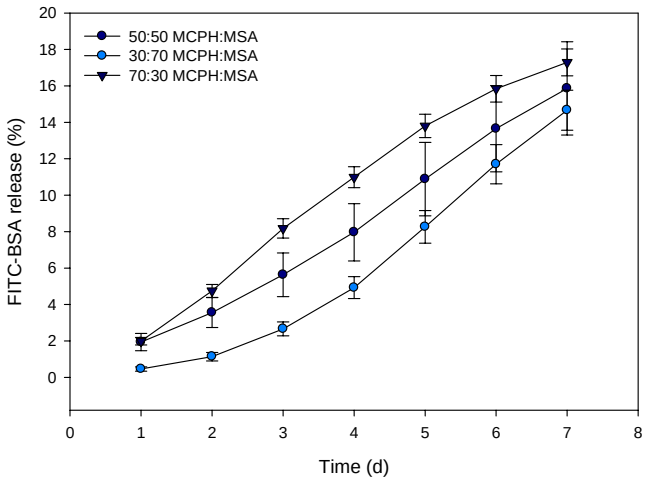

Fig. 2 Cumulative release kinetics of insulin (A), HRP (B), and FITC-BSA (C) from photocrosslinked PA networks (containing 10 wt% PEGDA) into PBS at 37°C with agitation (60 rpm) expressed as normalized protein release. Error bars represent means ± SD for n=3-5

Differences in release between the three proteins can be attributed to several different parameters – the physiochemical properties of the protein itself, the nature of the detection strategy, or the loading levels of protein within the photocrosslinked networks. Interestingly, the quantity of insulin released was less than 1% of the total loaded protein as determined by ELISA, significantly less than HRP or FITC-BSA after one week. Similarly, slow release of insulin in comparison to larger molecular weight proteins such as BSA and lysozyme has been seen in other sustained release systems

(37). If the mechanism for protein release were dictated purely by erosion of the polymer network, it would be expected that the release profile and amount of protein release would be unrelated to protein molecular weight. However, molecular weight appeared to play a dominant role. One suggested mechanism was that sustained release occurred via diffusion through matrix channels. As a result, release was dictated by protein properties (solubility and diffusivity) as well as matrix properties (porosity and tortuosity). Small molecular weight macromolecules such as insulin were incapable of inducing substantial matrix porosity, therefore hindering release. Additionally, insulin can be trapped in micropores throughout the system, while macromolecules of larger molecular weight were able to bypass the smallest conduits in the network to be more rapidly released into the surrounding buffer.

An additional mechanism that explains the slow insulin release is that low insulin solubility in the aqueous solutions slowed transfer of insulin from the matrix to the release buffer. In our previous study we have shown that contrary to prevailing logic, the incorporation of the hydrophilic PEGDA reduced water uptake and swelling in comparison with unaugmented matrices, most likely through increased network crosslink density (25). However, even with 10 wt% PEGDA incorporation into the system, water uptake of 200% (by mass) has been seen after two weeks of degradation. It was likely that a network of hydrated conduits formed within the crosslinked system, facilitating release of the more soluble HRP and FITC-BSA proteins with minimal effect on the less soluble insulin. However, this proposed mechanism would play a minimal role during short-term release from photocrosslinked PA matrices, as acidity produced by the degrading system improves insulin solubility. An alternative

theory is that insulin aggregation into insoluble fibrils occurred within the system. Aggregation occurs when hydrophobic residues within the interior of monomeric insulin become exposed to the protein surface (38). Degradation-induced acidity would not be sufficient to solublize fibrils, resulting in insulin retention within the network.

Also contributing to this theory that matrix porosity and protein properties were dominant factors in protein release was the observation that MCPH:MSA ratio, the main contributor to degradation rate, was not a good predictor of amount of protein release during this short-term study. In both FITC-BSA and insulin release systems, formulations with a higher MCPH:MSA ratio (more slowly degrading) actually provided greater protein release during the seven day study.

Long-term release of HRP and FITC-BSA from photocrosslinked PA networks – effect of MCPH:MSA ratio

To evaluate the long-term release behavior and phases of release from photocrosslinked PA networks, HRP release was assessed over a 120 day period. Release profiles for three MCPH:MSA ratios are displayed in Fig. 3.. In all experiments, protein release is expressed a percentage of the theoretical quantity of protein loaded per sample. To quantify observed trends in release rate, release profiles were divided into 6 phases, similar to the four phase methodology (over 21 days of release) used to describe protein release from an oligo(poly(ethylene glycol) fumarate) hydrogel (39). Phase 1 was defined as the burst release after 24 hours of degradation. Phase 2 was a period of rapid release between days 1-3. Distinct release rates were also noted between days 3-6 (Phase 3), days 6-28 (Phase 4) and days 28-60 (Phase 5). A less distinct phase (Phase 6) was seen in the long-term, between days 60 and 120. In the

context of regenerative medicine, phases 1 and 2 constitute priming the environment with a bolus of the therapeutic macromolecule. The remaining long-term release phases aid in maintenance of a sustained response, a strategy desired for a single-dose vaccine such as tetanus toxoid (40).

Final cumulative release values are reported for the end of the experiment; however significant (>50%) polymer mass remained even at later (120 day) timepoints. The burst release cumulative release, and rates of release for each phase can be seen in Table 3. The 70:30 MCPH:MSA network formulation displayed the lowest burst effect (3.81±0.62%) after 24 hours of release, while the 50:50 MCPH:MSA and 70:30 MCPH:MSA displayed similar burst releases (6.22±1.36% and 7.33±0.37% respectively). Phase 2 and 3 release rates were similar for all polymer formulations. However, between days 6 and 28 (Phase 4) as well as days 28-60 (Phase 5), significantly different rates of HRP release were observed for all three formulations. The 30:70 MCPH:MSA formulation had the highest rate of protein release during these phases, while the 70:30 MCPH:MSA formulation had the slowest protein release. The slowest overall protein release was seen during the final phase, Phase 6. As a result of a high matrix hydrophobicity, the lowest cumulative release during the study was seen in the 70:30 MCPH:MSA formulation. The 30:70 MCPH:MSA formulation exhibited the highest cumulative release. The release from the 70:30 MCPH:MSA formulation was significantly lower than the 50:50 and 30:70 formulations throughout the experiment, an expected result since this was the most hydrophobic formulation.

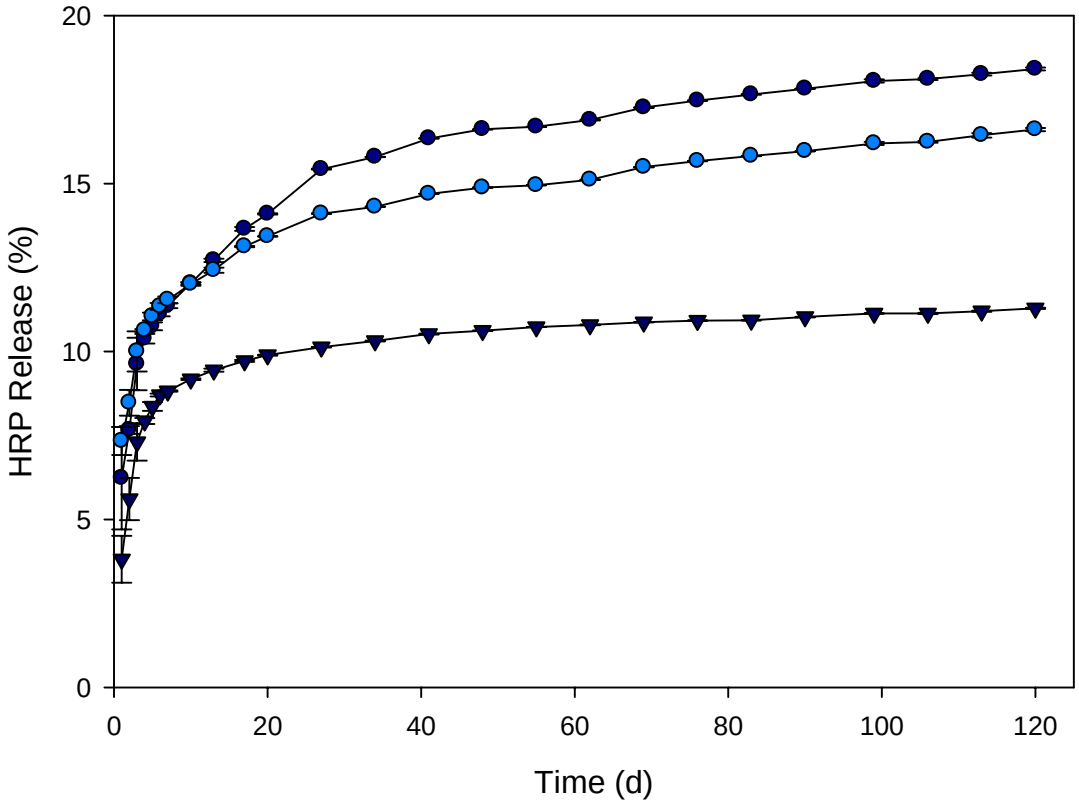

Fig. 3: Cumulative release kinetics of HRP from photocrosslinked PA networks (containing 10 wt% PEGDA) into PBS at 37°C with agitation (60 rpm) expressed as normalized active protein release. Error bars represent means ± standard deviation for n=5.

Table 3: Burst release, Phase 2-6 release rate and cumulative HRP release from photocrosslinked PA networks containing 10 wt% PEGDA. # denotes release that is significantly greater than other formulations, ^ denotes release that is significantly less than other formulations ($p<0.05$).

Formulation	Burst release (%)	Phase 2 (day 1-3) rate (%/day)	Phase 3 (day 3-6) rate (%/day)	Phase 4 (day 6-28) rate (%/day)	Phase 5 (day 28-60) rate (%/day)	Phase 6 (day 60-120) rate (%/day)	Cumulative release (%)
30:70 MCPH:MSA	6.22±1.36	1.94±0.36	0.48±0.09	0.20±0.02#	0.04±0.003#	0.02±0.01	18.41±3.0
50:50 MCPH:MSA	7.33±0.37	1.33±0.41^	0.44±0.07	0.13±0.02	0.03±0.004	0.025±0.01	16.61±1.5
70:30 MCPH:MSA	3.81±0.62^	1.74±0.24	0.46±0.07	0.06±0.02^	0.02±0.01^	0.01±0.01^	11.35±1.4^

These long-term release studies suggested that the mechanism of protein release from photocrosslinked PA networks changes during the course of the experiment. The initial burst release most likely occurred as a result of both water uptake and the release of protein that is immediately available for dissolution at the matrix surface. In the short-term release period following the initial burst, matrix porosity and protein properties presumably play a dominant role as protein release is dictated by diffusion. Finally, in the long-term release phases (Phases 4 - 6), dependence on matrix hydrophobicity (MCPH:MSA ratio) was observed.

Surprisingly, FITC-BSA release profiles (Fig. 4) and phases of release (Table 4) were dramatically different from the release curves for HRP with the same polymer network formulations. For the first 10 days of release, MCPH:MSA ratio appeared to play no significant role in dictating rate of protein release. Interestingly, the Phase 2 (day 1-3) rates were statistically different for all formulations; although, the highest MCPH:MSA ratio formulation (most hydrophobic and most slowly degrading) had the greatest rate of FITC-BSA release during this time. The release behavior during the initial phases (burst release and Phases 2-3) suggests that matrix degradation was not a predominant factor during the short term release. During this time, a gradual wetting of the matrix may have led to induction of porosity and diffusion of the protein into the release buffer. However, in Phase 4 (days 6-27), significantly different release rates were again seen in all formulations. In this phase, the MCPH:MSA ratio was a good predictor of the rate of release. More rapid FITC-BSA release was seen in the more rapidly degrading 30:70 MCPH:MSA formulation. Correspondingly, the lowest rate of FITC-BSA release was seen in the slowest degrading 70:30 MCPH:MSA formulation

during Phase 4. The reliance on matrix degradation during Phase 4 was a common factor in release of both HRP and FITC-BSA, despite differences in the overall rate of release and release profiles between the two proteins.

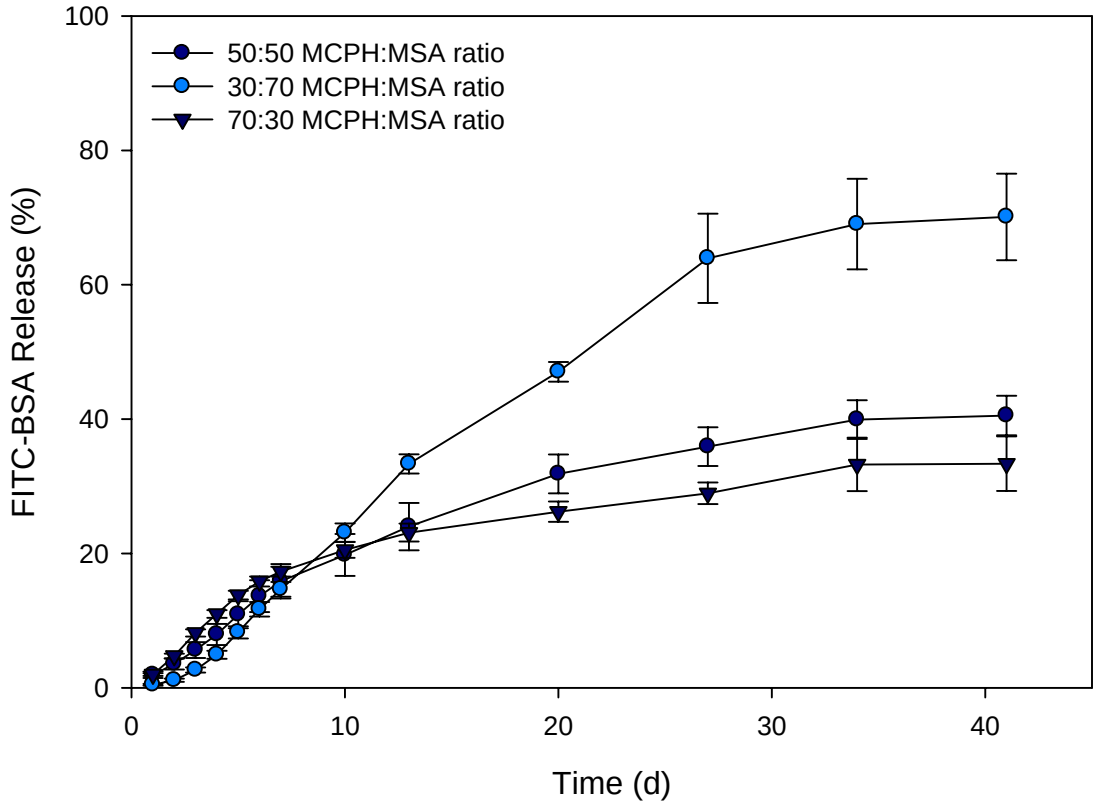

Fig. 4: Cumulative release kinetics of FITC-BSA from photocrosslinked PA networks (containing 10 wt% PEGDA) into PBS at 37°C with agitation (60 rpm) expressed as normalized protein release. Error bars represent means ± standard deviation for n=4

Table 4: Burst release, Phase 2-5 release rate and cumulative FITC-BSA release from photocrosslinked PA networks containing 10 wt% PEGDA. . # denotes release that is significantly greater than other formulations, ^ denotes release that is significantly less than other formulations ($p<0.05$).

Formulation	Burst release (%)	Phase 2 (day 1-3) rate (%/day)	Phase 3 (day 3-6) rate (%/day)	Phase 4 (day 6-27) rate (%/day)	Phase 5 (day 27-41) rate (%/day)	Cumulative release (%)
30:70 MCPH:MSA	0.46±0.25^	1.10±0.32^	3.04±0.51	2.24±0.09#	0.42±0.22	64.74±5.89#
50:50 MCPH:MSA	1.94±0.94	1.84±0.74	2.70±0.81	1.06±0.20	0.33±0.06	40.54±5.89
70:30 MCPH:MSA	1.99±0.41	3.09±0.35#	2.57±0.23	0.61±0.11^	0.31±0.37	33.36±8.14

Long-term release of HRP – effect of PEGDA concentration

Previous studies in our laboratory have shown that incorporation of PEGDA into photocrosslinked matrices minimizes water uptake and buffer acidity during *in vitro* degradation. Although we have determined that inclusion of PEGDA is beneficial for performance of the material in *in vitro* degradation, some dose dependence was seen with different percentages of PEGDA in photocrosslinked PA formulations. To assess the effect of PEGDA loading on protein release, HRP-containing formulations described in Table 2 were evaluated. Interestingly, samples containing 0 wt% PEGDA did not remain intact for more than 4 days of *in vitro* degradation (data not shown). This result provides conclusive evidence that PEGDA is a critical component of photocrosslinked PA systems for protein release. In earlier studies, the proposed mechanism for reduction in water uptake by PEGDA (despite the molecule's hydrophilicity) was the introduction of a more densely crosslinked network and a reduction in the concentration of unreacted monomer. A system that was not augmented by PEGDA most likely lacked sufficient crosslinking density and elasticity to maintain structural integrity with the inclusion of protein granules.

Formulations containing 5% or 20% PEGDA displayed a similarly shaped release profile (Fig 5.) as previously described for the 10% PEGDA formulations (Fig. 3). Burst releases and Phase 1 release rates for the 20% PEGDA formulations were higher than the 5% PEGDA formulations (Table 5). As expected from earlier experiments, the MCPH:MSA ratio did not play a significant role in protein release during these phases. However, during Phases 3 and 4, the MCPH:MSA ratio was a better predictor of release rate, with the 30:70 MCPH:MSA ratio yielding more rapid release. Final cumulative HRP release was significantly greater for the 20% PEGDA loading than for the 5% PEGDA loading within a given MCPH:MSA ratio. Final cumulative HRP release was greater for the 30:70 MCPH:MSA ratio within a given PEGDA loading. These data suggested that matrix hydrophilicity played a role in increasing protein release since both high PEGDA concentrations and low MCPH:MSA ratios yielded greater protein release, thus presenting a novel mechanism for controlling macromolecular release from hydrophobic matrices. FITC-BSA release was quantified from similar formulations; however no difference in release rate was seen with alternative PEGDA loading (5 or 20 wt%) (data not shown). This finding suggested that physical properties of the protein may alter the effect of PEGDA on release profiles.

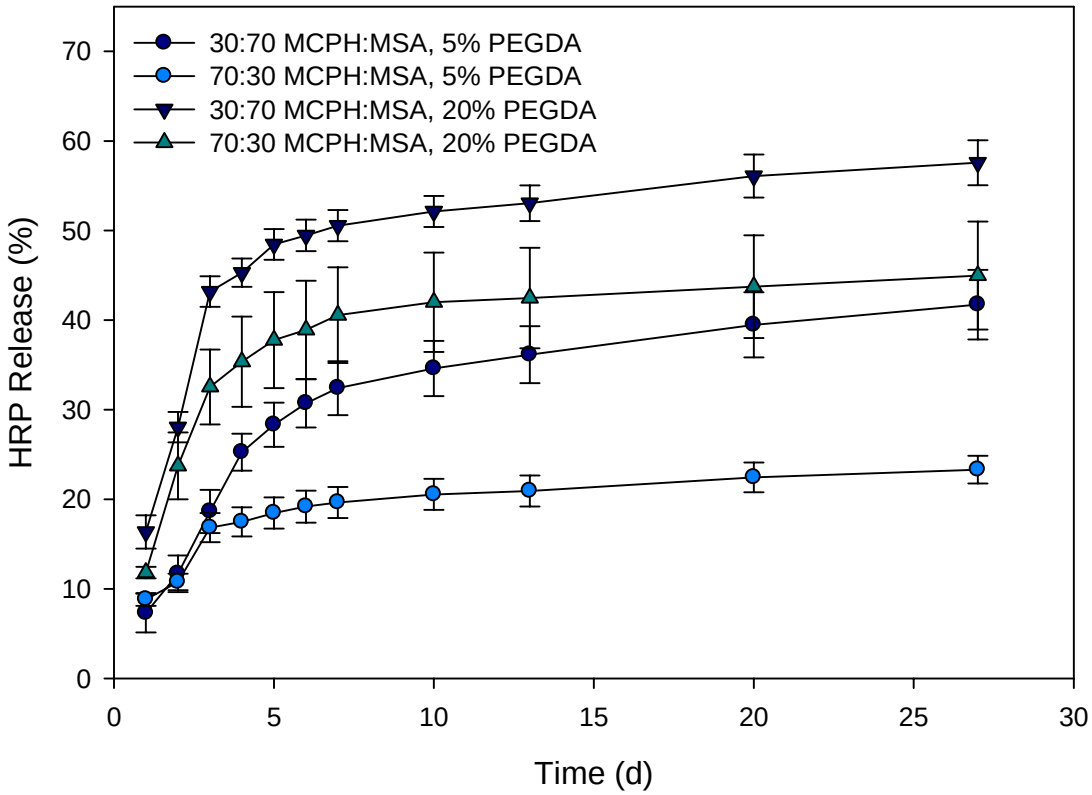

Fig. 5: Cumulative release kinetics of HRP from photocrosslinked PA networks (containing 5 or 20 wt% PEGDA) into PBS at 37°C with agitation (60 rpm) expressed as normalized active protein release. Error bars represent means ± SE for n=4.

Table 5: Burst release, Phase 2-4 release rate and cumulative HRP release from photocrosslinked PA networks containing 5 or 20 wt% PEGDA.

Formulation	Burst release (%)	Phase 2 (day 1-3) rate (%/day)	Phase 3 (day 3-6) rate (%/day)	Phase 4 (day 6-27) rate (%/day)	Cumulative release (%)
5% PEGDA 30:70 MCPH:MSA	7.30±2.17	5.67±0.86	3.93±0.69	0.50±0.08	41.73±3.89
5% PEGDA 70:30 MCPH:MSA	8.82±0.71	4.01±0.51	0.81±0.08	0.19±0.02	23.30±1.54
20% PEGDA 30:70 MCPH:MSA	16.36±1.85	13.38±0.94	2.20±0.06	0.38±0.04	57.57±2.52
20% PEGDA 70:30 MCPH:MSA	11.82±0.64	10.36±1.84	2.13±0.46	0.25±0.04	44.96±6.02

Conclusions

This study is the first to evaluate protein release from photocrosslinked PA networks. More importantly, sustained long-term release (> 4 months) of macromolecules in their active form from photocrosslinked PA networks has been demonstrated. Three model proteins, that differ in their physicochemical and detection modalities have been incorporated into the matrices and released *in vitro*. By varying the network hydrophobicity (MCPH:MSA ratio or PEGDA content) the release profiles were tuned to achieve varying rates of protein release from the matrices, although these effects were seen primarily in the later phases of release. This observation constitutes a novel mechanism for controlling macromolecular release from hydrophobic matrices. Interestingly, especially during the early phases of protein release, the physicochemical properties of individual proteins are a dominant factor in determining protein release. These findings validate the photocrosslinked PA system as an injectable vehicle for macromolecule delivery with broad clinical applications.

Acknowledgements

The authors would like to thank Xiao-Jun Xu for assistance with monomer synthesis. This work was supported by the Vanderbilt Institute for Integrative Biosystems Research and Education (VIIBRE) and the Vanderbilt University Discovery Grant program. AAW would like to acknowledge the National Science Foundation for support through their Graduate Research Fellowship Program.

References

1. Shastri, V. P. (2003) Non-degradable biocompatible polymers in medicine: past, present and future. *Curr Pharm Biotechnol* 4, 331-337.

2. Shastri, P. V. (2002) Toxicology of polymers for implant contraceptives for women. *Contraception* 65, 9-13.

3. Jain, J. P., Modi, S., Domb, A. J., and Kumar, N. (2005) Role of polyanhydrides as localized drug carriers. *J Control Release* 103, 541-563.

4. Gopferich, A., and Tessmar, J. (2002) Polyanhydride degradation and erosion. *Adv Drug Deliv Rev* 54, 911-931.

5. Park, E. S., Maniar, M., and Shah, J. C. (1998) Biodegradable polyanhydride devices of cefazolin sodium, bupivacaine, and taxol for local drug delivery: preparation, and kinetics and mechanism of in vitro release. *J Control Release* 52, 179-189.

6. Yang, X. F., Zeng, F. D., Zhou, Z. B., Huang, K. X., and Xu, H. B. (2003) In vitro release and antibacterial activity of poly (oleic/linoleic acid dimer: sebacic acid)-gentamicin. *Acta Pharmacol Sin* 24, 306-310.

7. Masters, D. B., Berde, C. B., Dutta, S., Turek, T., and Langer, R. (1993) Sustained local anesthetic release from bioerodible polymer matrices: a potential method for prolonged regional anesthesia. *Pharm Res* 10, 1527-1532.

8. Mylonas, C. C., Tabata, Y., Langer, R., and Zohar, Y. (1995) Preparation and Evaluation of Polyanhydride Microspheres Containing Gonadotropin-Releasing-Hormone (Gnrh), for Inducing Ovulation and Spermiation in Fish. *Journal of Controlled Release* 35, 23-34.

9. Teomim, D., Fishbien, I., Golomb, G., Orloff, L., Mayberg, M., and Domb, A. J. (1999) Perivascular delivery of heparin for the reduction of smooth muscle cell proliferation after endothelial injury. *J Control Release* 60, 129-142.

10. Shikani, A. H., and Domb, A. J. (2000) Polymer chemotherapy for head and neck cancer. *Laryngoscope* 110, 907-917.

11. Shikanov, A., Vaisman, B., Krasko, M. Y., Nyska, A., and Domb, A. J. (2004) Poly(sebacic acid-co-ricinoleic acid) biodegradable carrier for paclitaxel: in vitro release and in vivo toxicity. *J Biomed Mater Res A* 69, 47-54.

12. Storm, P. B., Moriarity, J. L., Tyler, B., Burger, P. C., Brem, H., and Weingart, J. (2002) Polymer delivery of camptothecin against 9L gliosarcoma: release, distribution, and efficacy. *J Neurooncol* 56, 209-217.

13. Li, Y., Owusu, A., and Lehnert, S. (2004) Treatment of intracranial rat glioma model with implant of radiosensitizer and biomodulator drug combined with external beam radiotherapy. *Int J Radiat Oncol Biol Phys* 58, 519-527.

14. Teomim, D., Nyska, A., and Domb, A. J. (1999) Ricinoleic acid-based biopolymers. *J Biomed Mater Res* 45, 258-267.

15. Berrada, M., Yang, Z., and Lehnert, S. (2002) Tumor treatment by sustained intratumoral release of 5-fluorouracil: effects of drug alone and in combined treatments. *Int J Radiat Oncol Biol Phys* 54, 1550-1557.

16. Brem, H., Kader, A., Epstein, J. I., Tamargo, R. J., Domb, A., Langer, R., and Leong, K. W. (1989) Biocompatibility of a biodegradable, controlled-release polymer in the rabbit brain. *Sel Cancer Ther* 5, 55-65.

17. Brem, H., Piantadosi, S., Burger, P. C., Walker, M., Selker, R., Vick, N. A., Black, K., Sisti, M., Brem, S., Mohr, G., and et al. (1995) Placebo-controlled trial of safety and efficacy of intraoperative controlled delivery by biodegradable polymers of chemotherapy for recurrent gliomas. The Polymer-brain Tumor Treatment Group. *Lancet* 345, 1008-1012.

18. Lin, H. H., Mathiowitz, E., and Langer, R. (1987) Controlled Insulin Release from Injectable, Bioerodible Polyanhydride Microspheres for Clinical Management of Diabetes-Mellitus. *Clinical Research* 35, A820-A820.

19. Tabata, Y., Gutta, S., and Langer, R. (1993) Controlled delivery systems for proteins using polyanhydride microspheres. *Pharm Res* 10, 487-496.

20. Hanes, J., Chiba, M., and Langer, R. (1998) Degradation of porous poly(anhydride-co-imide) microspheres and implications for controlled macromolecule delivery. *Biomaterials* 19, 163-172.

21. Determan, A. S., Trewyn, B. G., Lin, V. S., Nilsen-Hamilton, M., and Narasimhan, B. (2004) Encapsulation, stabilization, and release of BSA-FITC from polyanhydride microspheres. *J Control Release* 100, 97-109.

22. Lucas, P. A., Laurencin, C., Syftestad, G. T., Domb, A., Goldberg, V. M., Caplan, A. I., and Langer, R. (1990) Ectopic induction of cartilage and bone by water-soluble proteins from bovine bone using a polyanhydride delivery vehicle. *J Biomed Mater Res* 24, 901-911.

23. Kubek, M. J., Liang, D., Byrd, K. E., and Domb, A. J. (1998) Prolonged seizure suppression by a single implantable polymeric-TRH microdisk preparation. *Brain Res* 809, 189-197.

24. Anseth, K. S., Shastri, V. R., and Langer, R. (1999) Photopolymerizable degradable polyanhydrides with osteocompatibility. *Nat Biotechnol* 17, 156-159.

25. Weiner, A. A., Shuck, D. M., Bush, J. R., and Shastri, V. P. (2007, in review) Optimization of photocrosslinked anhydride systems for bone augmentation applications: characterization of in vitro degradation. *Biomaterials.*

26. Castellanos, I. J., Carrasquillo, K. G., Lopez, J. D., Alvarez, M., and Griebenow, K. (2001) Encapsulation of bovine serum albumin in poly(lactide-co-glycolide) microspheres by the solid-in-oil-in-water technique. *J Pharm Pharmacol* 53, 167-178.

27. Zhu, G., Mallery, S. R., and Schwendeman, S. P. (2000) Stabilization of proteins encapsulated in injectable poly (lactide- co-glycolide). *Nat Biotechnol* 18, 52-57.

28. Elisseeff, J., McIntosh, W., Fu, K., Blunk, B. T., and Langer, R. (2001) Controlled-release of IGF-I and TGF-beta1 in a photopolymerizing hydrogel for cartilage tissue engineering. *J Orthop Res* 19, 1098-1104.

29. Mellott, M. B., Searcy, K., and Pishko, M. V. (2001) Release of protein from highly cross-linked hydrogels of poly(ethylene glycol) diacrylate fabricated by UV polymerization. *Biomaterials* 22, 929-941.

30. Burdick, J. A., Mason, M. N., Hinman, A. D., Thorne, K., and Anseth, K. S. (2002) Delivery of osteoinductive growth factors from degradable PEG hydrogels influences osteoblast differentiation and mineralization. *J Control Release* 83, 53-63.

31. An, Y., and Hubbell, J. A. (2000) Intraarterial protein delivery via intimally-adherent bilayer hydrogels. *J Control Release* 64, 205-215.

32. Quick, D. J., Macdonald, K. K., and Anseth, K. S. (2004) Delivering DNA from photocrosslinked, surface eroding polyanhydrides. *J Control Release* 97, 333-343.

33. Baroli, B., Shastri, V. P., and Langer, R. (2003) A method to protect sensitive molecules from a light-induced polymerizing environment. *J Pharm Sci* 92, 1186-1195.

34. Tarcha, P. J., Su, L., Baker, T., Langridge, D., Shastri, V., and Langer, R. (2001) Stability of photocurable anhydrides: Methacrylic acid mixed anhydrides of nontoxic diacids. *J Polym Sci Pol Chem* 39, 4189-4195.

35. Conix, A. (1966) Poly[1,3-bis(p-carboxyphenoxy)propane anhydride]. *Macromol. Synth.* 2, 95-98.

36. Davis, M. E., and Brewster, M. E. (2004) Cyclodextrin-based pharmaceutics: past, present and future. *Nat Rev Drug Discov* 3, 1023-1035.

37. Rhine, W. D., Hsieh, D. S., and Langer, R. (1980) Polymers for sustained macromolecule release: procedures to fabricate reproducible delivery systems and control release kinetics. *J Pharm Sci* 69, 265-270.

38. Brange, J., and Langkjoer, L. (1993) Insulin structure and stability. *Pharm Biotechnol* 5, 315-350.

39. Holland, T. A., Tabata, Y., and Mikos, A. G. (2005) Dual growth factor delivery from degradable oligo(poly(ethylene glycol) fumarate) hydrogel scaffolds for cartilage tissue engineering. *J Control Release* 101, 111-125.

40. Schwendeman, S. P., Costantino, H. R., Gupta, R. K., Siber, G. R., Klibanov, A. M., and Langer, R. (1995) Stabilization of tetanus and diphtheria toxoids against moisture-induced aggregation. *Proc Natl Acad Sci U S A* 92, 11234-11238.

CHAPTER IV

MODULATION OF PROTEIN RELEASE FROM PHOTOCROSSLINKED POLY(ANHYDRIDE) NETWORKS THROUGH INCORPORATION OF GELATIN MICROPARTICLES

Ashley A. Weiner
Marc C. Moore
Amanda H. Walker
V. Prasad Shastri

Department of Biomedical Engineering and Biomaterials, Drug Delivery & Tissue Engineering Laboratory (BDTL)
Vanderbilt University
Nashville, TN

Abstract

Injectable delivery systems are attractive as vehicles for localized delivery of therapeutics especially in the context of regenerative medicine. In this study, photocrosslinked polyanhydride (PA) networks were modified by incorporation of microparticles to enhance and modulate long-term delivery of macromolecules. The *in vitro* release of two model proteins (horseradish peroxidase (HRP) and bovine serum albumin labeled with fluorescein isothiocyanate (FITC-BSA)) were evaluated from photocrosslinked anhydride networks composed of sebacic acid dimethacrylate (MSA), 1,6-bis-carboxyphenoxyhexane dimethacrylate (MCPH), poly(ethylene glycol) diacrylate (PEGDA), and calcium carbonate (CaCO3), supplemented with gelatin microparticles or sodium chloride (NaCl) crystals. The proteins were formulated into granules first by dilution with a cyclodextrin excipient through tituration, followed by gelatin-based wet-granulation prior to incorporation into the networks. Protein release was quantified over predetermined time periods by activity assay (HRP) or fluorescence (FITC-BSA). Protein release profiles and rates of protein release were successfully modulated by incorporation of microparticles into photocrosslinked PA networks, presumably by enabling aqueous channels through the matrix. By loading the protein in the gelatin microparticles, additional control over protein release was achieved. Furthermore, a dual release system has been demonstrated by incorporation of protein in both the PA matrix and the gelatin microparticles. These results suggest that microparticle incorporation into photocrosslinked PA system may be a useful strategy to modulate protein release in injectable delivery systems for the long-term delivery of

macromolecules. These gelatin microparticle-photocrosslinked composites present an interesting class of materials for bone regeneration applications.

Introduction

In the recent past, our laboratory efforts have focused on the exploration of the photocrosslinked polyanhydride (PA) system as a scaffold for hard tissue regeneration and drug delivery. This system is based on anhydride monomers with reactive methacrylate functionalities and has been developed for use in orthopedic tissue repair and regeneration (1). Upon exposure to light radiation, this system can be rapidly crosslinked *in situ* into a high strength degradable network. This system has several advantages over traditional PLGA systems for drug delivery. First, as a result of the anhydride linkages, PA based systems are capable of undergoing surface erosion and achieving predictable near-zero order drug release. Additionally, the capability of *in situ* formation is of particular importance in TE applications in which physical conformation of the device to an implant site is an important prerequisite for optimal tissue healing.

We have shown that a traditional photocrosslinked PA system composed of MCPH and MSA can be easily modified with additives such as $CaCO_3$ and PEGDA to modulate degradation properties such as mass loss, water uptake, pH and mechanical strength while providing no adverse effects on the crosslinking capabilities of the system (2). Additionally, we have demonstrated that this system possesses a robust capability for long-term delivery of macromolecules (3). We have implemented a protein stabilization strategy previously developed in our laboratory to protect proteins from free radicals during polymerization (4), with some minor modifications to stabilize and disperse the protein in the PA system developed for the spinal fusion application. Using these strategies, we have demonstrated that the photocrosslinked PA system can serve as an injectable vehicle for the long-term delivery of active proteins. Although most

studies of the photocrosslinked PA system have focused on orthopedic applications, a more general application would involve intra-muscular and sub-dermal injectable systems capable of long-term delivery of macromolecules.

In our previous work, we were able to achieve long-term (over four months) release of enzymatically active protein (HRP), although relatively low levels of protein release were attained. The release rate and profile were modestly modulated by altering matrix hydrophobicity (MCPH:MSA ratio or PEGDA content). Significant modulation of protein release rates and profiles is difficult in this photocrosslinked system outside of altering matrix hydrophobicity. Although reactive and nonreactive additives can be incorporated with ease, an upper limit exists after which crosslinking and/or structural integrity of the system is impaired.

One proposed driving force for protein release (in addition to degradation) is protein diffusion through aqueous channels in the wetted network. Maximization of the channel volume within the matrix by incorporation of porogens would be one mechanism for increasing release. One possible methodology for induction of microscale channels is the incorporation of microparticles or salt crystals within the crosslinked matrix (5). In the field of TE, microparticles alone suffer limitations, since they do not provide a substrate for cellular or tissue ingrowth. However diverse uses have been identified for incorporation of microparticles into TE scaffolds. Initially, leachable porogens such as microparticles of gelatin or NaCl have been used to generate porosity in scaffolds by solvent casting or particulate leaching. More recently, drug or protein-loaded microparticles have been incorporated into TE scaffolds (such as polypropylene fumarate (5) or oligo(poly(ethylene glycol) fumarate) (6)) to form

composites with the capability of delivering bioactive molecules that aid in tissue regeneration. For these drug delivery applications, biodegradable microparticles composed of gelatin (7), co-polymers of lactic acid and glycolic acid (PLGA) (5), or polyanhydrides (PA) (8) have garnered much interest.

In the current study, two model proteins (HRP and FITC-BSA) were selected for release from porous photocrosslinked PA networks. The current strategies employed include both particulate leaching of NaCl and gelatin microparticles as well as release of protein from composites composed of protein loaded gelatin microparticles within photocrosslinked PA networks (see Fig. 1). This study is the first to evaluate the incorporation of porogens in the photocrosslinked PA system. In addition, it is the first to employ the particulate leaching strategy as a primary means of facilitating protein release. The overall objective of this study was therefore to demonstrate the ease of modulation of this system for improving delivery of peptides and proteins. Specifically, we aim to answer the following questions: (1) To what extent can the delivery of macromolecules be controlled by incorporation of porogens (NaCl and gelatin microparticles) within the matrix? (2) Can the protein carrier affect protein release? and (3) Does the physiochemical nature of the macromolecule affect release? By answering these questions, we have expanded on our previous studies to demonstrate versatility in release profiles from the photocrosslinked PA system for the long-term delivery of active macromolecules.

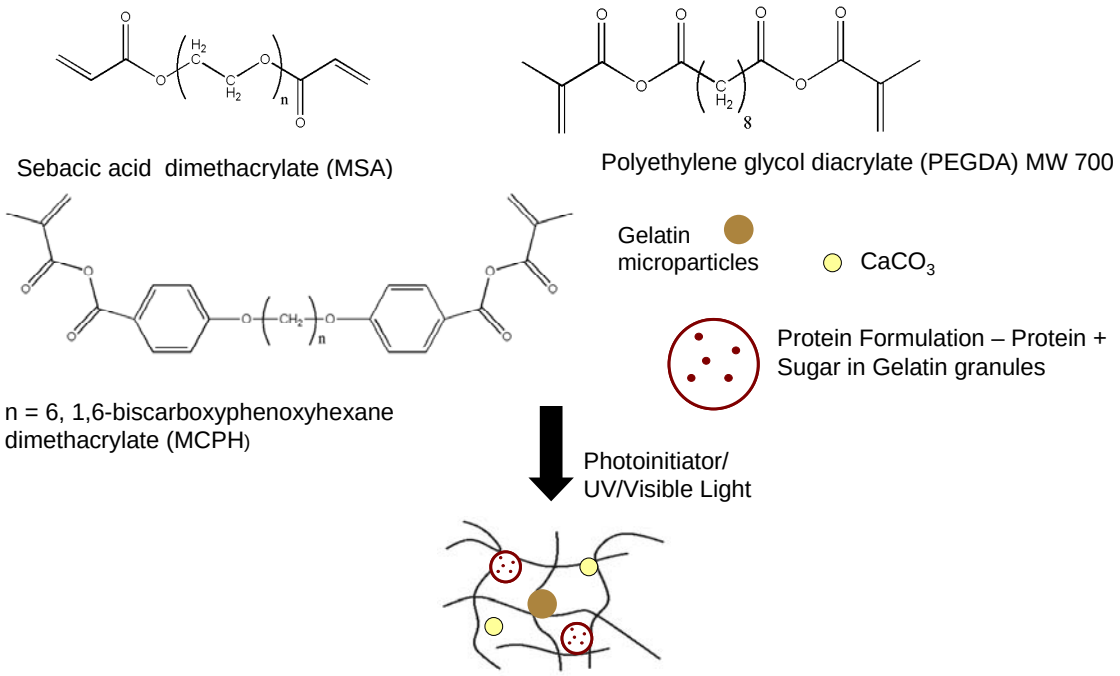

Fig. 1: Schematic of photocrosslinking. Anhydride monomers (MSA, MCPH), PEGDA, $CaCO_3$ and protein granules were mixed to form a paste. Mixtures were photocrosslinked after addition of photoinitiators and exposure to visible light.

Experimental

Materials

Methacrylic acid, sebacoyl chloride, triethylamine, methylene chloride, sodium bicarbonate, sodium sulfate, 4-hydroxybenzoic acid, 1,6-dibromohexane, methacryloyl chloride, poly(ethylene gycol) diacrylate (PEGDA), camphorquinone, ethyl 4-(dimethylamino)benzoate (4-EDMAB), benzoyl peroxide, dimethyl toluidine, n-methyl pyrrolidone, bovine serum albumin fluorescein isothiocyanate conjugate (FITC-BSA), calcium carbonate, bovine gelatin B, and glutaraldehyde were obtained from Sigma-Aldrich. Horseradish peroxidase, TMB substrate kits and Coomassie-based Bradford assay kits were purchased from Pierce. All materials were used as received.

Monomer synthesis

Sebacic acid dimethacrylate

Sebacic acid dimethacrylate (MSA) was synthesized from methacrylic acid and sebacoyl chloride as described by Tarcha (9). Methacrylic acid (9 g) and triethylamine (Et_3N) (11.63 g) were dissolved in methylene chloride (150 ml), and the mixture was stirred at 0°C for 30 min. Sebacoyl chloride (12.5 g) was added dropwise to the solution. Stirring was continued for 1 h at a reduced temperature, followed by vacuum filtration for removal of the precipitated triethyl ammonium chloride. The filtrate was diluted with an additional 100 mL of methylene chloride and cooled to 0°C. The solution was washed sequentially with saturated $NaHCO_3$ (250mL × 2) and distilled H_2O (250mL × 2) and dried over Na_2SO_4. Methylene chloride was then removed *in vacuo* at 0°C.

1,6-bis-carboxyphenoxyhexane

1,6-bis-carboxyphenoxyhexane (CPH) was synthesized from 4-hydroxybenzoic acid and 1,6-dibromohexane based on the synthesis of 1,3-bis-carboxyphenoxypropane described by Conix (10). NaOH (20 g) was dissolved in distilled water (100 ml) in a 500 ml round-bottom flask equipped with a reflux condenser, an addition funnel and a stirbar. 4-hydroxybenzoic acid (29 g) was added to this solution, and the system was heated until reflux. 1,6-dibromohexane (24.6 g) was added dropwise over 2 hours. The reaction was stirred for several hours under reflux. The product (disodium salt of CPH) was dried by vacuum filtration and washed twice with methanol. The product was dissolved in distilled water, warmed to 60°C and acidified to pH 2 with H_2SO_4. This resulted in the free acid of CPP or CPH as a white frothy precipitate. The product was then isolated by vacuum filtration and washed with distilled H_2O (200 ml × 2) and

acetone (200 ml × 2) to remove any trace organics, water, and unreacted 4-hydroxybenzoic acid. The final product was then dried overnight in a 60°C oven.

1,6-bis-carboxyphenoxyhexane dimethacrylate

1,6-biscarboxyphenoxyhexane dimethacrylate (MCPH) was synthesized from CPH and methacryloyl chloride as described by Tarcha (9). 1,6-bis(p-carboxyphenoxy)hexane (11.3 g) and Et_3N (8.08 g) were dissolved in methylene chloride (120 mL) and stirred at 0 °C for 45 min. Methacryloyl chloride (7.1g) was added dropwise to this solution. Stirring was continued at a reduced temperature for 3.5 h, followed by vacuum filtration for removal of precipitated triethyl ammonium chloride. The filtrate was washed sequentially with saturated $NaHCO_3$ (200 mL × 2) and distilled H_2O (200 mL × 2). The solution was dried over anhydrous Na_2SO_4, and CH_2Cl_2 was removed *in vacuo*; a slurry was thereby produced. Then, anhydrous ethyl ether was added and removed *in vacuo* to facilitate the removal of any remaining methylene chloride.

Protein formulation

HRP and FITC-BSA were used as model proteins. The formulation for incorporation into photocrosslinked polyanhydride matrices was based on methods described by Baroli (4). In brief, each protein (P) was first pulverized by trituration in a Teflon dish with a Teflon-coated spatula. Pulverized protein was then mixed with hydroxypropyl-β-cyclodextrin (HPβCD), in a ratio 1:50 (FITC-BSA) or 1:100 (HRP) w/w (P:HPβCD), by geometric dilutions until a homogeneous powder was obtained. Subsequently, this P–HPβCD mixture was granulated with a 5% aqueous solution of

gelatin B (100 mg of gelatin solution per 1 g of P–HPβCD mixture) to produce a slightly wet mass, which was then forced through a 250 μm sieve to yield granules. The granulated P–HPβCD mixture was stored at -20°C and analyzed for fluorescence (FITC-BSA) or enzymatic activity (HRP) prior to use.

To verify the homogeneity of the protein distribution in freshly prepared powders, a content uniformity test was used. Prior to granulation, the P–HPβCD mixtures were sampled uniformly over their entirety without mixing. Using a sample size of 10 mg (n=10 per each formulation), the mixtures were then quantified for enzyme content using a Coomassie-based Bradford Assay. For each set of 10 samples, the mean and the standard deviation was calculated. Requirements of the test were considered met if the amount of enzyme was within the limits of 85 and 115% of the expected values, and the relative standard deviation (expressed as a percentage) was less than or equal to 6%.

Preparation of gelatin microparticles

Gelatin microparticles were fabricated as described by Holland (6). Briefly, 5 g of basic gelatin was dissolved in 45 ml of deionized water by heating to 60°C under constant stirring. The aqueous gelatin solution was added dropwise via a syringe and 21-G needle to 250 ml of olive oil while maintaining a stirring rate of 500 rpm. Stirring was maintained while the emulsion temperature was decreased to 15°C to induce gelation. After 30 minutes, 100 ml of chilled acetone were added. The microparticles were removed by vacuum filtration and were washed 4 times with acetone to remove

residual olive oil. Microparticles were sized by passing through sieves of sizes ranging from 500 μm to 106 μm.

Crosslinking of gelatin microparticles

Gelatin microparticles were crosslinked by stirring in a 0.1% solution of Tween 80 containing 0.5% glutaraldehyde for 12 h at 15°C. Crosslinked microparticles were collected by vacuum filtration. The microparticles were washed in deionized water and then incubated in a 25 mM glycine solution for 1 h to block any unreacted gluteraldehyde. The microparticles were collected by vacuum, washed in deionized water, and vacuum-dried overnight. Crosslinked microparticles were then sized by passing through a gradient of sieves.

Protein loading of gelatin microparticles

Solutions of protein in phosphate buffered saline were prepared for loading of the crosslinked gelatin microparticles. Microparticle loading was achieved by incubating 5 μl of protein solution (2 mg/ml, HRP or FITC-BSA) per mg of gelatin microparticles. This solution volume was significantly below the theoretical equilibrium swelling volume of the microparticles, ensuring complete protein adsorption by the particles. The microparticle-protein mixture was vortexed completely and incubated overnight at 4°C to allow adsorption to occur.

In vitro protein release from gelatin microparticles

HRP and FITC-BSA release from crosslinked gelatin microparticles was assessed in PBS. Loaded microparticle were weighed and incubated with 1 ml of PBS. All specimens were incubated at 37°C with shaking (60 rpm). At predetermined timepoints, the specimens were pelleted by centrifugation. The release buffer was removed and replaced with fresh PBS. The presence of protein in the release buffer was quantified by correlation with a standard curve (see assays for HRP and FITC-BSA below). Cumulative protein release was quantified by calculating the cumulative protein release and normalizing to the total loaded protein in each specimen.

Sample preparation and photopolymerization

Photopolymerizations were initiated with a dual initiator strategy, composed of camphorquinone (CQ)/4-EDMAB for light-initiated crosslinking, and benzoyl peroxide (BPO)/dimethyl toluidine (DMT) for chemically-initiated crosslinking. as previously developed and described (2). Sample formulations were prepared by thoroughly mixing the monomers in appropriate amounts, followed by adding an appropriate quantity of a BPO/CQ in N-methyl pyrrolidone (NMP) followed by 4-EDMAB/DMT in NMP to yield a final quantity of up to 0.1 wt% for each of CQ, BPO, 4-EDMAB, and DMT in the formulation. Uniform discs (4 mm in height and 9 mm in diameter) were prepared in Teflon molds. Samples were polymerized with a blue dental lamp (CuringLight XL1500).

In vitro release studies

In vitro protein release was assessed in phosphate buffered saline, pH 7.4 at 37°C to mimic physiological conditions. Samples were maintained at 60 rpm on an orbital shaker throughout degradation studies. The discs were degraded in 10 ml of buffer. Buffer was replaced at predetermined timepoints for entire duration of the study to minimize the effects enzyme deactivation in solution and to maintain sink conditions for degradation.

HRP activity assay

Enzymatic activity of HRP was calculated by quantification of oxidized TMB substrate in a peroxide solution using a TMB Substrate Kit. Serial dilutions of HRP release buffer were performed in PBS. 100 μl of each appropriate dilution was added to a 96 well plate. Using a multichannel pipettor, 100 μl of TMB substrate in a peroxidase buffer was added and the plate was immediately transferred to a plate reader for analysis. The concentration of the oxidized product was measured every 5 minutes for 30 minutes total at 462 nm on a BioTek II microplate reader. HRP concentrations in release buffer were compared to freshly prepared HRP standards ranging from 0.01 mU/ml to1 mU/ml. The linear range for a 30 minute incubation was between 0.01 mU/ml and 0.25 mU/ml. The detection limit was 0.01 mU/ml.

Quantification of FITC-BSA fluorescence

Concentration of FITC-BSA was quantified by fluorescence at 488 nm on a BioTek II microplate reader. 200 μl FITC-BSA containing release buffer was loaded in

wells of a 96b well plate. FITC-BSA concentrations were compared to freshly prepared standards ranging from 0.01 to 2 μg/ml. The detection limit for the assay was 0.01 μg/ml.

Statistical analysis

Statistical analysis for comparison of burst release, cumulative release, and rates of release was performed using a Student's t-test with a minimum confidence level of 0.05 for statistical significance. All experiments were performed with n = 3-5 and are reported as mean ± standard deviation of the mean.

Results

HRP release from photocrosslinked PA matrices with NaCl-or gelatin microparticle-induced porosity

Although previous experimentation in our laboratory demonstrated capability of delivering active proteins over a long timeframe at a tunable rate, the cumulative HRP release was less than 20% of total loaded HRP after 35 days. We therefore hypothesized that the introduction water soluble porogens such as NaCl or gelatin microparticles might accelerate the release of HRP (see formulations in Table 1a). The most hydrophobic network (MCPH:MSA) was selected, as it resulted in the slowest protein release in unmodified systems. Introduction of 25 w/w% of 250 μm gelatin microspheres into the system resulted in the release of 56% of loaded HRP over a 5-week period which represents a five-fold increase over the 10% release seen in the unmodified system. A significant increase in protein release was seen both during the

24 hour burst release ($p=0.001$) as well as during the long term release phase (days 7-35, $p=0.005$) in the gelatin microparticle supplemented system. However, when NaCl particles (<106 μm) were incorporated into networks as a porogen, no difference in release rate occurred in comparison with the unmodified, nonporous matrix. This is an important result as it suggests that the leaching of dissolved gelatin leaves an aqueous path, whereas the complete ionic dissolution of NaCl does not result in new aqueous pathways or macroporosity for protein diffusion. Fig. 2 shows the release profiles over 35 days for these three formulations. In addition, Table 2 compares the 24 hour burst effect release, the cumulative release after 48 hours, the long-term release rate (between days 7 and 35), and the total cumulative release rate for the unmodified, nonporous network, and for the network containing 250 μm gelatin microparticles. There is a statistically significant difference for all calculated parameters in this table. There is only a difference in burst release between the unmodified, nonporous network and the network containing <106 μm NaCl crystals. This modification to our HRP release studies shows that we can modulate the rate of release of active protein from our crosslinked anhydride system. Further enhancement in protein release can be achieved by varying the size, volume fraction or type of porogen.

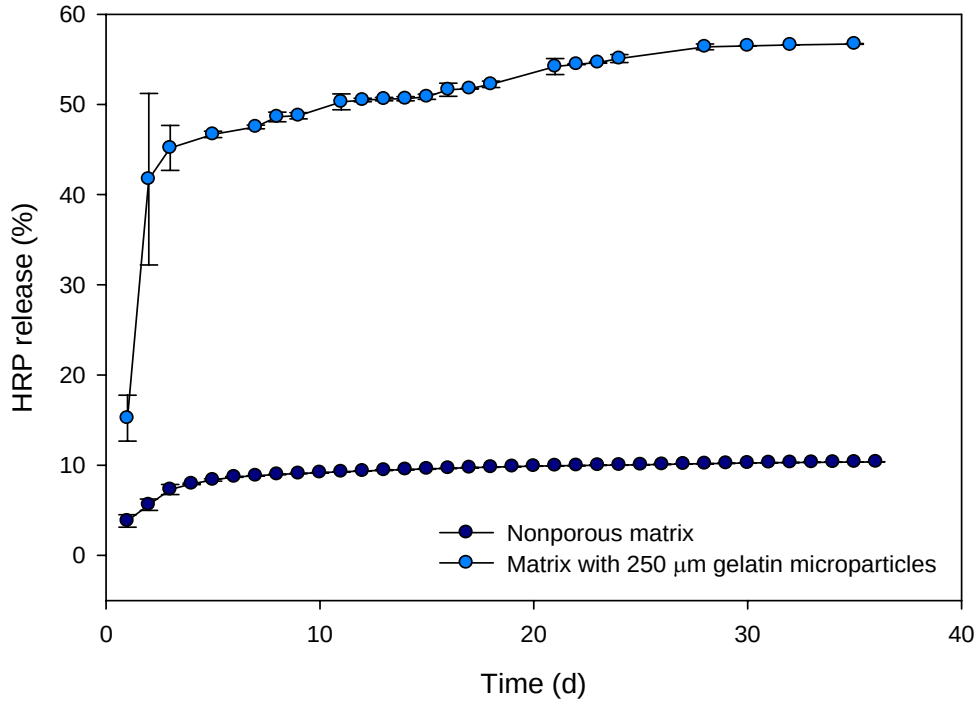

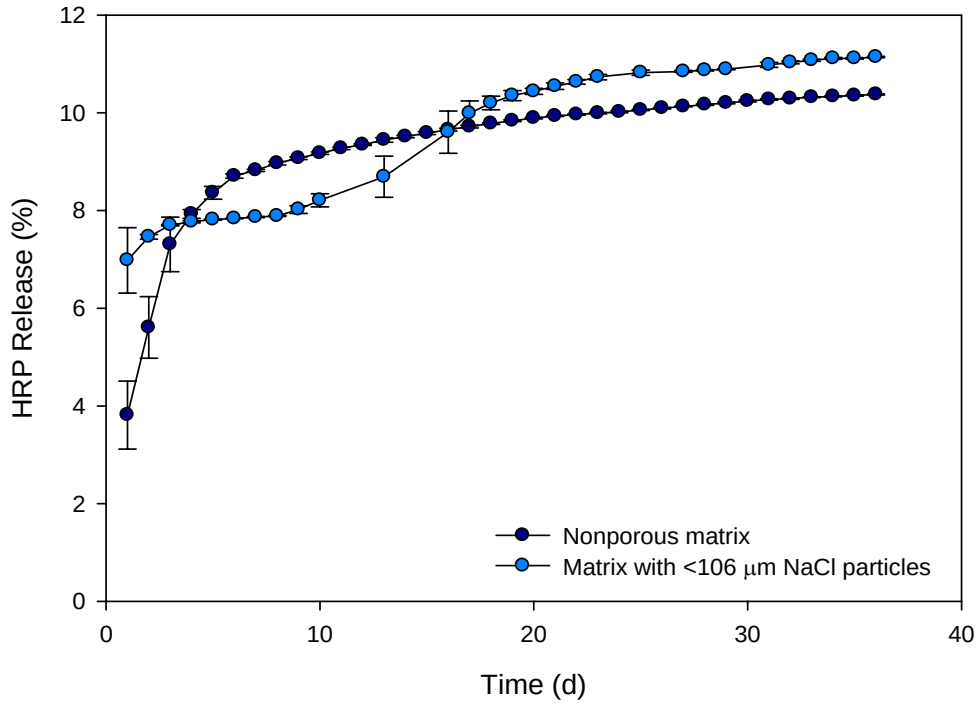

Fig. 2: Cumulative release kinetics of HRP from photocrosslinked anhydride networks containing gelatin microparticles (A) or NaCl particles (B) into PBS at 37°C with agitation (60 rpm). Error bars represent mean±S.E. for *n*=2-4.

Table 1: Experimental design for evaluation of microparticle leaching for modulation of protein release

	MCPH:MSA ratio	Granulated protein	Microparticle loading	Microparticle size	Microparticle type
a.	70:30	HRP	25 w/w%	< 106 µm	NaCl
	70:30	HRP	25 w/w%	250 µm	Gelatin B
b.	70:30	HRP	75 v/v%	180-250 µm	Gelatin B
	70:30	HRP	75 v/v%	250-300 µm	Gelatin B
c.	70:30	HRP	33 v/v%	106-180 µm	Gelatin B
	70:30	HRP	55 v/v%	180-250 µm	Gelatin B
	30:70	HRP	33 v/v%	180-250 µm	Gelatin B
	30:70	HRP	55 v/v%	106-180 µm	Gelatin B

Table 2: Release rates of HRP from crosslinked anhydride networks

Formulation	24 h Burst (%)	Cumulative release after 48 h (%)	Long term release (d7 – d35) (%/d)	Cumulative release (%)
70:30 MCPH:MSA	3.81±0.70	5.61±0.78	0.05±0.02	10.33±0.89
70:30 MCPH:MSA + gelatin µparticles	15.22±2.54	41.72±17.29	0.518±0.16	56.71±18.61

HRP release from photocrosslinked PA matrices with gelatin-microparticle-induced porosity: Effect of loading and particle size

Since gelatin microparticles were better modulators of protein release than NaCl crystals, preliminary studies were pursued with gelatin microparticles alone. Initially, gelatin microparticles of two size ranges (180-250 µm and 250-300 µm) were incorporated into photocrosslinked PA networks at a loading of 75 v/v%, the maximal loading allowable (formulations described in Table 1b). Large microparticles were selected to maximize the effect in these proof-of-concept studies. HRP release profiles

from these networks can be seen in Fig. 3. During the first eight days of degradation and release, the release profiles were identical, regardless of microparticle size. After day eight, the rate of HRP release from samples containing 180-250 μm microparticles was 0.48±0.11% per day, while the rate of HRP release from samples containing 250-300 μm microparticles was 1.22±0.06% per day ($p<0.05$). Since larger (250-300 μm) were often the result of the aggregation of smaller particles, additional studies utilized smaller, more uniform microparticles.

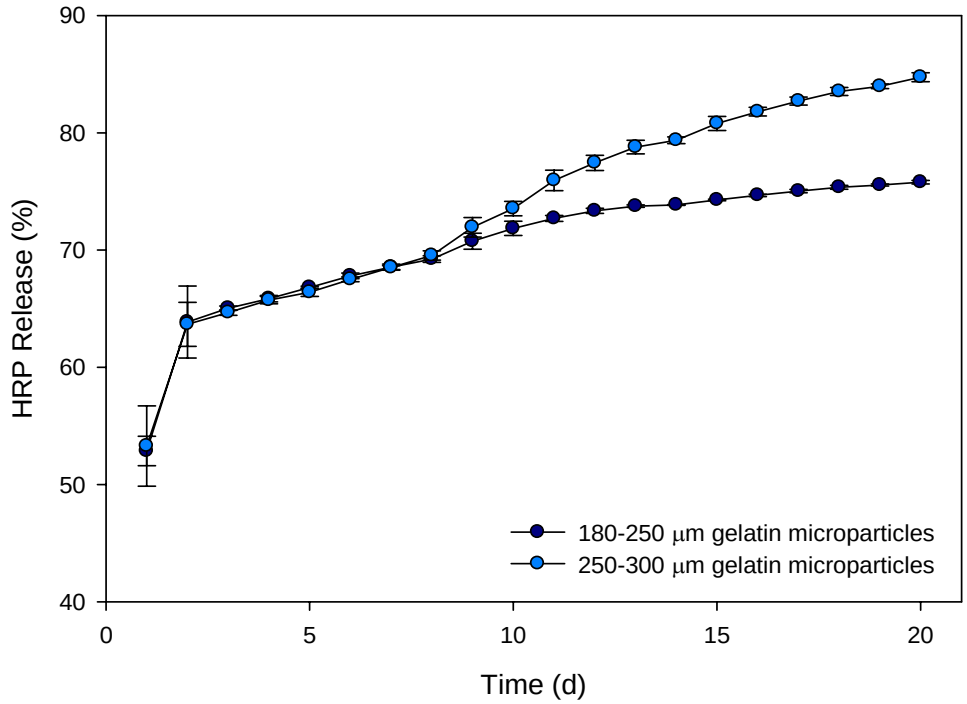

Fig. 3: Cumulative release kinetics of HRP from photocrosslinked anhydride networks containing gelatin microparticles into PBS at 37°C with agitation (60 rpm). (A) The cumulative normalized mass released from samples containing 75 v/v% gelatin microparticles, error bars represent mean±S.E. for *n*=2-4.

To evaluate the effect of gelatin microparticle size and loading on protein release, gelatin microparticles of two size ranges (106-180 μm and 180-250 μm) were utilized at loadings of 33 or 55 v/v%. Additionally, two MCPH:MSA ratios – 30:70 and 70:30 were evaluated. These formulations are described in Table 1c. Interestingly, the release profile was independent of microparticle loading and MCPH:MSA ratio (Fig. 4). As expected based on percolation theory, gelatin microparticle size was the dominant factor in dictating HRP release. The larger microparticles (180-250 μm) yielded greater cumulative protein release than the smaller microparticles (106-180 μm) ($p<0.05$) regardless of MCPH:MSA ratio or microparticle loading percentage. This long-term release profile was primarily dominated by the release of HRP over the first 48 hours.

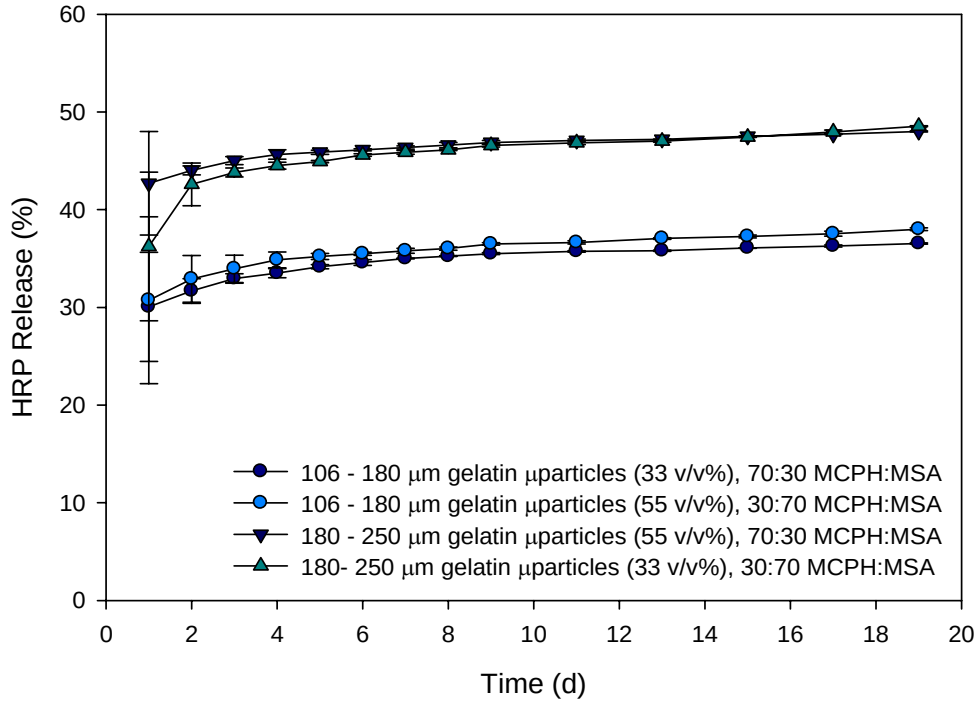

Fig. 4: Cumulative release kinetics of HRP from photocrosslinked anhydride networks containing gelatin microparticles into PBS at 37°C with agitation (60 rpm). The cumulative normalized mass released from samples containing 106-180 μm or 180-250 μm gelatin microparticles, error bars represent mean±S.D. for *n*=4.

Gelatin microparticles as protein delivery vehicles

Gelatin microparticles were also studied as a vehicle for protein delivery. Microparticles were loaded with a 2 mg/ml solution of FITC-BSA or HRP in PBS by swelling. Ten mg samples of loaded microparticles were then incubated in PBS release buffer. Combinations of protein type and microparticle size are described in Table 3a. The buffer was removed at predetermined timepoints and protein release was quantified (Fig. 5). Microparticles (106-180 μm) loaded with FITC-BSA exhibited a 24 hour burst release of 59.98±0.79% of loaded protein, while those loaded with HRP exhibited a smaller burst release than that of FITC-BSA (14.01±2.13%). Larger

microparticles (180-250 μm) loaded with HRP exhibited the smallest burst release (11.43±1.15%). Since the 180-250 μm particles were less uniform than smaller microparticles (data not shown), these were not used to evaluate FITC-BSA release nor were they utilized in future studies. Final cumulative release was the greatest for FITC-BSA (93.49±2.2% of loaded protein after 18 days). In contrast, 81.64±0.07% of loaded HRP was released from the 106-180 μm microparticles and 60.57±0.01% of loaded HRP was released from 180-250 μm microparticles. As expected, the total cumulative release of HRP was greater from the smaller microparticles, presumably a result of the increased surface area to volume ratio over the larger microparticles.

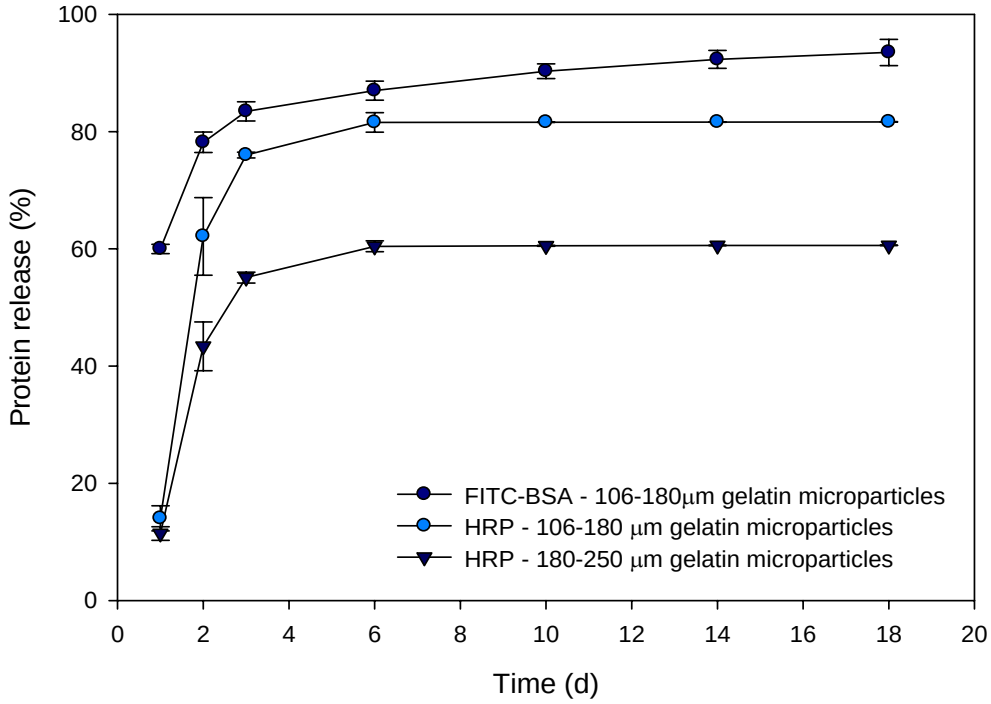

Fig. 5: Crosslinked gelatin microparticles were loaded with a solution of FITC-BSA or HRP; protein was released in 1 ml of PBS.

Table 3: Experimental design for evaluation of protein release from loaded gelatin microparticles and from photocrosslinked PA networks

	Matrix	Granulated protein	Microparticle loading	Microparticle size	Protein loaded in microparticles
a.	N/A	N/A	N/A	106-180 µm	FITC-BSA
	N/A	N/A	N/A	106-180 µm	HRP
	N/A	N/A	N/A	180-250 µm	HRP
b.	70:30 MCPH:MSA	HRP	10 w/w%	106-180 µm	FITC-BSA
	70:30 MCPH:MSA	FITC-BSA	10 w/w%	106-180 µm	HRP

Dual release system for HRP and FITC-BSA from photocrosslinked PA matrix-gelatin microparticle composites

Composites of photocrosslinked PA networks and gelatin microparticles were fabricated to evaluate co-release of FITC-BSA and HRP. One set of composites was created which contained FITC-BSA in the traditional wet granulated protein and cyclodextrin formulation and HRP-loaded gelatin microparticles. Another set of composites contained HRP in the traditional wet granulated protein and cyclodextrin formulation and FITC-BSA-loaded gelatin microparticles. A schematic for protein and microparticle loading is shown in Fig. 6. Release profiles were dependent on both the phase of protein loading (within gelatin microparticles or within the granulated formulation) and the type of protein (formulations described in Table 3b). When HRP was incorporated into composites in the granulated formulation with FITC-BSA loaded gelatin microparticles (Fig. 7), there was a burst release of 9.66±2.45% of loaded HRP after 24 hours. After 18 days, the cumulative release of HRP was 11.20±0.002% of the theoretical loading. Interestingly, only 0.02+0.008% of FITC-BSA from the composites was released after 18 days, with no detectable burst release. In contrast, when FITC-BSA was incorporated into composites in the granulated formulation with HRP loaded gelatin microparticles (Fig. 8), there was a burst release of 5.73±0.87% of loaded FITC-BSA after 24 hours. After 18 days, the cumulative release of FITC-BSA was 82.7±0.47% of the theoretical loading. HRP release from gelatin microparticles within the composite yielded a burst release of 30.32±0.19%. Final cumulative release of HRP after 18 days was 34.00±0.20% of the theoretical loading.

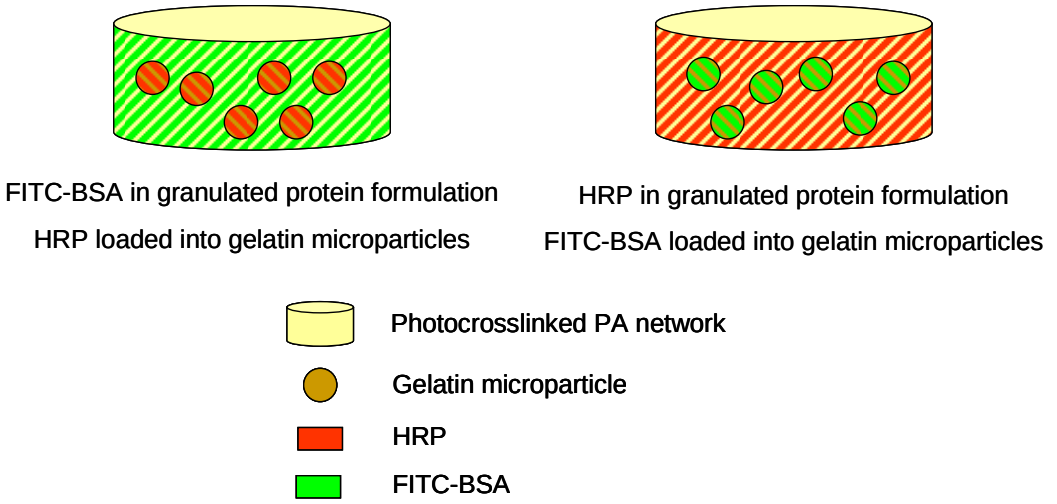

Fig. 6: Schematic for dual release strategy. Specimen contained HRP in the wet-granulated formulation and FITC-BSA-loaded gelatin microparticles or FITC-BSA in the wet-granulated formulation and HRP-loaded gelatin microparticles.

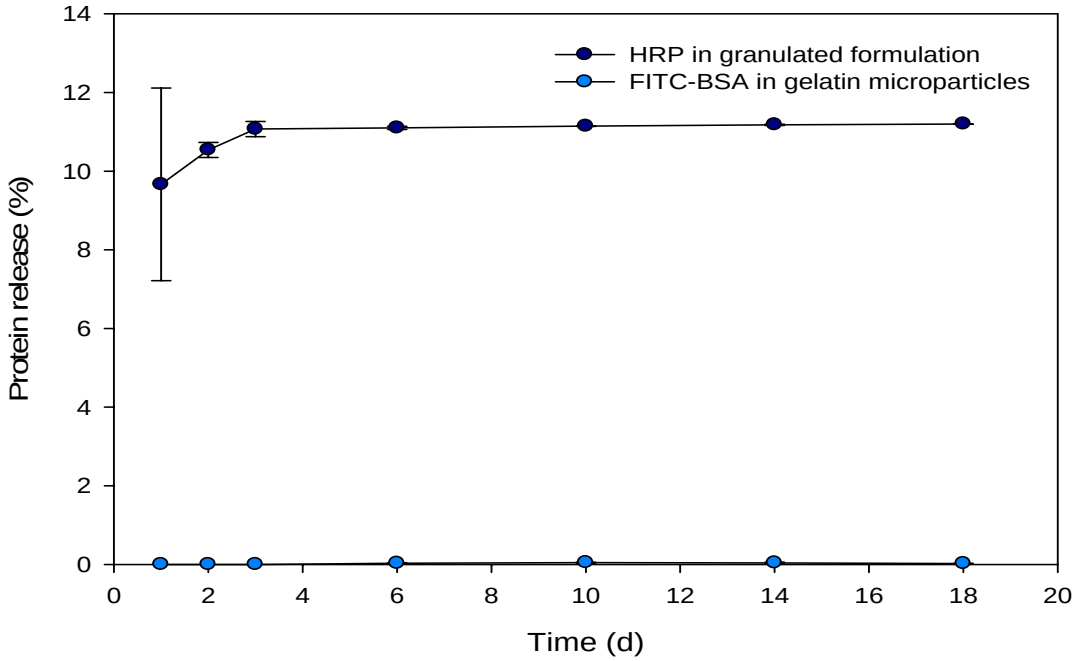

Fig. 7: Cumulative release kinetics of HRP and FITC-BSA from photocrosslinked anhydride networks containing gelatin microparticles into PBS at 37°C with agitation (60 rpm). Samples contained traditionally formulated HRP (sugar+ protein+ granulation) (10 wt%) and FITC-BSA loaded gelatin microparticles (10 wt%).The cumulative normalized mass released from samples is shown, error bars represent mean±S.D. for *n*=2-4.

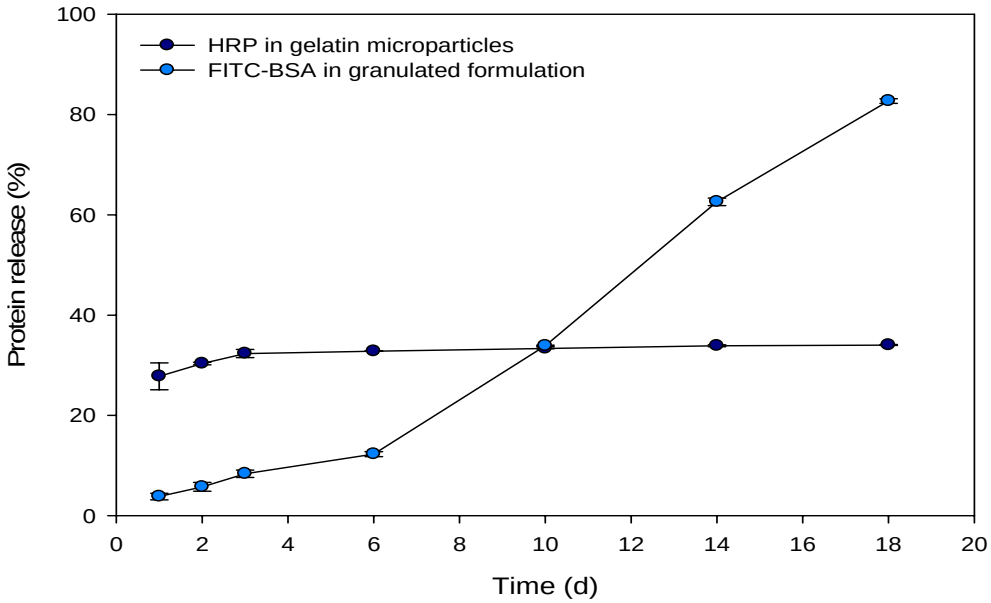

Fig. 8: Cumulative release kinetics of HRP and FITC-BSA from photocrosslinked anhydride networks containing gelatin microparticles into PBS at 37°C with agitation (60 rpm). Samples contained traditionally formulated FITC-BSA (sugar+ protein+ granulation) (10 wt%) and HRP loaded gelatin microparticles (10 wt%).The cumulative normalized mass released from samples is shown, error bars represent mean±S.D. for *n*=2-4.

Discussion

Our laboratory has been the first to evaluate protein release from photocrosslinked PA networks (3). This delivery system was initially selected as a result of numerous properties including the potential for predictable near-zero order release profiles, the capability of formation *in situ* by virtue of photocrosslinking, and the relative ease of system modification. In our initial study, sustained long-term release (> 4 months) of macromolecules in their active form from photocrosslinked PA networks was demonstrated. Additionally, the release profiles of the evaluated macromolecules led to new conclusions regarding the mechanism of protein release from these networks. As expected, varying the network hydrophobicity (MCPH:MSA ratio or

PEGDA content) altered the release profiles to achieve varying rates of protein release from the matrices. Surprisingly, these effects were seen primarily in the later phases (>7 days) of release. Interestingly, especially during the early phases of protein release, the physicochemical properties of individual proteins were a dominant factor in determining protein release.

If the mechanism for protein release were dictated purely by erosion of the polymer network, it would be expected that the release profile would be near-zero order and unrelated to protein molecular weight. However, protein molecular weight played a dominant role. The mechanism for protein release in the short-term appeared to be diffusion through matrix channels. As a result, release was dictated by protein properties (solubility and diffusivity) as well as by matrix properties (porosity and tortuosity). Small molecular weight macromolecules were incapable of inducing substantial matrix porosity, therefore hindering release. Also contributing to this theory that matrix porosity and protein properties were dominant factors in protein release was the observation that MCPH:MSA ratio, the main contributor to degradation rate, was not a good predictor of amount of protein release during the short-term. In contrast, after roughly 7 days of release, network hydrophobicity began to play the expected role in modulating protein release.

In prior work, alteration of monomers failed to achieve modulation of protein release in the short-term, therefore other avenues have been explored. Since porosity played a dominant role in dictating protein release, modifications in network porosity have been explored. Particulate leaching strategies are used in TE to induce porosity in scaffolds. In this process, leachable porogens such as salt or gelatin microparticles are

incorporated uniformly into a scaffold. By incubation in aqueous buffer, the leachables are removed, leaving a uniformly porous scaffold. In the current study, the particulate leaching strategy was employed to fine tune protein release from photocrosslinked PA networks. Gelatin microparticles (250 μm) or NaCl particles (<106 μm) were incorporated into photocrosslinked PA matrices of identical formulations. In specimen with gelatin microparticles, burst effect, long-term release rate, and total cumulative release rate of HRP were increased in comparison with unmodified networks (Fig. 2). However, in specimen containing NaCl particles, there was only a significant increase in burst release behavior. This suggests that the leaching of dissolved gelatin leaves an aqueous path, whereas the complete ionic dissolution of NaCl does not result in new aqueous pathways or macroporosity for protein diffusion and release.

Particulate leaching of gelatin microparticles for facilitation of HRP release from photocrosslinked PA networks was further pursued. Initially, gelatin microparticles of two sizes (180-250 μm or 250-300 μm) were incorporated into photocrosslinked PA networks at a loading of 75 v/v%. In this system, microparticle size played no role in the burst release or release rate during the first 8 days (Fig 3). However, after eight days, matrices with larger microparticles resulted in a higher rate of protein release. Since 75 v/v% was the upper limit for microparticle loading, and did result in some fracture during degradation, lower levels of loading were explored. A fractional factorial design of formulations was prepared with a high and low MCPH:MSA ratio (70:30 and 30:70), microparticle loading (55 v/v% and 33 v/v%) and gelatin microparticle size (180-250 μm and 106-180 μm). Interestingly, protein release was independent of both MCPH:MSA ratio and microparticle loading (Fig. 4). The larger gelatin microparticle size significantly

increased cumulative protein release, although this was primarily a result of protein release during the initial 48 hours. These data demonstrate that protein release can be modulated by a particulate leaching strategy. Regardless of gelatin microparticle size or loading, burst release and cumulative release were increased in comparison to nonporous matrices in previous studies. Experimental differences between the 75 v/v% loading and the lower (55 and 33 v/v %) loadings could be a result of a failure of the lower loadings to reach the percolation threshold for the material This critical threshold concentration of porogens would result in an “infinite cluster” of conducting links, or pores through which the buffer can infiltrate (11). In this system, achieving the percolation threshold was not generally feasible; as structural integrity was compromised by high (75 v/v%) microparticle loading.

In addition to their usage in particulate leaching, gelatin microparticles have also been utilized for controlled delivery of growth factors as a result of ionic complexation capabilities (12). Microparticles were loaded with protein solutions by partial swelling. During release, poorly associated protein was released into the release buffer during the initial 24 hours as the microparticles reach equilibrium swelling (Fig 5). FITC-BSA demonstrated a high burst release from gelatin microparticles, yet also appeared to yield sustained release throughout the 18 day experimental conditions. HRP demonstrated less of a burst response than FITC-BSA; however HRP release after 6 days was negligible. HRP release from smaller microparticles (106-180 μm) was greater than HRP release from larger microparticles (180-250 μm), presumably an effect of a higher surface area to volume ratio in the smaller microparticles. This

difference in cumulative release was primarily dictated by HRP release between days 2 and 6.

Finally, further experiments examined the dual release of FITC-BSA and HRP from photocrosslinked PA network – gelatin microparticle composites. The goal of this dual release strategy was to create a system that could provide sustained release of two or more growth factors at different rates or release profiles. For example, in a system for tissue regeneration, a proliferative growth factor could undergo substantial release in the short-term, while a release of a differentiative growth factor could dominate in the long-term. In this study, protein-loaded microparticles were encapsulated into the photocrosslinked network along with a wet-granulated protein-cyclodextrin formulation. One composite formulation contained FITC-BSA-loaded gelatin microparticles and HRP in the wet-granulated phase (Fig. 7). The other composite formulation contained HRP-loaded gelatin microparticles and FITC-BSA in the wet-granulated phase (Fig. 8). The strategy of encapsulating drug- or protein-loaded microparticles in a matrix is commonly used to localize delivery to a specific site. In this system, the microparticles additionally confer porosity to the matrix to facilitate release of the protein in the wet-granulated phase.

When FITC-BSA was loaded into gelatin microparticles and HRP was present in the wet-granulated phase, surprisingly, there was no detectable release of FITC-BSA from the composite. Additionally, HRP release profiles were similar to profiles from a nonporous matrix. Alternatively, when HRP was loaded into gelatin microparticles and FITC-BSA was present in the wet-granulated phase, significant release of both HRP and FITC-BSA occurred. Release was greater than from nonporous matrices in

previous studies. It was surprising that no appreciable release of FITC-BSA was detected from the composites containing FITC-BSA in the gelatin phase, although FITC-BSA does release from gelatin microparticles and HRP release from the matrix was observed. The phenomenon is presumably explained by protein molecular weight (MW) and hydrodynamic radius (HR). The protein in the wet-granulated phase was readily solubilized when in contact with buffer. When the higher molecular weight protein (FITC-BSA, MW 67 kDa, HR 36Å) was present in the wet-granulated phase, protein diffusion created channels through which the smaller protein (HRP, MW 43 kDa, HR 30Å) could diffuse as well. However when the larger protein was in the gelatin microparticle phase, the channels created by the smaller protein probably are insufficient for the larger protein to transport through (Scheme in Fig. 9).

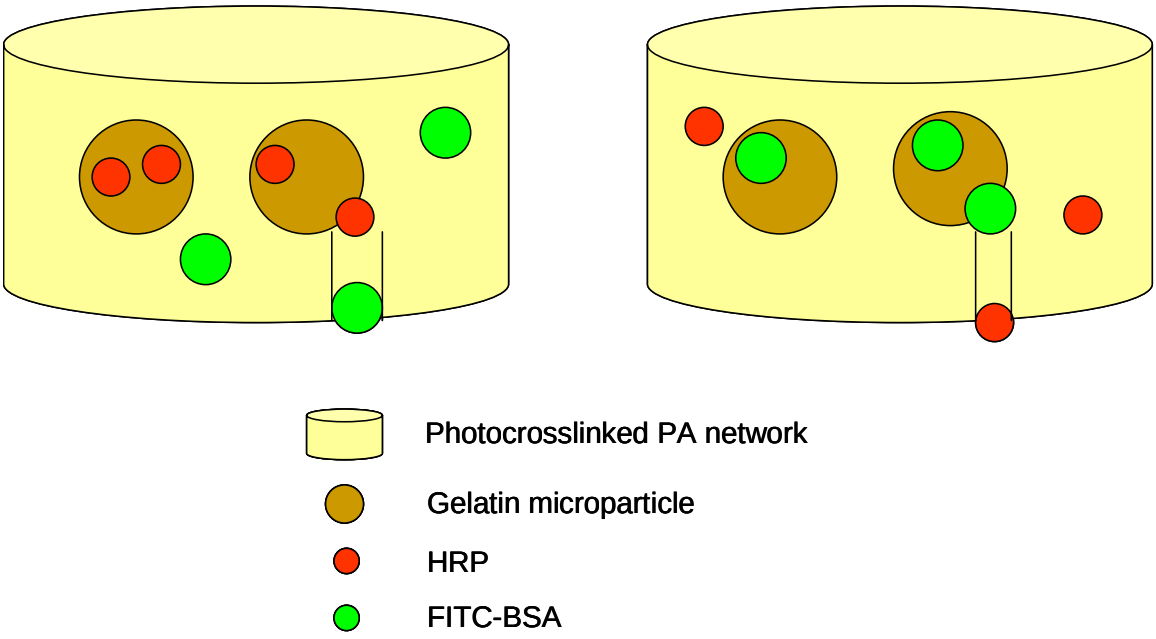

Fig. 9: Proposed mechanism for dual protein release from photocrosslinked PA network-gelatin microparticle composites.

Conclusions

This study details a means of modulating delivery of proteins from an injectable degradable system by incorporation of gelatin microparticles into the photocrosslinked PA system. Since protein diffusivity and matrix porosity in addition to matrix degradation were dominant factors in controlling protein release in previous studies, here we have focused on incorporation of porogens for increasing levels of protein release. When gelatin microparticles were included in matrices, microparticle size appeared to be the predominant factor affecting HRP release, with microparticle loading having no appreciable effect. Gelatin microparticles were also explored as a delivery vehicle. Both microparticle size and protein type (FITC-BSA or HRP) affected protein release from gelatin microparticles. By loading the protein in the gelatin microparticles, additional control over protein release was achieved. Furthermore, a dual release system has been demonstrated by incorporation of protein in both the PA matrix and the gelatin microparticles. Variation of system parameters – microparticle size, loading percentage, and protein loading of the microparticles – provide a versatile methodology for tailoring release profiles from photocrosslinked PA system. Future work will include further elucidation of the mechanisms of release, including porosity and aqueous channel formation.

Acknowledgements

The authors are grateful for financial support from the Vanderbilt Institute for Integrative Biology and Education (VIIBRE) and from a Vanderbilt University Discovery Grant.

They would also like to acknowledge support for AAW from the National Science Foundation Graduate Research Program.

References

1. Anseth, K. S., Shastri, V. R., and Langer, R. (1999) Photopolymerizable degradable polyanhydrides with osteocompatibility. *Nat Biotechnol* 17, 156-159.

2. Weiner, A. A., Shuck, D. M., Bush, J. R., and Shastri, V. P. (2007, in review) Optimization of photocrosslinked anhydride systems for bone augmentation applications: characterization of in vitro degradation. *Biomaterials*
.
3. Weiner, A. A., Gipson, M. E., Bock, E. A., and Shastri, V. P. (2007, in submission) Photocrosslinked anhydride systems for long-term protein release. *Journal of Controlled Release.*

4. Baroli, B., Shastri, V. P., and Langer, R. (2003) A method to protect sensitive molecules from a light-induced polymerizing environment. *J Pharm Sci* 92, 1186-1195.

5. Hedberg, E. L., Kroese-Deutman, H. C., Shih, C. K., Crowther, R. S., Carney, D. H., Mikos, A. G., and Jansen, J. A. (2005) Effect of varied release kinetics of the osteogenic thrombin peptide TP508 from biodegradable, polymeric scaffolds on bone formation in vivo. *J Biomed Mater Res A* 72A, 343-353.

6. Holland, T. A., Tabata, Y., and Mikos, A. G. (2005) Dual growth factor delivery from degradable oligo(poly(ethylene glycol) fumarate) hydrogel scaffolds for cartilage tissue engineering. *J Control Release* 101, 111-125.

7. Muvaffak, A., Gurhan, I., and Hasirci, N. (2004) Prolonged cytotoxic effect of colchicine released from biodegradable microspheres. *J Biomed Mater Res B Appl Biomater* 71, 295-304.

8. Determan, A. S., Trewyn, B. G., Lin, V. S., Nilsen-Hamilton, M., and Narasimhan, B. (2004) Encapsulation, stabilization, and release of BSA-FITC from polyanhydride microspheres. *J Control Release* 100, 97-109.

9. Tarcha, P. J., Su, L., Baker, T., Langridge, D., Shastri, V., and Langer, R. (2001) Stability of photocurable anhydrides: Methacrylic acid mixed anhydrides of nontoxic diacids. *J Polym Sci Pol Chem* 39, 4189-4195.

10. Conix, A. (1966) Poly[1,3-bis(p-carboxyphenoxy)propane anhydride]. *Macromol. Synth.* 2, 95-98.

11. Romm, F. (2002) Theories and theoretical models for percolation and permeability in multiphase systems: comparative analysis. *Adv Colloid Interface Sci* 99, 1-11.

12. Yamamoto, M., Ikada, Y., and Tabata, Y. (2001) Controlled release of growth factors based on biodegradation of gelatin hydrogel. *J Biomater Sci Polym Ed* 12, 77-88.

CHAPTER V

CONCLUSIONS AND FUTURE WORK

Summary of Manuscripts

This dissertation is composed of three manuscripts which detail the optimization of the photocrosslinked polyanhydride (PA) system for tissue engineering and drug delivery applications. Each manuscript corresponds to one of the three specific aims detailed in Chapter I. Together, these three aims describe the development of a versatile biomaterial for usage in spinal fusion applications.

In Chapter II, the photocrosslinked PA system was enhanced by the inclusion of PEGDA and $CaCO_3$ as additives. The incorporation of additives did not alter the curing ability or formability of the system. Incorporation of PEGDA and $CaCO_3$ served both to decrease water uptake and to modulate local acidity during degradation. The inclusion of $CaCO_3$ enabled maintenance of compressive modulus throughout the degradative lifetime of the material. In this study, we have revealed additional mechanisms for tuning material properties via incorporation of additive agents to expand the scope and functionality of the system. Finally, this study demonstrated that additives can be easily and successfully incorporated into photocrosslinked PA networks to address a variety of physical characteristics.

Chapter III detailed the first study to evaluate protein release from photocrosslinked PA networks. The modifications described in Chapter II were used in this system. One important result of this work was that sustained long-term release (> 4

months) of macromolecules in their active form from photocrosslinked PA networks was feasible. Three model proteins, that differ in their physicochemical and detection modalities have been incorporated into the matrices and released *in vitro*. By varying the network hydrophobicity (MCPH:MSA ratio or PEGDA content) the release profiles were tuned to achieve varying rates of protein release from the matrices. This observation constituted a novel mechanism for controlling macromolecular release from hydrophobic matrices. Interestingly, especially during the early phases of protein release, the physicochemical properties of individual proteins were a dominant factor in determining protein release. These findings validated the photocrosslinked PA system as an injectable vehicle for macromolecule delivery with broad clinical applications.

Chapter IV is a direct extension of the studies described in Chapter III. The release rate of proteins in Chapter III was slower than may be desirable for *in vivo* applications. This study detailed a means of modulating delivery of proteins from an injectable degradable system by incorporation of gelatin microparticles into the photocrosslinked PA system. Since protein diffusivity and matrix porosity in addition to matrix degradation were dominant factors in controlling protein release in previous studies, here we focused on incorporation of porogens for increasing levels of protein release. When gelatin microparticles were included in matrices, microparticle size appeared to be the predominant factor affecting HRP release, although microparticle loading was also evaluated. Gelatin microparticles were also explored as a delivery vehicle. Both microparticle size and protein type (FITC-BSA or HRP) affected protein release from gelatin microparticles. When protein-loaded microparticles were incorporated into photocrosslinked PA networks, release behavior was greatly

dependent on the protein. Variation of these parameters – microparticle size, loading percentage, and protein loading of the microparticles – provided a versatile methodology for tailoring release profiles from photocrosslinked PA system.

In summary, the studies this from dissertation have optimized the photocrosslinked PA system. By incorporation of additives, the material properties have been modulated to minimize water uptake and acidity during degradation, while preserving mechanical strength. Next, the system was further modified to enable long-term release of active proteins. Theories were developed as to mechanisms of protein release during different phases. Finally, based on these theories, protein release from the system was enhanced through the incorporation of water soluble porogens. These results demonstrate progress toward the development of an injectable, biodegradable material for spinal fusion, with an end goal of releasing osteoinductive factors for promotion of new bone growth in spinal fusion applications.

Future Work

The photocurable polyanhydride system has numerous advantages for applications in spinal fusion. First, the photocurable nature of the system, by virtue of methacrylate groups, allows formation of the network *in situ*, thereby enabling conformability of the material to the desired region. Second, upon crosslinking, the network's modulus is comparable to that of cortico-cancellous bone, and hence is less likely to shield the bone from normal stresses, allowing for bone remodeling. The ratios of monomers can be altered to fit nearly any degradation rate. Up to 30 wt% of the formulation can consist of non-reactive additives (inorganic fillers or porogens, growth

factors, or viscosity modifiers) without altering crosslinking kinetics. Photocuring allows a more extensive handling time prior to crosslinking than is typically possible with chemical crosslinking. By combining chemical and photo crosslinking, both the handling time and depth of cure are increased. Finally, system biodegradability eliminates the need for secondary surgeries to remove the device.

Development of this photo-curable poly(anhydride) system into an osteoconductive, osteoinductive biomaterial for use in spinal applications will be a paradigm shift. There is currently no material that provides immediate structural stability and is biodegradable over time. While minimally invasive procedures such as vertebroplasty and kyphoplasty are also envisioned as a long-term application for this biomaterial, the initial future studies will focus on spinal fusion. We feel that by evaluating our material in a well-validated animal model for spinal fusion (posterolateral intertransverse arthrodesis in the New Zealand white rabbit) we can demonstrate the full range of material capabilities and biocompatibility.

The New Zealand white rabbit model for posterolateral intertransverse (PLIT) lumbar arthrodesis has been a well-described, well-accepted and prevalent model for spinal fusion since its description by Boden in 1995 (1-3). Model utility is based on several factors, including approximation to human surgical procedure, healing environment, and nonunion rate (4). The surgical anatomy (4) and operative technique (5) have been thoroughly described in the literature. The model has been applied to study the effects of diverse parameters on the bone biology of lumbar fusion – including bone graft substitutes, growth factors, or gene therapy (6-11). We have selected this model to demonstrate the potential of our PA system to facilitate spinal fusion.

Initial animal studies will involve the use of the photocrosslinked PA system as an extender to autograft. Morselized autograft from iliac crest will be mixed with the monomer paste, and used in the PLITF model. Three experimental groups will be assessed to accomplish this aim. In the control group, the fusion material will be morselized autograft bone, harvested from iliac crest during surgery. In experimental group 1, the fusion material will be the poly(anhydride) network, which will be crosslinked *in situ*. In experimental group 2, the fusion material will be a mixture of the PA network and morselized autograft bone. Data collected from this study will include: histology, histomorphometry, planar x-ray, microCT, and DEXA imaging. Biocompatibility, as well as osteogenicity will be evaluated. Subsequent studies will involve the replacement of the autograft + polymer group with a group that receives polymer mixed with formulated BMP-2, for osteoinduction. Success of this material (defined as fusion that is comparable to that of autograft) in spinal fusion applications is the end goal. In summary, the research that stems from the work in this dissertation will provide a major advance in osteoconductive, osteoinductive biomaterials for use in spine applications.

References

1. Boden, S. D., Schimandle, J. H., and Hutton, W. C. (1995) An experimental lumbar intertransverse process spinal fusion model. Radiographic, histologic, and biomechanical healing characteristics. *Spine* 20, 412-420.

2. Boden, S. D., Schimandle, J. H., Hutton, W. C., and Chen, M. I. (1995) 1995 Volvo Award in basic sciences. The use of an osteoinductive growth factor for lumbar spinal fusion. Part I: Biology of spinal fusion. *Spine* 20, 2626-2632.

3. Boden, S. D., Schimandle, J. H., and Hutton, W. C. (1995) 1995 Volvo Award in basic sciences. The use of an osteoinductive growth factor for lumbar spinal fusion. Part II: Study of dose, carrier, and species. *Spine* 20, 2633-2644.

4. Palumbo, M., Valdes, M., Robertson, A., Sheikh, S., and Lucas, P. (2004) Posterolateral intertransverse lumbar arthrodesis in the New Zealand White rabbit model: I. Surgical anatomy. *Spine J* 4, 287-292.

5. Valdes, M., Palumbo, M., Appel, A. J., McAllister, S., and Ehrlich, M. (2004) Posterolateral intertransverse lumbar arthrodesis in the New Zealand White rabbit model: II. Operative technique. *Spine J* 4, 293-299.

6. Lindfors, N. C., Tallroth, K., and Aho, A. J. (2002) Bioactive glass as bone-graft substitute for posterior spinal fusion in rabbit. *J Biomed Mater Res* 63, 237-244.

7. Namikawa, T., Terai, H., Suzuki, E., Hoshino, M., Toyoda, H., Nakamura, H., Miyamoto, S., Takahashi, N., Ninomiya, T., and Takaoka, K. (2005) Experimental spinal fusion with recombinant human bone morphogenetic protein-2 delivered by a synthetic polymer and beta-tricalcium phosphate in a rabbit model. *Spine* 30, 1717-1722.

8. Minamide, A., Kawakami, M., Hashizume, H., Sakata, R., Yoshida, M., and Tamaki, T. (2004) Experimental study of carriers of bone morphogenetic protein used for spinal fusion. *J Orthop Sci* 9, 142-151.

9. Hile, D. D., Kandziora, F., Lewandrowski, K. U., Doherty, S. A., Kowaleski, M. P., and Trantolo, D. J. (2005) A poly(propylene glycol-co-fumaric acid) based bone graft extender for lumbar spinal fusion: in vivo assessment in a rabbit model. *Eur Spine J.*

10. Alden, T. D., Pittman, D. D., Beres, E. J., Hankins, G. R., Kallmes, D. F., Wisotsky, B. M., Kerns, K. M., and Helm, G. A. (1999) Percutaneous spinal fusion using bone morphogenetic protein-2 gene therapy. *J Neurosurg* 90, 109-114.

11. Mooney, V., Massie, J. B., Lind, B. I., Rah, J. H., Negri, S., and Holmes, R. E. (1998) Comparison of hydroxyapatite granules to autogenous bone graft in fusion cages in a goat model. *Surg Neurol* 49, 628-633; discussion 633-624.

APPENDIX A

RATIONALE FOR SELECTION OF POLYMER FORMULATIONS FOR SPECIFIC AIMS TWO AND THREE

Based on our preliminary results, we have selected a formulation of monomers, inorganic fillers and photoinitiators that have yielded the most desirable properties *in vitro*. First, the anhydride portion of the formulation will be composed of MCPH and MSA in a ratio of 70:30. The balance of this parameter is responsible for the rate of mass loss, the pH profile on degradation, as well as the mechanical strength. Next, the overall composition should be 10 wt% PEGDA (MW 700). This amount is sufficient to provide viscosity modification and to improved depth of cure and crosslinking resultant from the highly reactive diacrylate functionality. The improvement in crosslinking diminishes swelling during network degradation. The inorganic filler calcium carbonate ($CaCO_3$) should be present at 10 wt%, to serve as a moderate porogen and as a significant pH buffer during the course of degradation. Finally, the photoinitiators should be included at 0.1 wt%. This photoinitiator concentration provides excellent depth of cure within 10 minutes in our human cadaver corpectomy model, while allowing a reasonable working time after adding initiators. In addition, we have demonstrated that photocrosslinking can occur with an additional 10 wt% of nonreactive fillers, allowing the supplementation of this formulation with proteins without affecting the polymerization efficacy. This level of in vitro testing will provide our collaborators and others in the field with an unprecedented level of insight, thereby enabling tests of function in a direct and highly efficient manner. Table 1 summarizes the network components.

Table 1: Rationale for polymer formulation

Parameter	Composition	Rationale
Anhydride ratio (MCPH:MSA)	70:30	Mass loss pH Mechanical properties
PEGDA	10 wt%	Viscosity modification Depth of cure
Calcium carbonate	10 wt%	pH buffer Porogen
Benzoyl Peroxide	0.1 wt%	Chemical crosslinking
Dimethyl Toluidine	0.1 wt%	
Camphorquinone	0.1 wt%	Photo-crosslinking
Ethyl 4-dimethylaminobenzoate	0.1 wt%	

APPENDIX B

INCORPORATION OF BARIUM SULFATE INTO PHOTOCROSSLINKED POLY(ANHYDRIDE) NETWORKS

Radio-opacity must be conferred to the polymer if it is to be visualized after implantation. This allows the clinical outcome to be easily followed via x-ray. In a proof-of-concept experiment, barium sulfate ($BaSO_4$) was mixed into a mixture of methacrylated anhydride monomers and photocrosslinked. The specimen were embedded in agarose phantoms and imaged by planar x-ray. In Fig. 1, two samples containing $BaSO_4$ (top and bottom right) show more contrast than a photocrosslinked poly(anhydride) network without $BaSO_4$ (bottom left). $BaSO_4$ incorporation within the network clearly improves contrast on x-ray without affecting curing parameters.

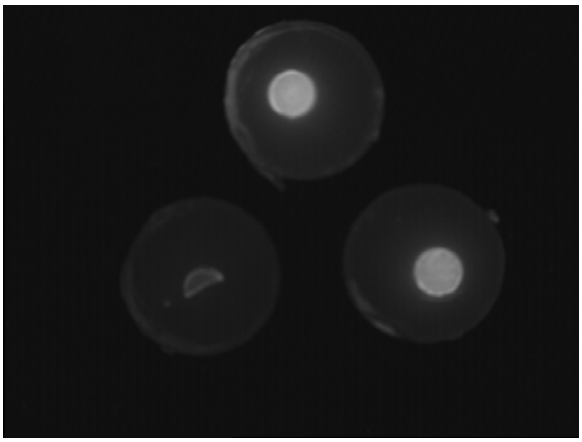

Fig. 1: Photocrosslinked poly(anhydride) networks without $BaSO_4$ (bottom left) or with $BaSO_4$ (top and bottow right). $BaSO_4$ incorporation within the network clearly improves contrast on x-ray without affecting curing parameters.

APPENDIX C

INCORPORATION OF MORSELIZED BONE INTO PHOTOCROSSLINKED POLY(ANHYDRIDE) NETWORKS

Producing crosslinked poly(anhydride) matrices containing autogenous bone from the iliac crest is a vital component of future work. To evaluate feasibility of an experimental group containing a mixture of autograft and polymer, two formulations were crosslinked. The first contained 50% iliac crest autograft and 50% polymer formulation (by mass), and the second contained 35% iliac crest autograft and 75% polymer formulation. Both formulations crosslinked into uniform discs (5 mm height, 10 mm diameter), although after a curing time of 10 minutes, the 50:50 sample required showed evidence of inhomogeneous curing. The 25:75 samples polymerized in less than 5 minutes. Samples containing morselized bone (Fig. 1 a 25:75, b 50:50) were imaged by scanning electron microscopy (SEM, Hitachi S-4200) to demonstrate more porous network architecture than unmodified polymer formulations. As a result of the lengthened crosslinking time and inhomogeneous curing for the 50:50 formulation, the 25:75 formulation has been selected for future studies.

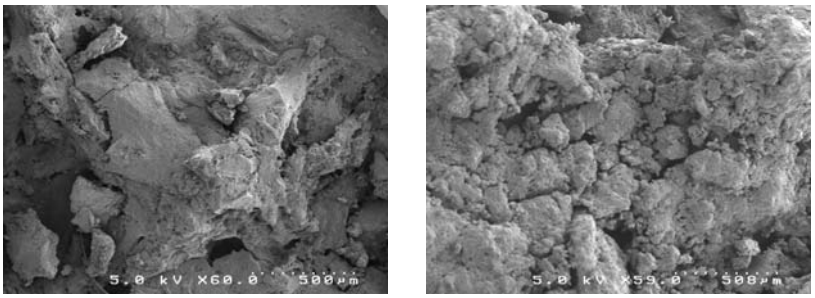

Fig. 1: SEM images of photocrosslinked poly(anhydrides) containing A) 25% morselized bone and B) 50% morselized bone.

APPENDIX D

IN SITU PHOTOCROSSLINKING IN HUMAN CADAVER SPINE

To evaluate proof of principle for photocrosslinking the poly(anhydride) system in the spine, a modified corpectomy model was assessed in a human cadaver spine (Fig. 1). A partial corpectomy was performed on a thoracic vertebral body. The polymer formulation was mixed and poured into the excised region. The polymer network was formed via curing with a blue dental lamp (CuringLight XL1500) for 10 minutes. The crosslinked network was removed from the defect. The polymer network meshed with existing bone and perfectly filled the defect, verifying feasibility of this strategy *in vivo*. The crosslinked polymer in this scenario was 3 cm in width and 1.5 cm in height, demonstrating that complete curing can occur in a reasonable timeframe even on larger samples.

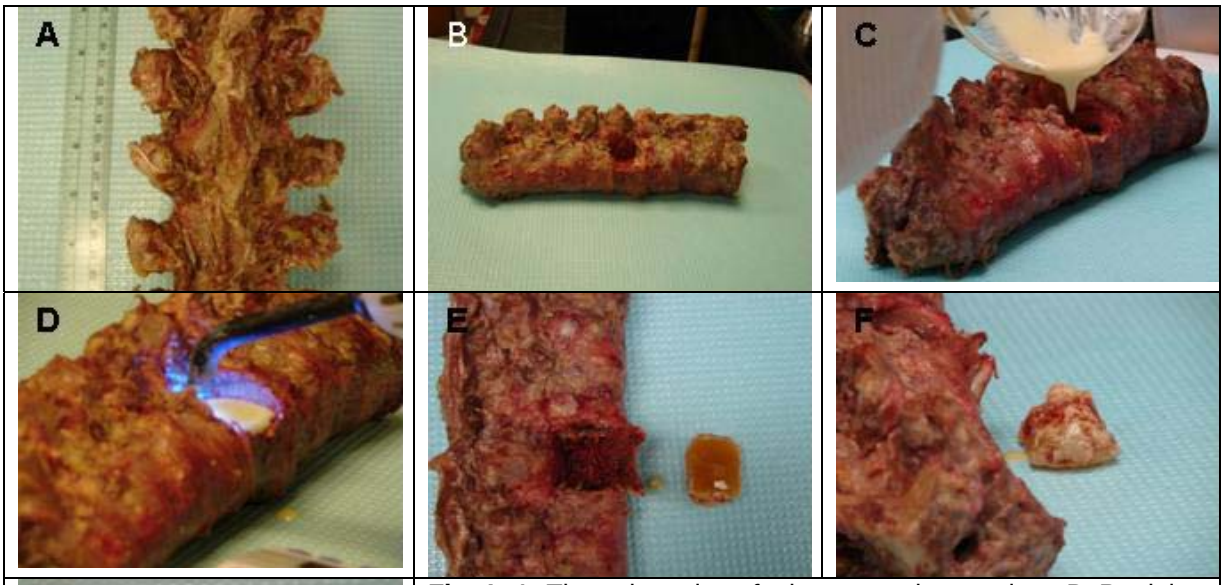

Fig. 1: A. Thoracic region of a human cadaver spine. B. Partial corpectomy of a thoracic vertebral body. C. Mixture of anhydride monomers was poured into the corpectomy region. D. Photocrosslinking the PA network in the corpectomy region of a human cadaver spine. E. Photocrosslinked PA network removed from the corpectomy region. F. Alternative view of the back of the photocrosslinked PA network, demonstrating a complete filling of the void space. G. Cross-section of the photocrosslinked PA) network, demonstrating crosslinking throughout the depth of the material.

APPENDIX E

PHOTOCROSSLINKED POLY(ANHDRIDES) IN A RABBIT MODEL FOR POSTEROLATERAL INTERTRANSVERSE FUSION

Surgical procedure

Posterolateral intertransverse arthrodesis was performed as described by Valdes et al (1). The dorsal aspect of the lumbar spine was shaved. The skin was prepared using sterile technique, and the spinal level to be fused, L5-L6, was identified by palpation. A dorsal midline incision of approximately 6 cm in length was made over the L5-L6 level. The skin and subcutaneous tissue was retracted. A 4-6 cm incision through the lumbar fascia was made, approximately 2 cm lateral to the midline. The iliocostalis muscle was divided to reveal the longissimus muscle, which underwent blunt dissection at the lateral border to reveal the transverse processes. The graft material was placed over the intertransverse ligament, spanning the distance between the L5 and L6 transverse processes. Fig. 1A shows the crosslinked matrices during the surgical procedure. Harvest of iliac crest autograft was carried out concurrently with the posterolateral intertransverse spinal fusion procedure, as described by Valdes et al (1). The middle two thirds of the iliac crest was exposed (greatest amount of cancellous bone at this location). For this study, the harvest of only one iliac crest was required. The graft on the right side of the animal consisted of polymer alone, supplemented with 10 mg $BaSO_4$ to provide radio-opacity. The graft on the left side of the spine was composed of polymer + 25% iliac crest autograft. Photocrosslinking of the polymer graft required 3 minutes of exposure to a blue dental lamp for the BaSO4 modified side

and 6 minutes of exposure for the polymer+autograft side. A 3-0 vicryl suture was used for muscle and lumbodorsal fascia. 2-0 nylon sutures were used along the incision.

Following this, the lumbar spine was explanted for analysis using microCT. The planar x-ray and DEXAscan were carried out with the assistance of Dr. Ed Donnelly at the Vanderbilt Institute of Imaging Sciences (VUIIS) Small Animal Imaging Facility. The microCT was carried out with the assistance of Dr. Todd Peterson at the VUIIS Small Animal Imaging Facility.

Planar x-ray

Radiographs were taken in the anteroposterior plane using a Faxitron Radiography X-ray (Wheeling, IL). Radiographs were taken at 60 kV with a 10 s exposure and a digital acquisition system. Both the specimen containing $BaSO_4$ and the specimen containing morselized autograft had sufficient contrast to be visualized on the x-ray image (Fig. 1B).

microCT

The Imtek MicroCAT II scanner is an X-ray computed tomography system capable of performing imaging studies of small animals in vivo or specimens. The microCT images were reconstructed and analyzed using Amide software. The 3D reconstruction can be seen in Fig. 1C. In Fig. 1D and 1E, slices of the coronal plane and transverse plane can be seen respectively. In both Fig.s 1D and E, the specimen containing autograft is seen on the left, and the specimen with $BaSO_4$ can be seen on the right. Both the polymer specimen containing $BaSO_4$ and morselized autograft were

clearly visible on the microCT reconstructions. The specimen containing $BaSO_4$ showed more contrast than the specimen containing morselized autograft. However, the pieces of morselized bone in the polymer + autograft specimen were clearly evident in most CT slices. This finding validates our strategy for using microCT as a metric for determining fusion in our studies as we will be able to detect bone within the polymer.

Dual energy x-ray absorptiometry (DEXA)

A GE Lunar PIXImus bone densitometer was used to evaluate the bone density in the regions of polymer and polymer + autograft. The image obtained from the densitometer is seen in Fig. 1F. From this image, six fields of 10 by 11 pixels were evaluated for bone density (g/cm^2). The specimen containing bone autograft had a significantly greater bone density than the $BaSO_4$ specimen ($p<0.05$). This data is shown in Fig. 1G. This result suggests that bone within the polymer can be both detected and quantified within the polymer specimen.

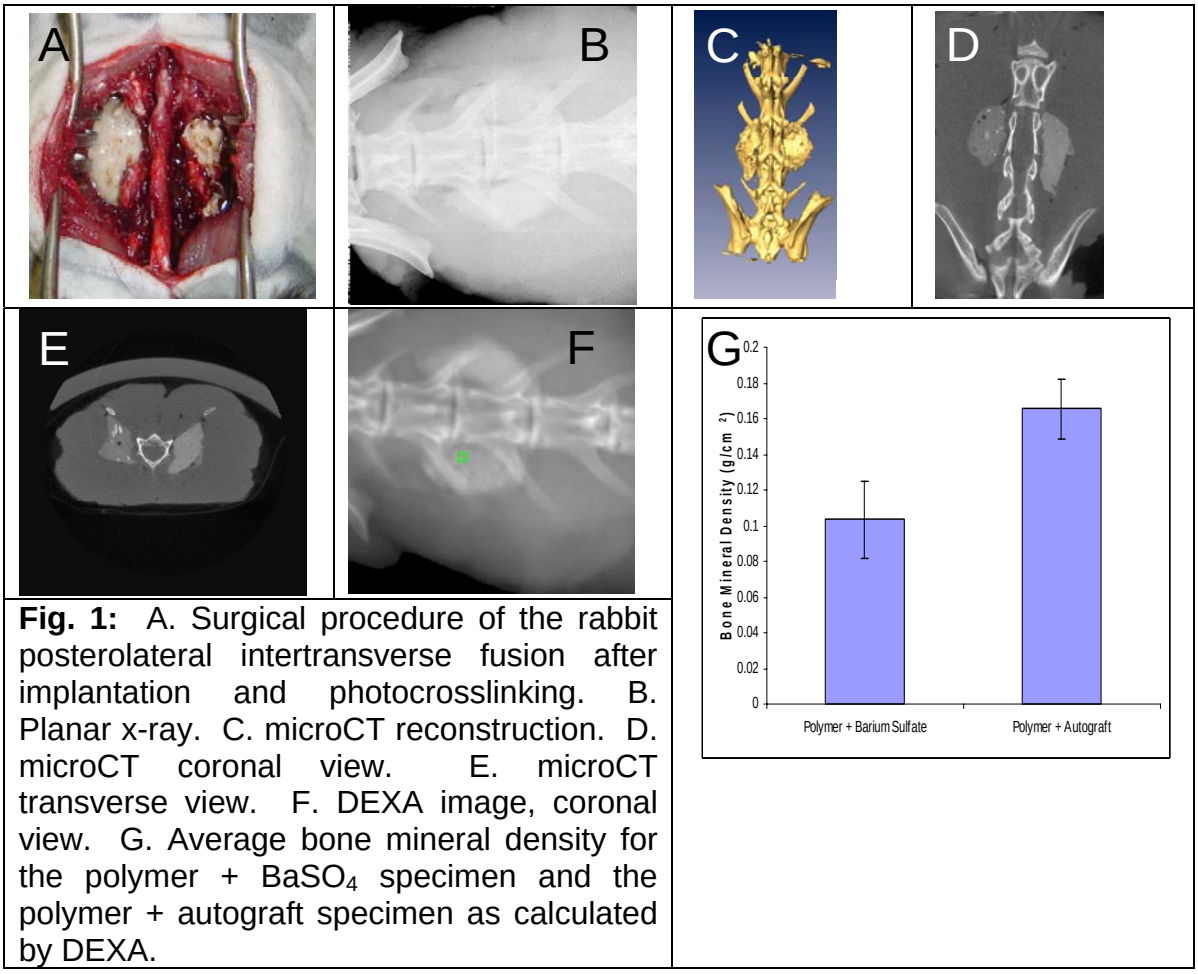

Fig. 1: A. Surgical procedure of the rabbit posterolateral intertransverse fusion after implantation and photocrosslinking. B. Planar x-ray. C. microCT reconstruction. D. microCT coronal view. E. microCT transverse view. F. DEXA image, coronal view. G. Average bone mineral density for the polymer + $BaSO_4$ specimen and the polymer + autograft specimen as calculated by DEXA.

References

1. Valdes, M., Palumbo, M., Appel, A. J., McAllister, S., and Ehrlich, M. (2004) Posterolateral intertransverse lumbar arthrodesis in the New Zealand White rabbit model: II. Operative technique. *Spine J* 4, 293-299.